AFRL-SR-BL-TR-98-

0251

REPORT DOCUMENTATION PAGE

1. AGENCY USE ONLY (Leave blank)	2. REPORT DATE	3. REPORT TYPE AND DATES COVERED
	02/11/98	Final Technical 09/01/94-08/31/97

4. TITLE AND SUBTITLE
Seeded Grain Growth for Textured Silicon Carbide and Mullite

5. FUNDING NUMBERS
F49620-94-1-0429 G

6. AUTHOR(S)
Michael D. Sacks

7. PERFORMING ORGANIZATION NAME(S) AND ADDRESS(ES)
University of Florida
219 Grinter Hall
Gainesville, FL 32611

8. PERFORMING ORGANIZATION REPORT NUMBER
4910 4509484-12

9. SPONSORING/MONITORING AGENCY NAME(S) AND ADDRESS(ES)
Dr. Alexander Pechenik
AFOSR/NA
110 Duncan Ave. Suite B115
Bolling AFB, DC 20332-8080

NA

10. SPONSORING/MONITORING AGENCY REPORT NUMBER
B732/02

11. SUPPLEMENTARY NOTES

12a. DISTRIBUTION/AVAILABILITY STATEMENT
Un limited

12b. DISTRIBUTION CODE

13. ABSTRACT (Maximum 200 words)

Textured fibers and bulk samples were fabricated using seeded grain growth. For bulk SiC samples, small amounts of SiC platelets were incorporated with preferred orientation during green-state processing of powder compacts. Upon heat treatment, the platelet seeds grew with preferred orientation by consuming the fine grains of the surrounding sintered SiC matrix. The volume fraction, size, and morphology of the *in-situ* grown plate-like grains could be controlled through variables such as heat-treatment temperature, matrix particle size, seed concentration, additive type, etc. Samples prepared with alumina/yttria additives were used to prepare *in-situ* toughened SiC bulk samples. SiC fibers were prepared using organosilicon polymer precursors. Textured fibers were fabricated using SiC whiskers or platelets as seed crystals, but these fibers had relatively low strengths because the seeds (and large grains formed during heat treatment) acted as strength-degrading flaws. Unseeded SiC fibers with textured boron nitride (BN) coatings were formed by an *in-situ* reaction method. These fibers had high tensile strength and excellent creep resistance. Textured Si_3N_4 fibrous monoliths were fabricated using extruded, powder-derived fibers which contained Si_3N_4 whiskers as seeds. The textured Si_3N_4 showed fracture toughness anisotropy.

14. SUBJECT TERMS	15. NUMBER OF PAGES
Textured Materials, Silicon Carbide, Grain Growth, Seeding, Fibers	71
	16. PRICE CODE

17. SECURITY CLASSIFICATION OF REPORT	18. SECURITY CLASSIFICATION OF THIS PAGE	19. SECURITY CLASSIFICATION OF ABSTRACT	20. LIMITATION OF ABSTRACT
			UL

NSN 7540-01-280-5500

Standard Form 298 (Rev. 2-89)
Prescribed by ANSI Std. Z39-18
298-102

THIS DOCUMENT IS COMPLETE AS IS

THE FIGURE PAGE ARE NOT NUMBERED

THERE ARE NO MISSING PAGES

PER: MICHAEL D. SACKS

(352) 392-6676

UNIVERSITY OF FLORIDA

GAINESVILLE, FL.

SEEDED GRAIN GROWTH FOR TEXTURED SILICON CARBIDE AND MULLITE

Final Technical Report (9/1/94 - 8/31/97)

AFOSR Grant No. F49620-94-1-0429

SEEDED GRAIN GROWTH FOR TEXTURED SILICON CARBIDE AND MULLITE

Final Technical Report (9/1/94 - 8/31/97)

AFOSR Grant No. F49620-94-1-0429

Submitted to: Dr. Alexander Pechenik
Air Force Office of Scientific Research
110 Duncan Ave., Suite B115
Bolling Air Force Base, DC 20332

Submitted by: M.D. Sacks
Dept. of Materials Science and Engineering
University of Florida
Gainesville, FL 32611

TABLE OF CONTENTS

1.0 EXECUTIVE SUMMARY

Materials with anisotropic physical properties can be produced by developing microstructural texture. In this program, textured materials were fabricated by controlling grain growth behavior. The overall objectives of the project were to: (i) produce textured fibers and bulk samples via seeded anisotropic grain growth and (ii) determine the effects of important processing variables (e.g., seed crystal characteristics, matrix powder characteristics, etc.) on grain growth behavior and texture development. In addition, preliminary information was obtained on the effect of textured microstructures on the mechanical properties.

The primary emphasis of the program was on the fabrication of highly textured SiC. The feasibility of producing textured SiC fibers and bulk samples via seeded anisotropic grain growth was demonstrated. Bulk SiC samples were formed by two powder processing techniques, i.e., sequential slip casting and tape casting/lamination. Small concentrations ($\sim$0.6-6%) of SiC platelets were incorporated with preferred orientation during the green-state processing of the powder compacts. Upon heat treatment, the platelet seeds grew with preferred orientation by consuming the fine grains of the surrounding sintered SiC matrix. The dominant growth direction was along the close-packed planes of the platelets. The volume fraction, size, and morphology of the *in-situ* grown platelike grains could be controlled through variables such as heat treatment temperature, particle size of the matrix powder, seed platelet concentration, type of additives used, etc. Samples prepared with alumina/yttria additives were used to fabricate *in-situ* toughened SiC.

Textured SiC fibers were prepared from pre-ceramic polymer solutions which contained small amounts ($\sim$0.2-2%) of SiC whiskers or SiC platelets as seed crystals. The whiskers and

platelets were oriented along the fiber length during the fiber spinning process. Whiskers seeded the growth of platelike grains along closed-packed planes perpendicular to the long axis of the whiskers. This resulted in textured fibers with a "stacked plate" morphology. Platelets seeded the development of elongated grains along the long axis of the fibers, but growth was sluggish in samples prepared with ~ 0.2 wt% seeds. The fibers produced to this point by these methods have low tensile strengths (i.e., compared to unseeded fibers) because (i) the seeds acted as strength-degrading flaws and (ii) the high processing temperatures resulted in large grain sizes.

SiC fibers with textured boron nitride (BN) coatings were formed by in-situ processing. The resulting fibers had high tensile strength and excellent creep resistance.

Textured Si_3N_4 was fabricated using extruded, powder-derived fibers which contained β-Si_3N_4 whiskers as seed crystals. The fibers were hot pressed to form a fibrous monolith. The seeds promoted oriented growth of rodlike β-Si_3N_4 grains. The textured Si_3N_4 showed fracture toughness anisotropy.

2.0 BACKGROUND

The development of anisotropic grain structures in ceramics and composites can result in improved physical properties. For example, increases in fracture toughness have been achieved when ceramic matrices are reinforced with rodlike or platelike grains.[1-18] In conventional fabrication methods, the reinforcing phase (e.g., whiskers or platelets) is mixed with the matrix phase powder during the initial stages of processing. Hot pressing is often required in order to obtain high sintered densities. A significant cost advantage can be realized by utilizing alternative processing approaches in which anisotropic particles are grown *in-situ*, i.e., after the sample has been substantially densified by pressureless sintering. This method has been very successful in producing silicon nitride-based and sialon-based ceramics with high strength and high fracture toughness.[3-10]

Microstructural texture is often developed in materials with anisotropic grain structures. This results in bulk samples which have orientation-dependent properties (e.g., mechanical, electrical, thermal, etc.).[2-4,11-15,17-24] There are several commons mechanism for development of microstructural texture in ceramic and composite materials. For example, anisotropic particles often become oriented in preferred directions due to non-isotropic applied stresses during powder consolidation/shape forming operations such as extrusion, tape casting, slip casting, dry pressing, etc.[10-16,24-34] Alternatively, texture may develop by rotation of rigid anisotropic particles under applied stresses during high temperature consolidation and deformation of bulk compacts (e.g., hot pressing, hot forging, etc.).[2-4,14-22,28] It has also been observed that texture can develop via anisotropic grain growth.[11,26,28,34]

In this project, a processing strategy which combines in-situ growth of anisotropic grain

structures with in-situ microstructural texturing is under investigation. The approach utilizes small amounts ($\leq 2\%$) of seed particles which are incorporated with preferred orientation during green state processing and which subsequently promote oriented growth of anisotropic grains during the heat treatment stage. This processing strategy is being applied to materials of interest for high temperature structural applications (e.g., silicon carbide, silicon nitride, and mullite). The method has potential for producing composites with improved fracture toughness and fibers with oriented grains for improved creep resistance.

3.0 RESULTS AND DISCUSSION

3.1 Textured Silicon Carbide

3.1.a Bulk Silicon Carbide

The development of highly textured bulk SiC samples via platelet-seeded grain growth has been investigated. Papers describing the initial work in this area are attached in the Appendix. Additional manuscripts are in preparation based on the work summarized below.

SiC platelet-seeded green bodies were prepared by slip casting and tape casting methods using suspensions of fine SiC particles. SiC platelets (hexagonal alpha phase) were added to the suspensions prior to casting. As illustrated schematically in Fig. 1, platelets tend to align during the forming operation such that the major faces of the platelets are parallel to the casting surface. In the case of tape cast samples, bulk samples were prepared by stacking and laminating individual tapes.

Platelet-Seeded Solid-State Grain Growth

SiC compacts were sintered using conventional boron and carbon dopants to ~96-99% of theoretical density at ~1950-2050°C. Figure 2 shows typical plots of relative density vs. temperature and open porosity vs. temperature for slip-cast samples prepared with and without 2% SiC platelets. Due to their low concentration, the platelets had essentially no effect on densification of the fine SiC powder compacts. The platelets underwent only minimal growth during the densification process.

Microstructure observations showed that significant growth of platelike grains occurred with post-densification heat treatments at higher temperatures. At sufficiently high temperatures,

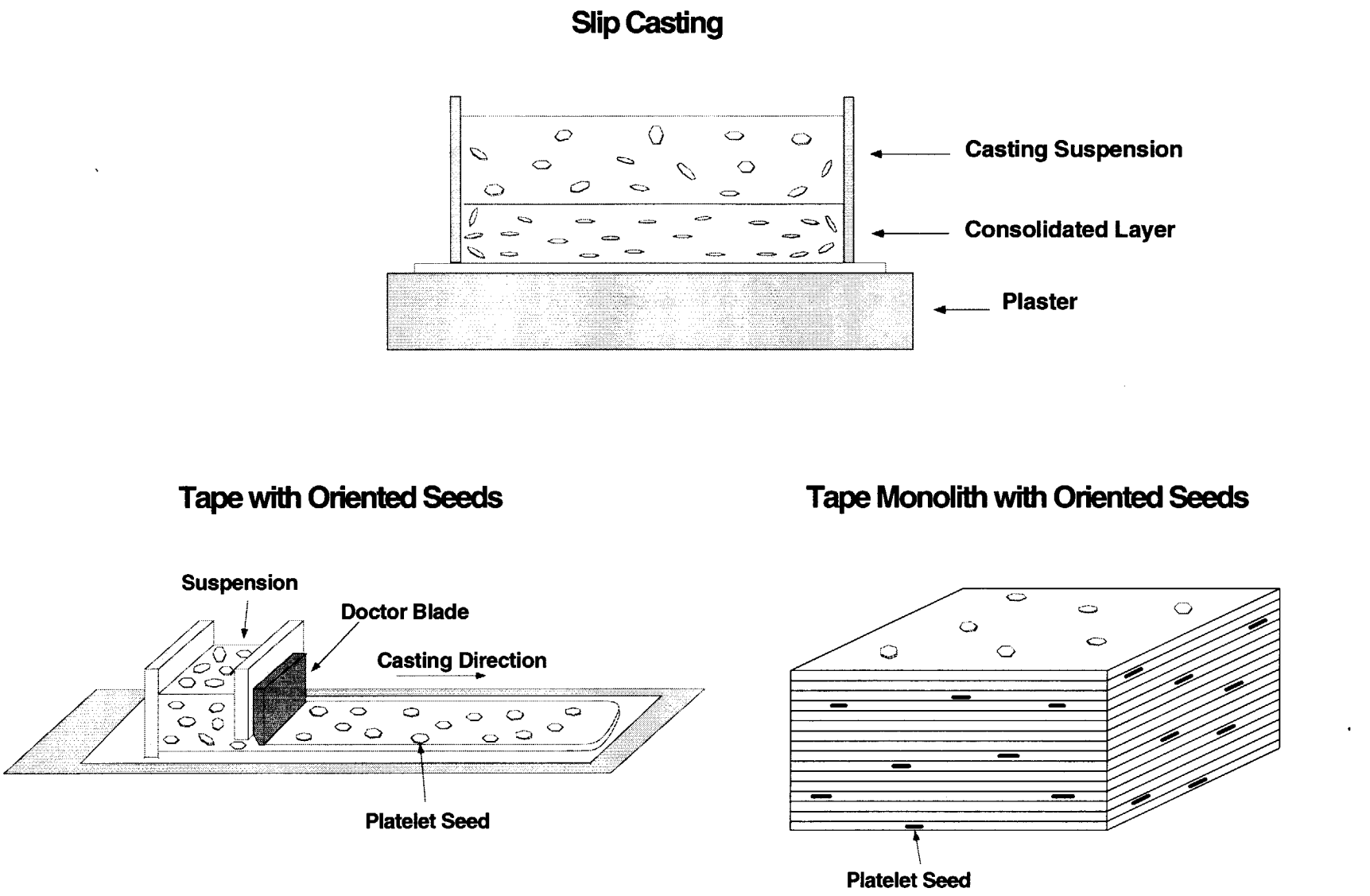

Figure 1. Schematic illustrations of the forming methods used to prepare green bodies with oriented platelets.

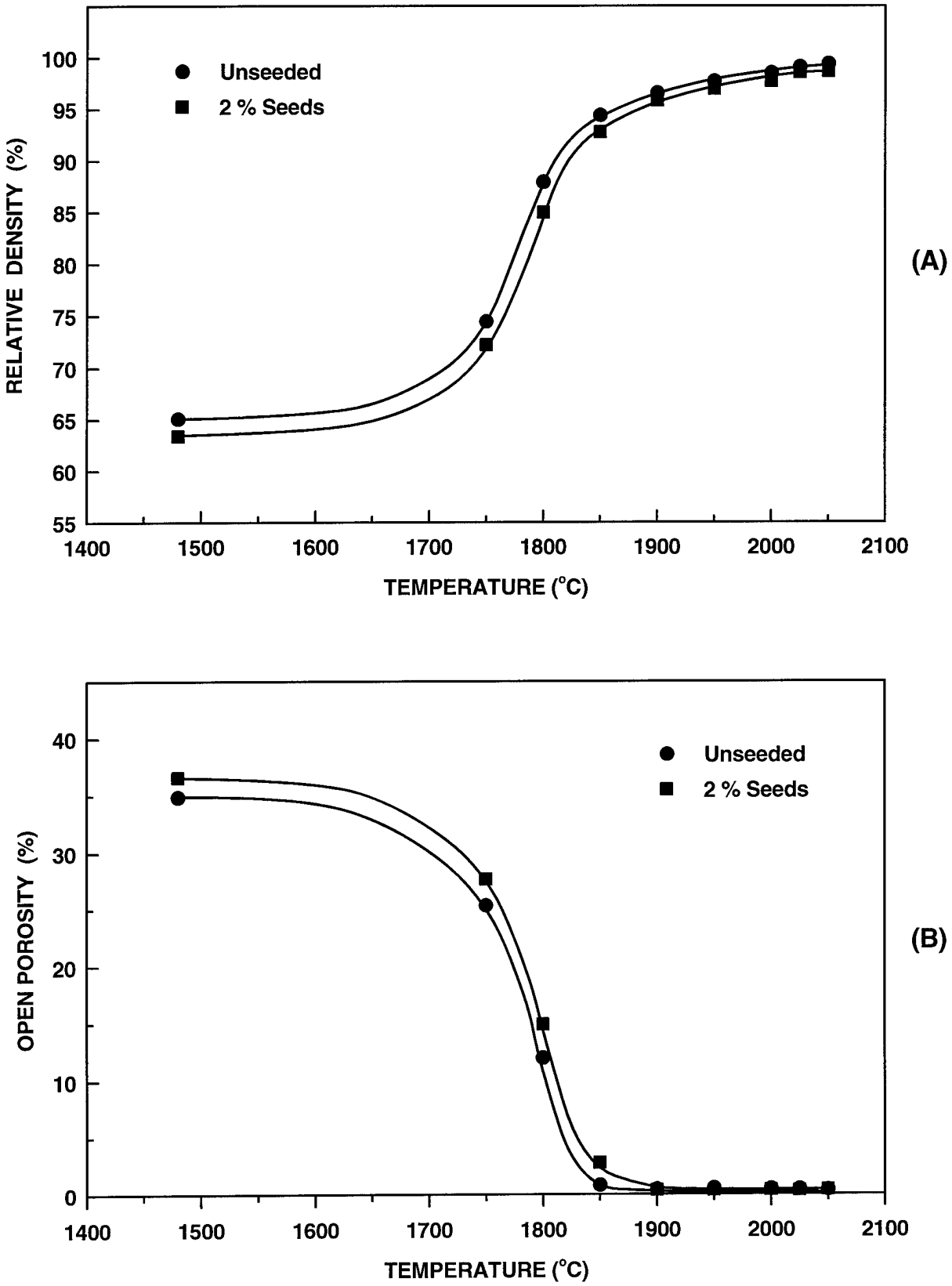

Figure 2. Plots of (A) relative density and (B) open porosity vs. heat treatment temperature for samples with and without 2% SiC platelet seeds.

the microstructure consisted almost entirely of large, oriented, platelike grains (see Fig. 3). The orientation of the platelike grains in the heat-treated samples was determined by the initial orientation of the seed platelets in the green compact. Thus, most of the large, platelike grains were aligned with the major faces parallel to the casting surface, i.e., the same as observed for the seed platelets in pre-sintered compacts (e.g., see Fig. 1 in the first paper attached in the Appendix). The preferred crystallographic orientation of the platelike grains was indicated by X-ray diffraction (XRD) characterization of the compact bottom surfaces which showed sharp increases in intensities for the (00·ℓ) reflections, i.e., the (00·6) and (00·12) closed-packed basal planes for the 6H polytype (Fig. 4). The XRD results and microstructure observations are consistent with development of the large grains by preferential (seeded) growth of the original platelets, i.e., in which the closed-packed basal planes of the original platelets grow by "consuming" fine grains of the surrounding matrix, as schematically illustrated in Fig. 5.

Microstructure evolution was monitored as a function of temperature using quantitative microscopy. Measurements were made from polished sections taken perpendicular to the casting surface. Figure 6 shows the volume percentage of the large, platelike grains in the microstructure as a function of temperature. The samples consist almost entirely of platelike grains after heat treatment at temperatures above ~2300°C. Figures 7 and 8 show the changes in length and thickness of the platelike grains as a function of temperature and platelet concentration, respectively. It is evident that platelet growth occurs primarily by increases in length rather than thickness. Figure 9 shows plots of the average platelet length/thickness ratio as a function of temperature and platelet concentration. Since the measurements were taken from sections taken perpendicular to the casting surface, the increases in length and aspect ratio

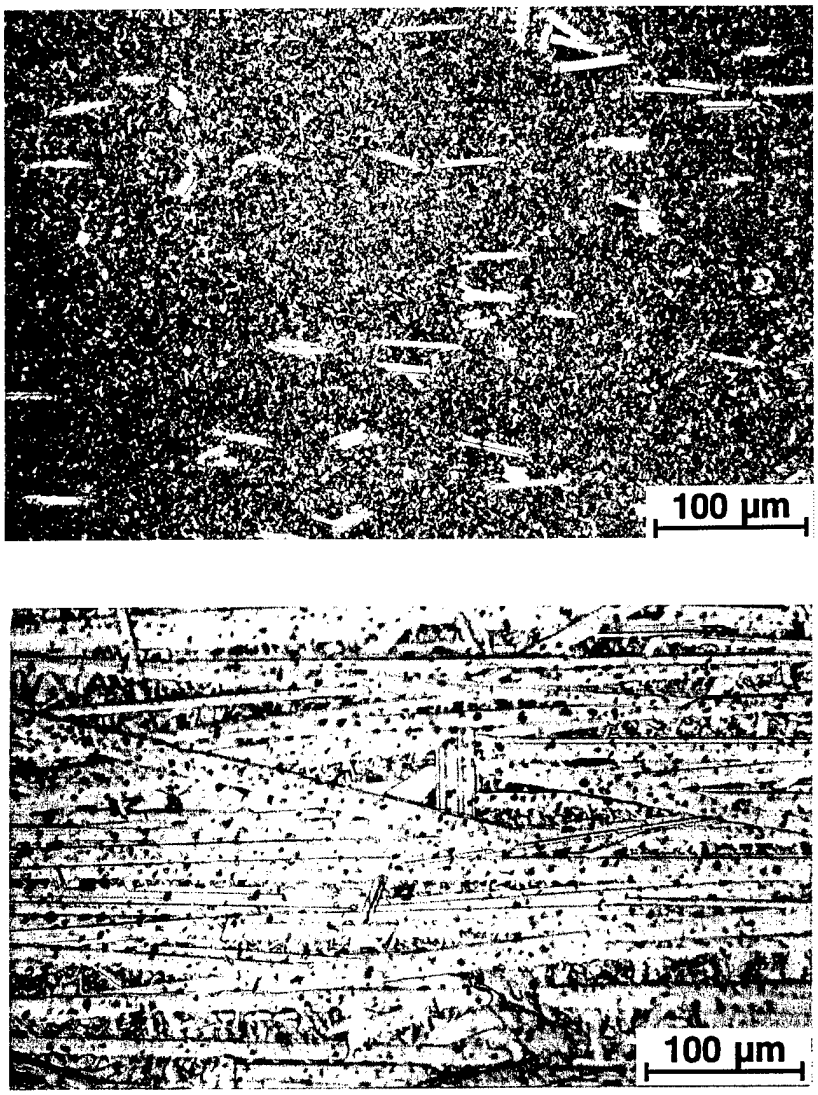

Figure 3. SEM micrographs of polished sections (taken perpendicular to the casting surface) of SiC samples showing the development of large, oriented platelike grains via growth from the oriented platelet seeds.

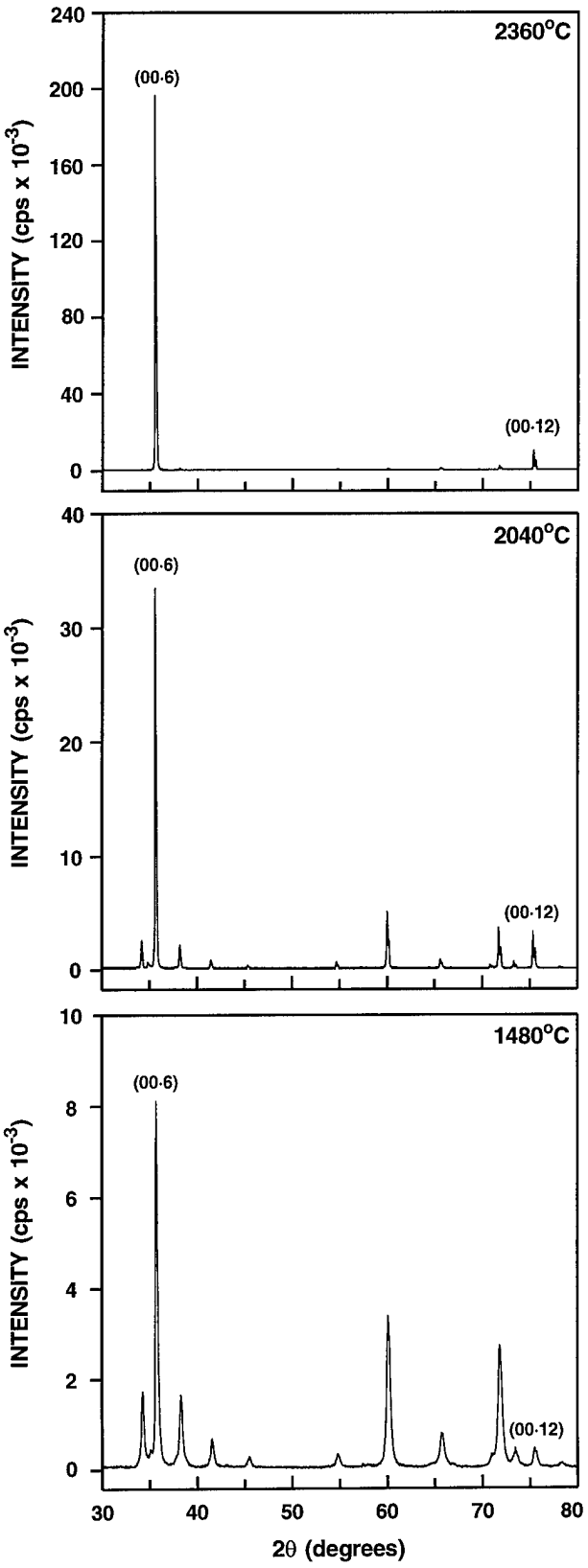

Figure 4. XRD patterns for seeded (2% platelets) SiC samples which were heat treated at the indicated temperatures.

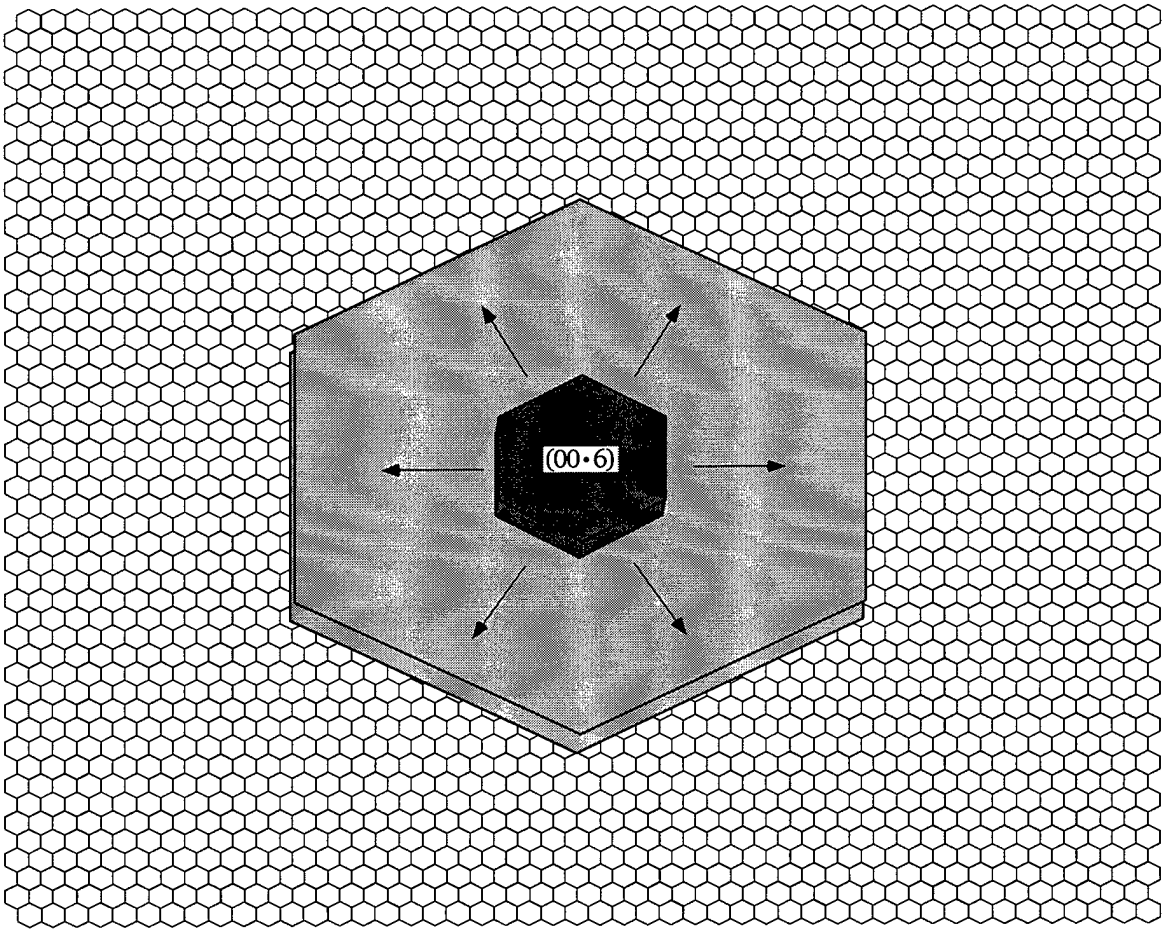

Figure 5. **Schematic illustration of seeded grain growth in which the closed-packed basal planes of the hexagonal SiC platelets are extended by consuming the fine grains of surrounding matrix.**

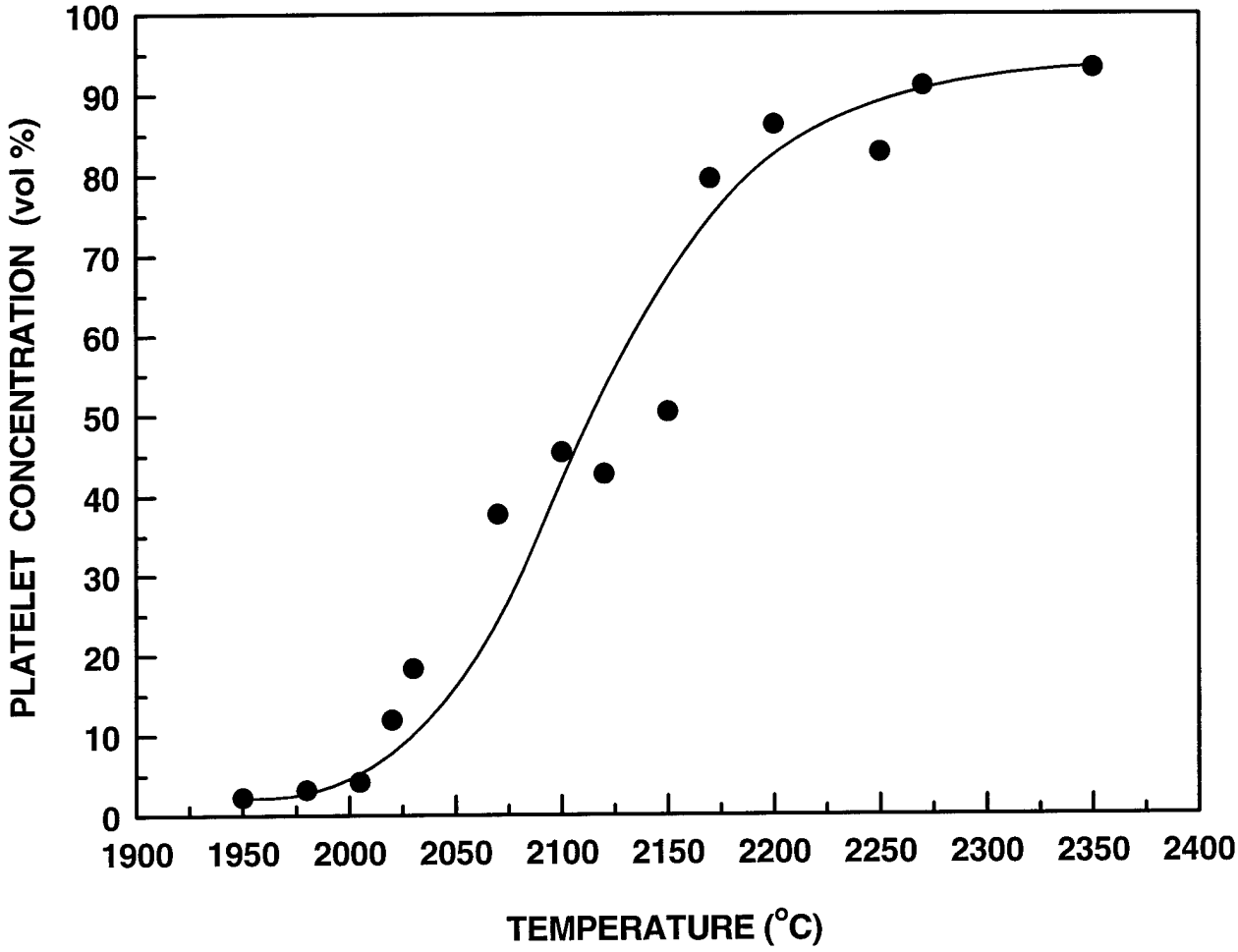

Figure 6. Plot of the volume percentage of platelet grains in the microstructure as a function of the heat treatment temperature for seeded (2% platelets) SiC samples.

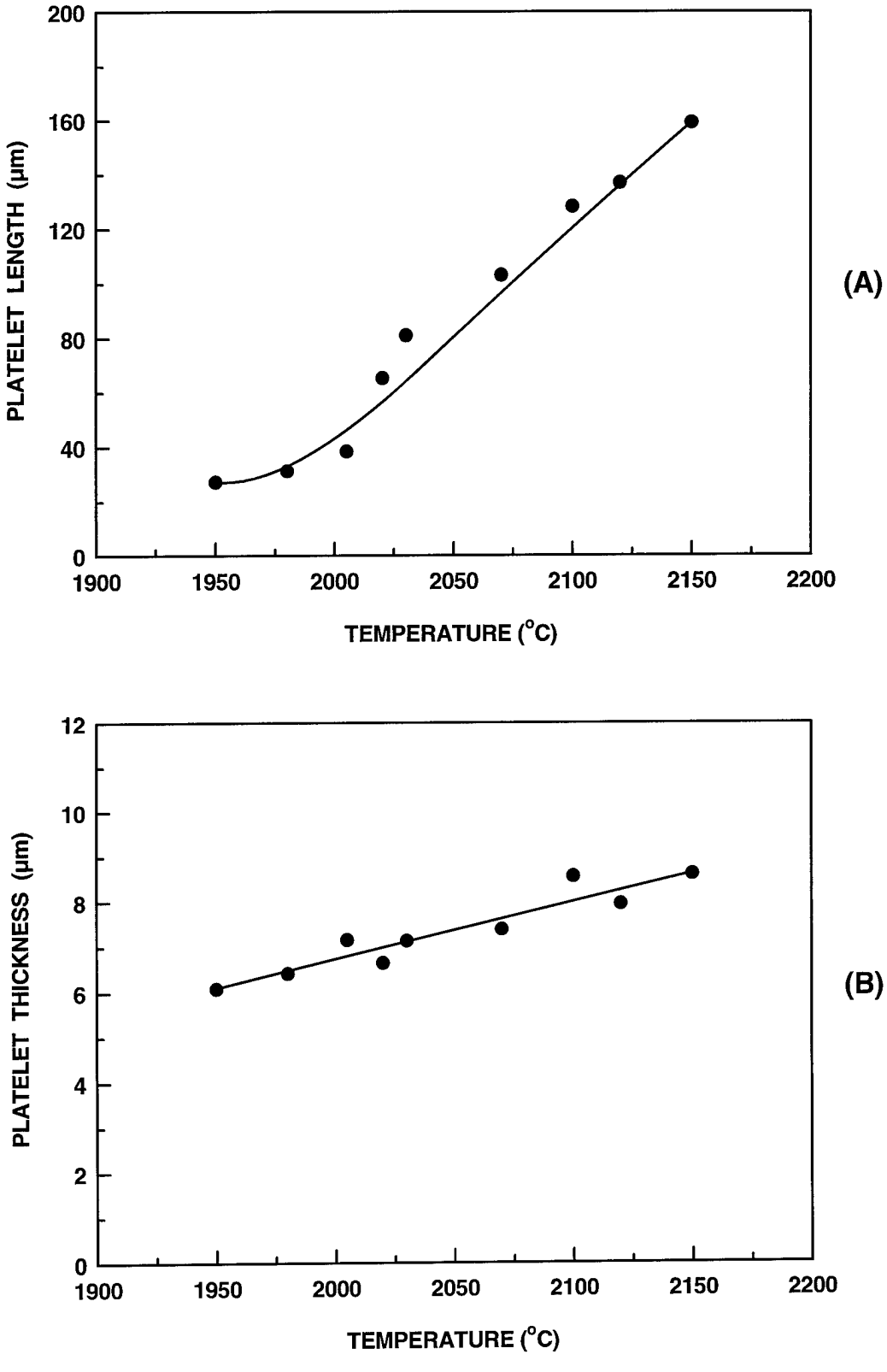

Figure 7. Plots of the (A) length and (B) thickness of the platelet grains as a function of the heat treatment temperature for seeded (2% platelets) SiC samples.

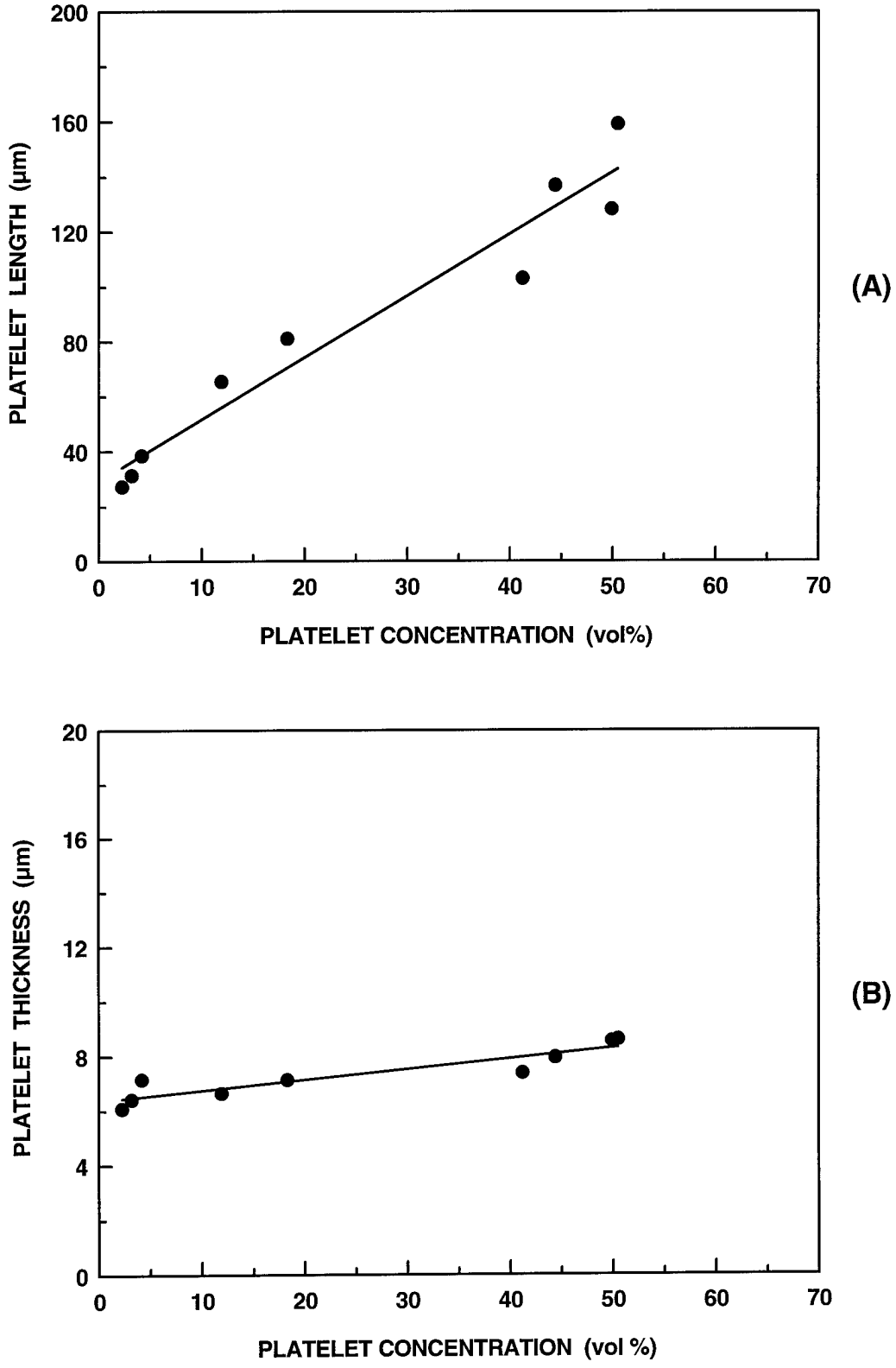

Figure 8. Plots of the (A) length and (B) thickness of the platelet grains as a function of the overall platelet concentration for seeded (2% platelets) SiC samples.

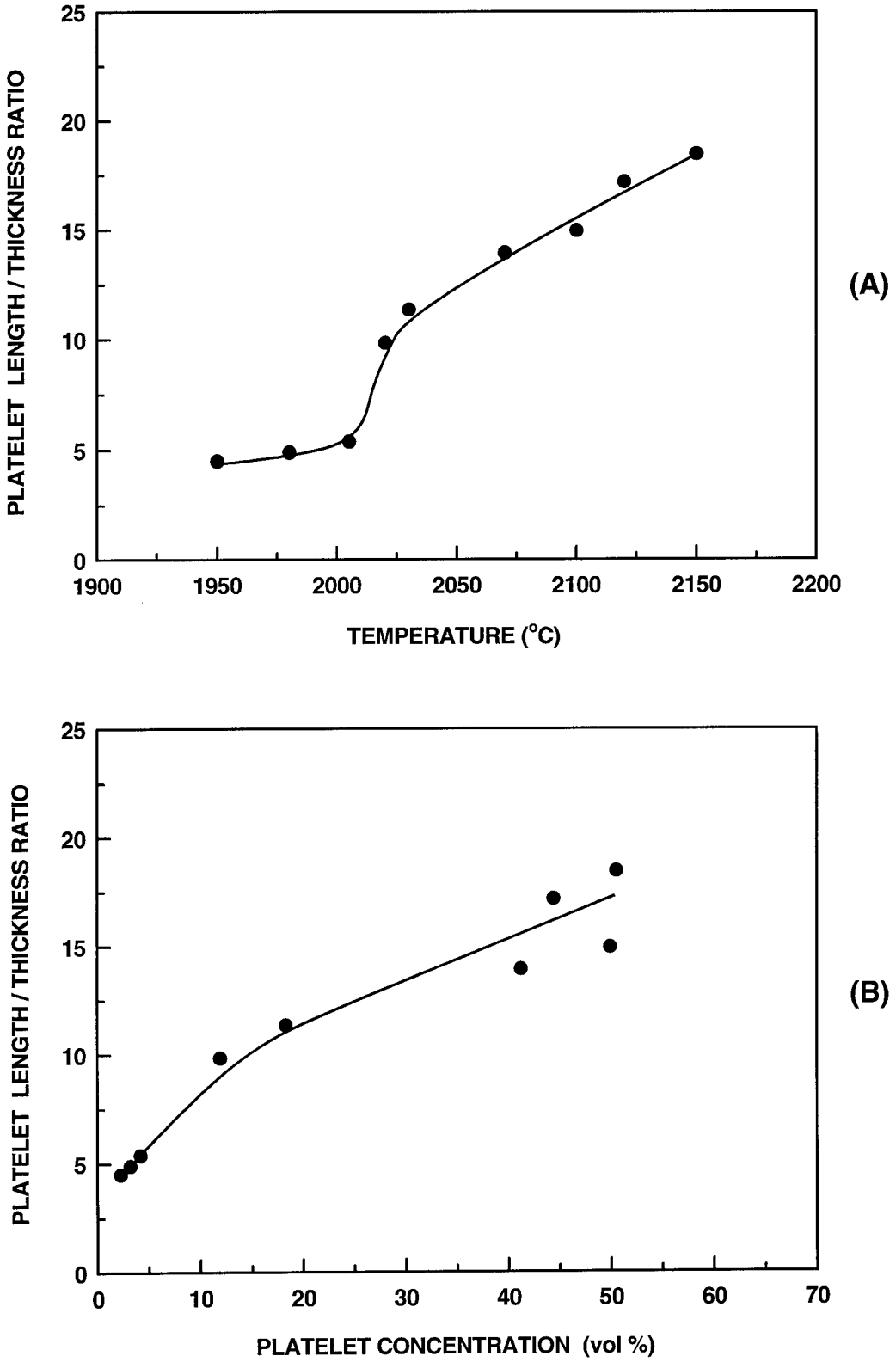

Figure 9. Plots of the length/thickness ratio of the platelet grains as a function of the (A) heat treatment temperature and (B) platelet concentration for seeded (2% platelets) SiC samples.

are actually representative of the two-dimensional growth of the major faces of the platelike grains. Based on the XRD results discussed above, it is evident that growth occurred preferentially in the close-packed hexagonal basal planes of the platelets.

The effect of heat treatment temperature on the orientation of the platelike grains was also monitored by quantitative microscopy. The grain orientation was determined from the angle formed by the intersection of a line drawn parallel to the grain length with a line drawn parallel to the casting surface. Thus, grains with the lengths parallel and perpendicular to the casting surface would have orientation angles of 0° and 90°, respectively. Figures 10 and 11 show the average and median orientation angles as a function of heat treatment temperature and platelet concentration, respectively. Data are shown for both slip cast and tape cast samples. Several observations are noted: (i) The median and average angle values for all the slip cast samples are in the range of 14° $\pm$ 4° and 23° $\pm$ 5°, respectively. Thus, there is substantial preferred orientation of the platelike grains parallel to the casting surface since random orientation would give an angle of 45°. The average orientation angles are higher than the median angles because of small amounts of platelets with high orientation angles. Figure 12 shows a plot of the orientation angle distribution for a sample heat treated at 1950°C. (ii) Tape cast samples have lower orientation angles than slip cast samples. This is not surprising since the shear forces in tape casting result in better alignment of the platelets parallel to the casting surface. (iii) The orientation angles do not change substantially with increasing heat treatment temperature (and increasing platelet concentration). This is consistent with the view that the growth of the platelike grains proceeds primarily from the initial seed platelets. It is evident, however, that there is a trend of slightly increasing orientation angles as platelet growth occurs. This appears

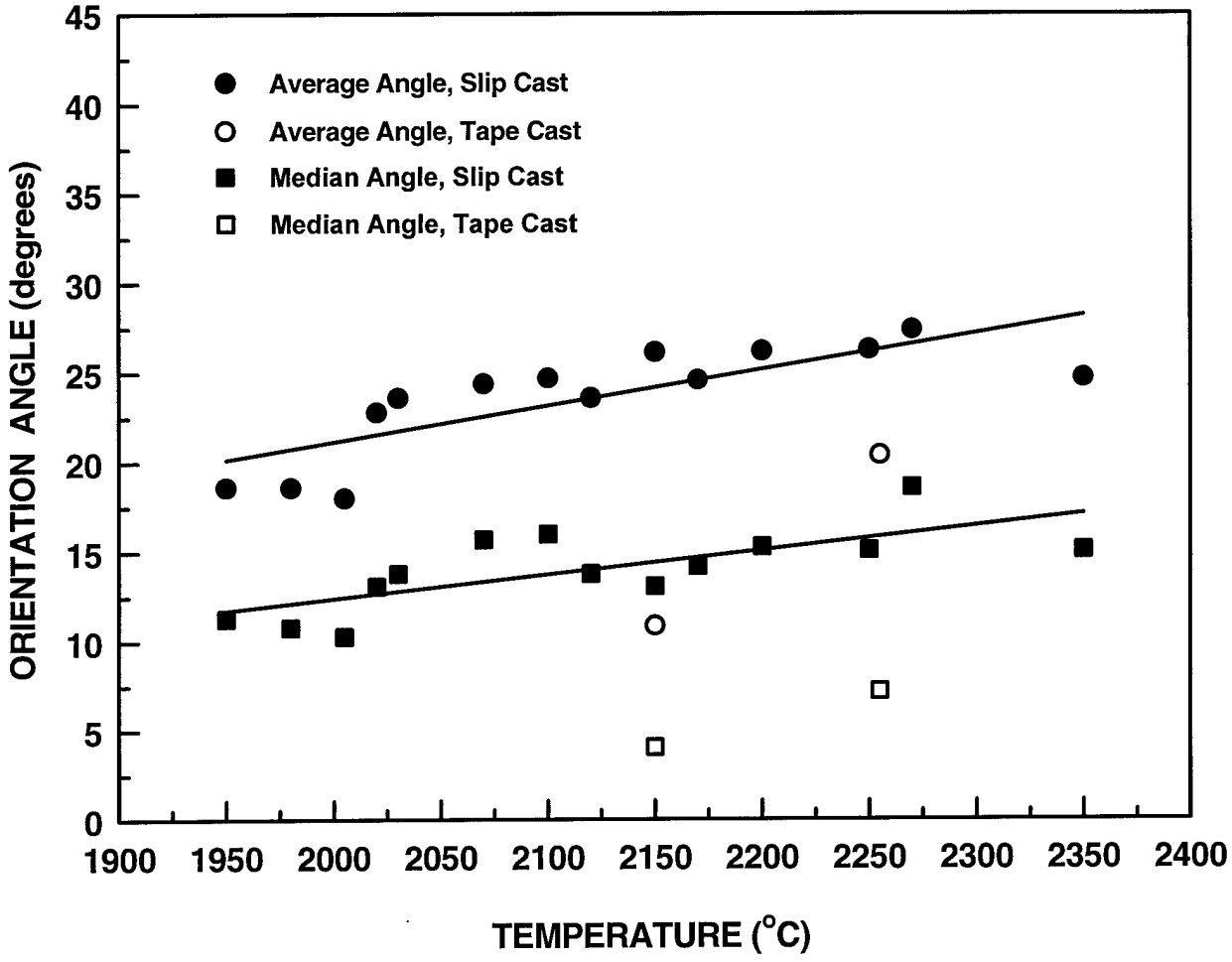

Figure 10. Plots of the median and average orientation angles for the platelet grains as a function of the heat treatment temperature for slip cast and tape cast for seeded (2% platelets) SiC samples.

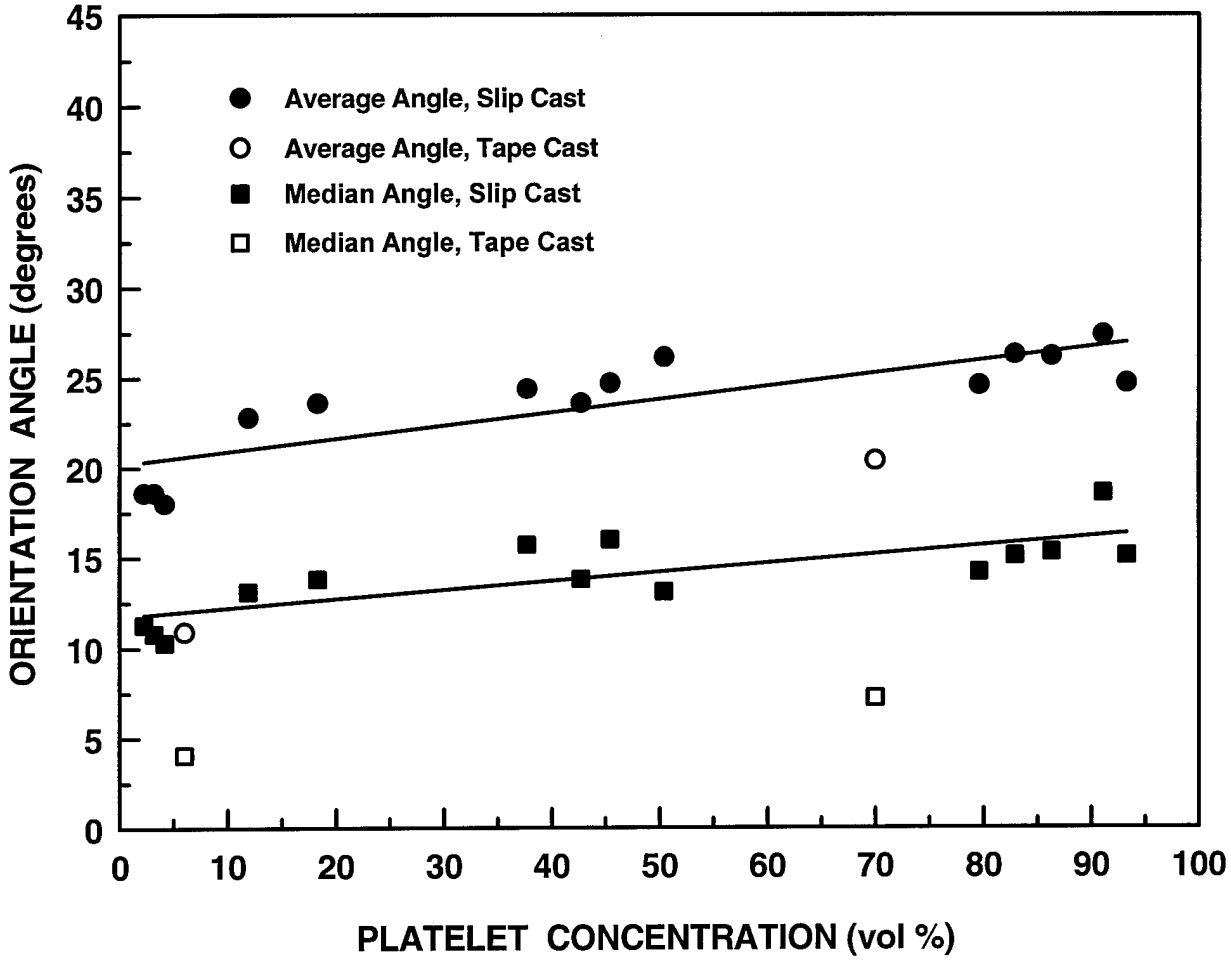

Figure 11. Plots of the median and average orientation angles for the platelet grains as a function of the platelet concentration for slip cast and tape cast for seeded (2% platelets) SiC samples.

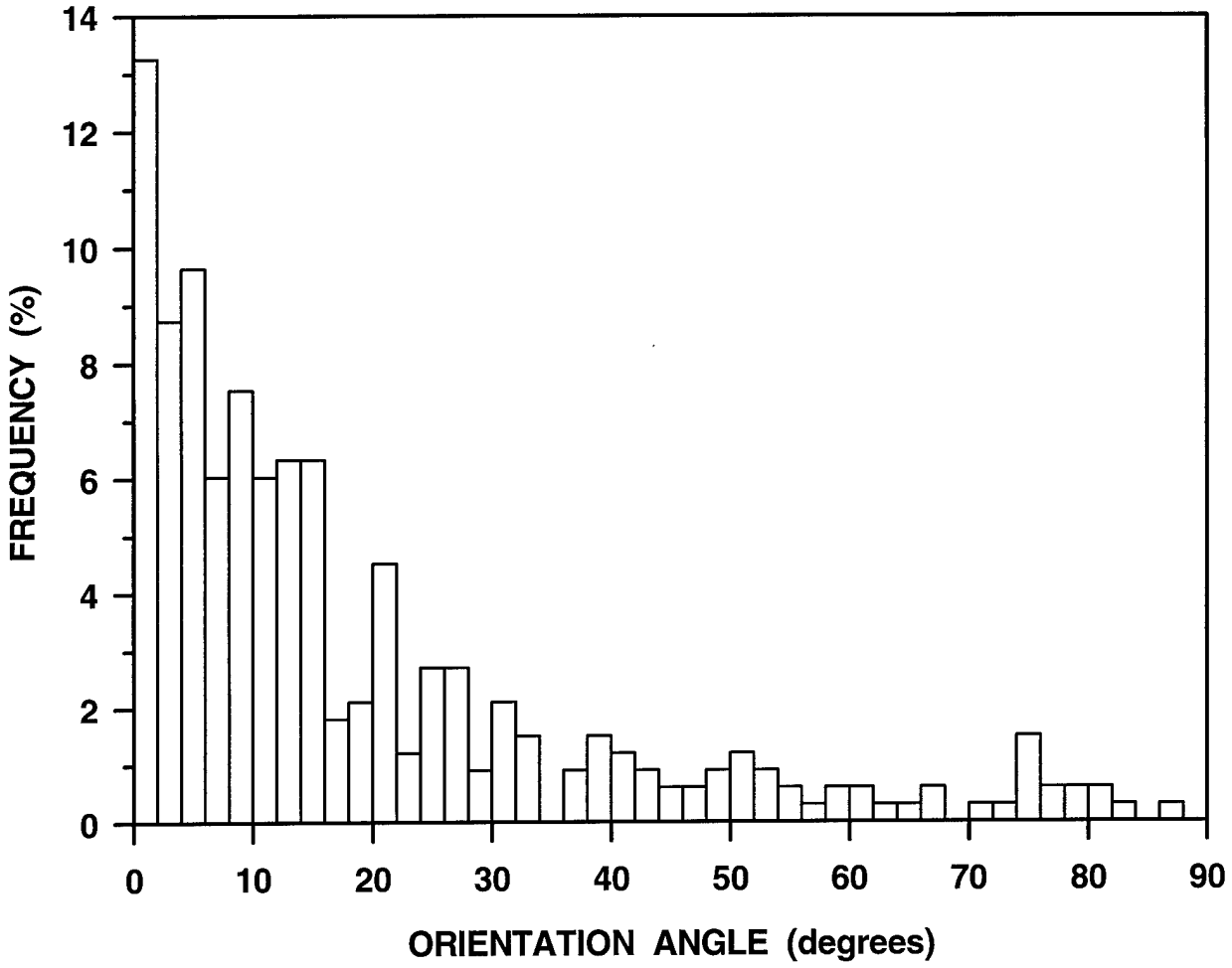

Figure 12. Frequency histogram plot of the orientation angle distribution for the platelet grains in a slip cast seeded (2% platelets) SiC sample.

to be associated with growth arising from a small amount of the SiC seeds with a somewhat equiaxed, particulate morphology, i.e., compared to the typical anisotropic, platelike morphology. Such particles are not expected to develop a preferred orientation during the casting operation. Nevertheless, these seeds would still be expected to show preferred growth along the closed-packed basal planes and, hence, anisotropic, platelike grains should still develop from them. However, the platelike grains would grow with nearly random orientation because of the lack of preferred orientation in the green state. This would account for the observation of occasional large platelike grains with high orientation angles in heat treated samples with only moderate overall platelike grain concentration. Figure 13 shows such an example in which a large platelike grain developed with an approximately 90° orientation to the casting surface. The development of such grains would account for the increase in the average orientation angle as the platelet concentration increases.

Preferred orientation of grains was also observed in the "matrix regions" between the large, platelike grains. The sample matrix is originally comprised of fine, equiaxed α-SiC particles. After densification (but prior to significant growth of the large, platelike grains), the SiC grains in the matrix initially retain a mostly equiaxed morphology. Figure 14 shows micrographs of a sample with ~98% relative density which was sintered at 2050°C. Figs. 14A and 14B show the fine, mostly equiaxed grains, while Fig. 14C shows that the platelet concentration is still relatively low (~5%) in this sample. With further heat treatment, the matrix grains grow with both an anisotropic morphology and a preferred orientation. The preferred orientation was demonstrated from lineal intercept measurements in which grain intercept sizes were determined both parallel and perpendicular to the casting surface. Figure

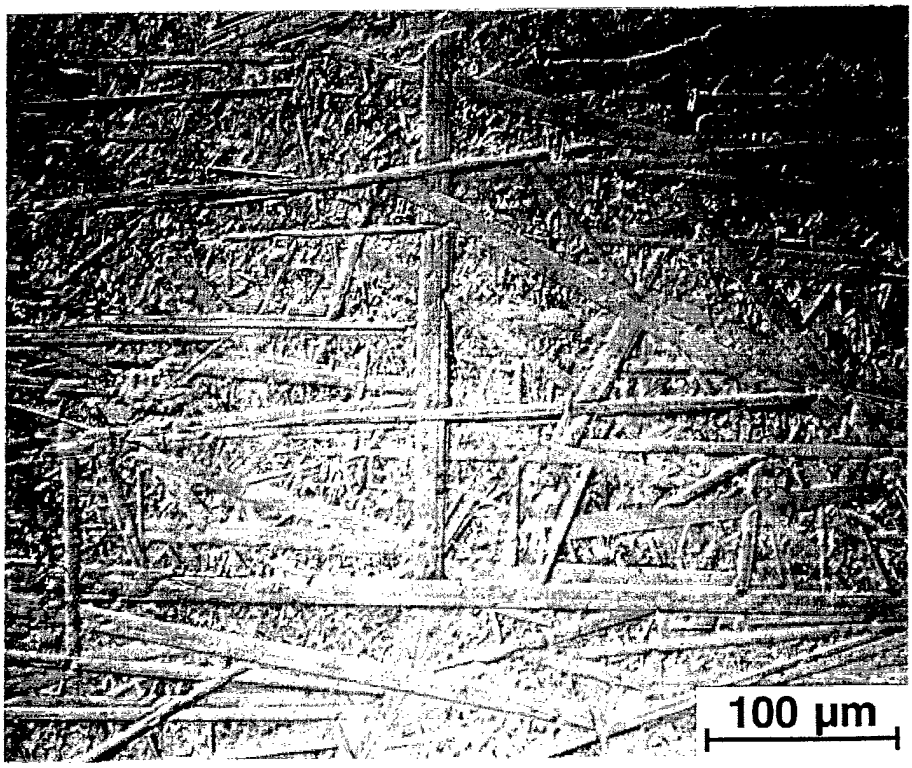

Figure 13. **Optical micrograph of a polished section (taken perpendicular to the casting surface) in a seeded (2% platelets) SiC sample showing the development of a large platelike grain approximately perpendicular to the casting surface.**

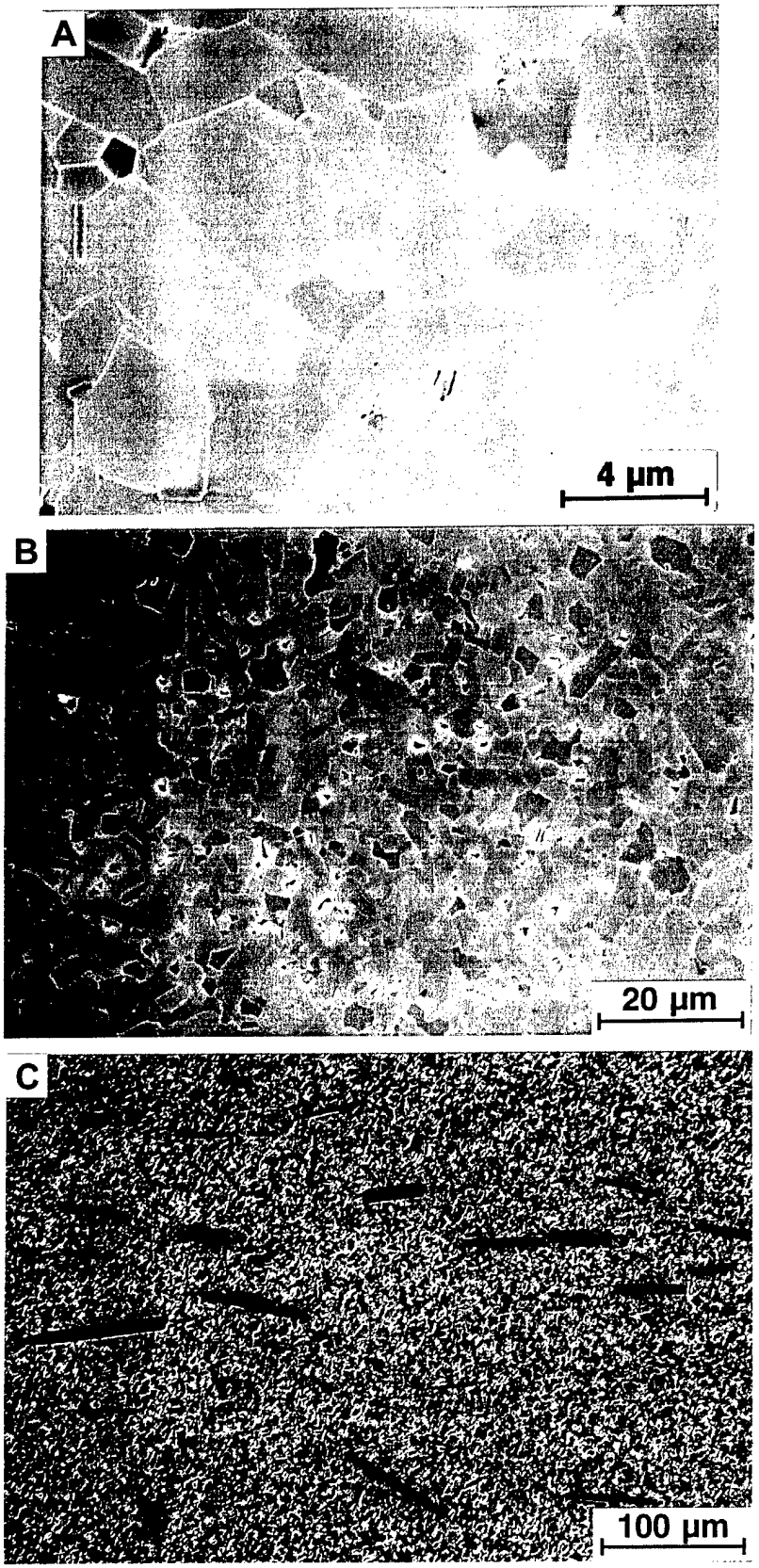

Figure 14. (A) and (B) SEM micrographs of a polished section (taken perpendicular to the casting surface) in a seeded (2% platelets) SiC sample showing the matrix grain structure after heat treatment at 2050°C. (C) Lower magnification optical micrograph showing the oriented platelet grains.

15 shows the matrix grain intercept sizes as a function of heat treatment temperature and platelet concentration. The grain size increases with increasing heat treatment temperature (as expected), but larger increases are measured in the direction perpendicular to the casting surface. Figure 16 shows SEM micrographs of a region in which the matrix grains have grown with a significant preferred orientation. These matrix grains, which have grown with platelike morphology, develop this extreme orientation when they grow between the much larger platelike grains that have developed from the original seeds (and which are oriented parallel to the casting direction). This suggests that the large seed-derived grains increase in thickness (i.e., undergo growth perpendicular to the casting direction) by preferentially consuming matrix grains which have similar initial orientation (i.e., matrix grains which have formed low angle boundaries with the large seed-derived grains). As a consequence, grain growth within the matrix regions would then be dominated by the "unconsumed" matrix grains which have high orientation angles relative to large seed-derived grains. The importance of the large seed-derived grains in this process can be illustrated by directly comparing the microstructure development in samples processed with and without 2% seed platelets. Figure 17A shows the average grain intercept ratio (i.e., ratio of the intercept sizes measured perpendicular and parallel to the casting direction) as a function of the heat treatment temperature for both seeded and unseeded samples. (Figure 17B shows the grain intercept ratio as a function of the platelet concentration.) The matrix grains in the unseeded sample maintain an intercept ratio of approximately 1, indicating that growth of the matrix grains did not occur with preferred orientation.

An investigation of the platelet growth kinetics has been initiated. The preliminary results in Fig. 18 show plots of the platelet amount and platelet length vs. heat treatment time

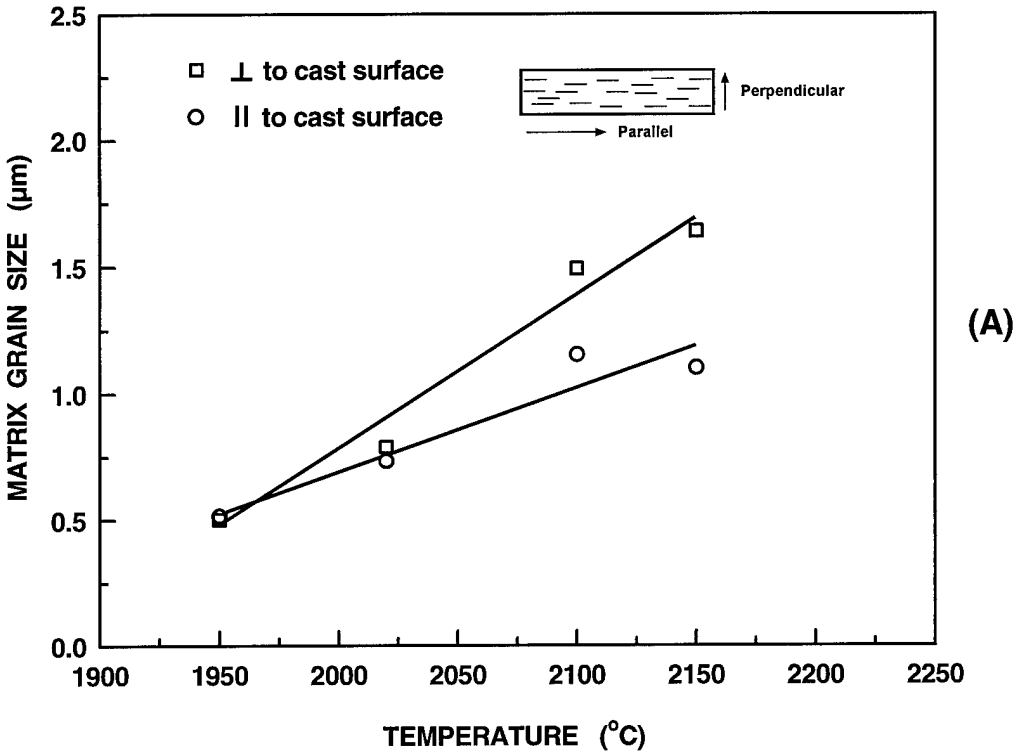

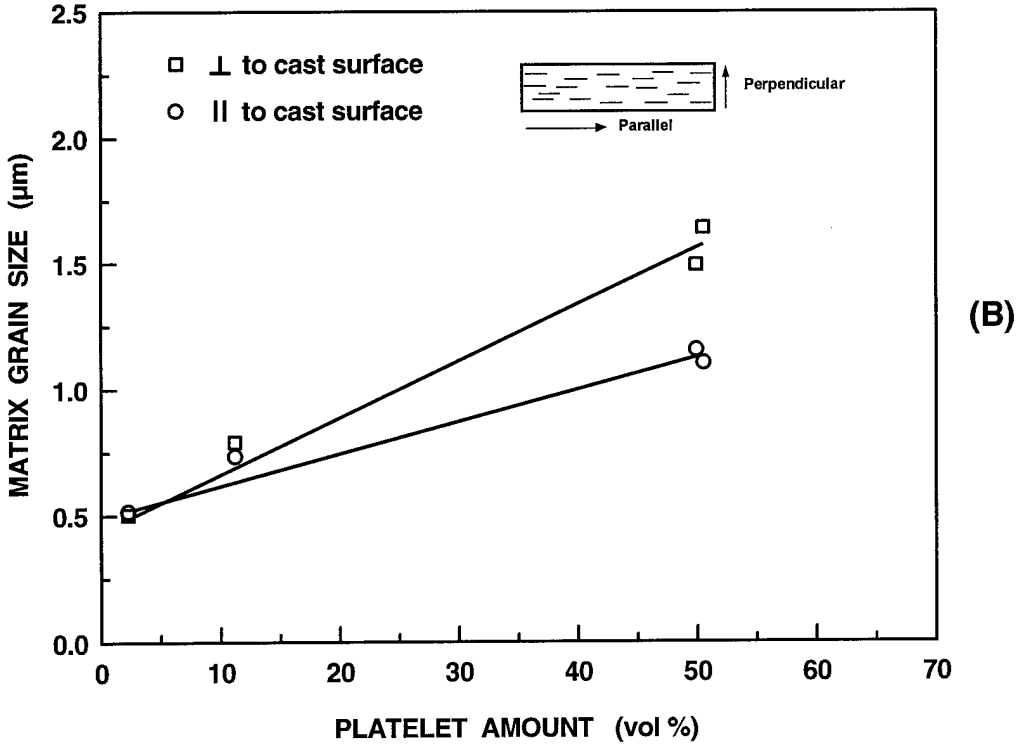

Figure 15. Plots of the matrix grain intercept sizes measured both perpendicular and parallel to the casting surface as a function of the (A) heat treatment temperature and (B) platelet concentration.

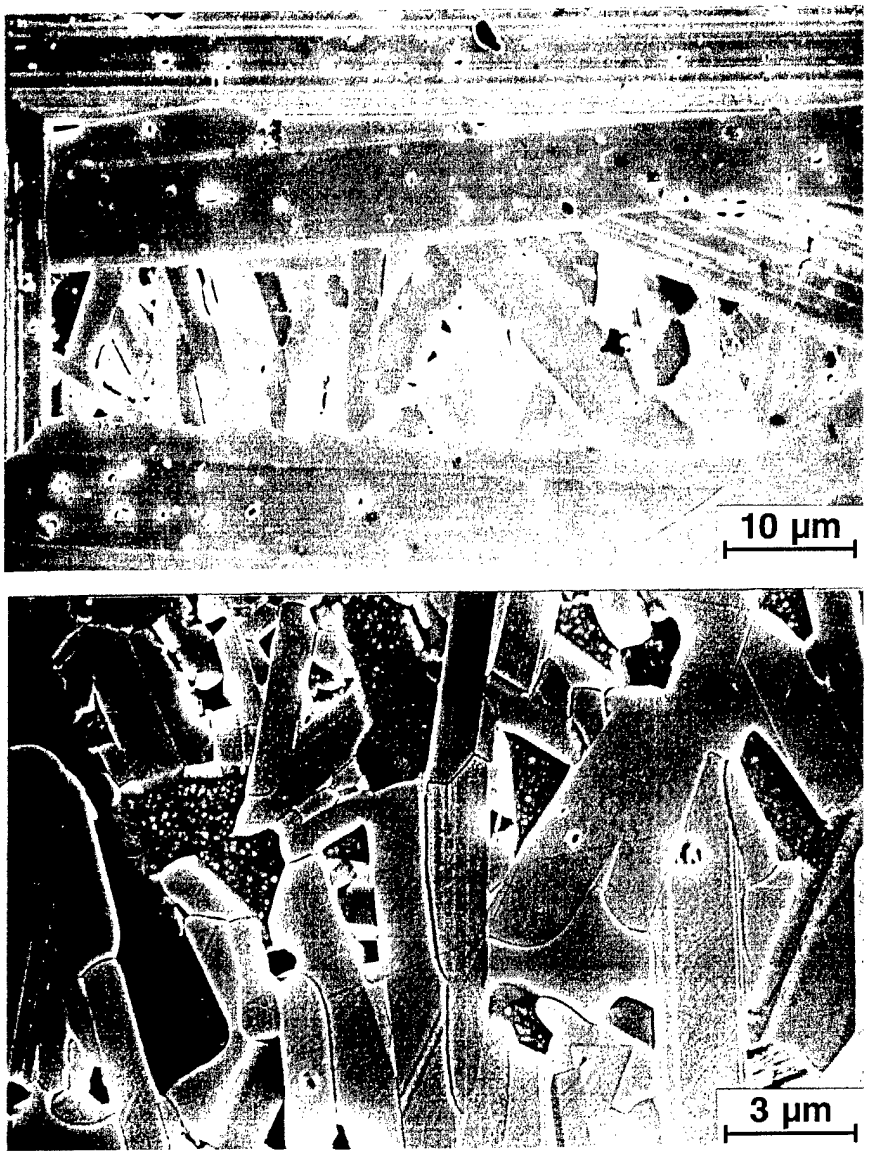

Figure 16. **SEM micrographs of a polished section (taken perpendicular to the casting surface) in a seeded (2% platelets) SiC sample showing a region in which the matrix grains have grown with significant preferred orientation.**

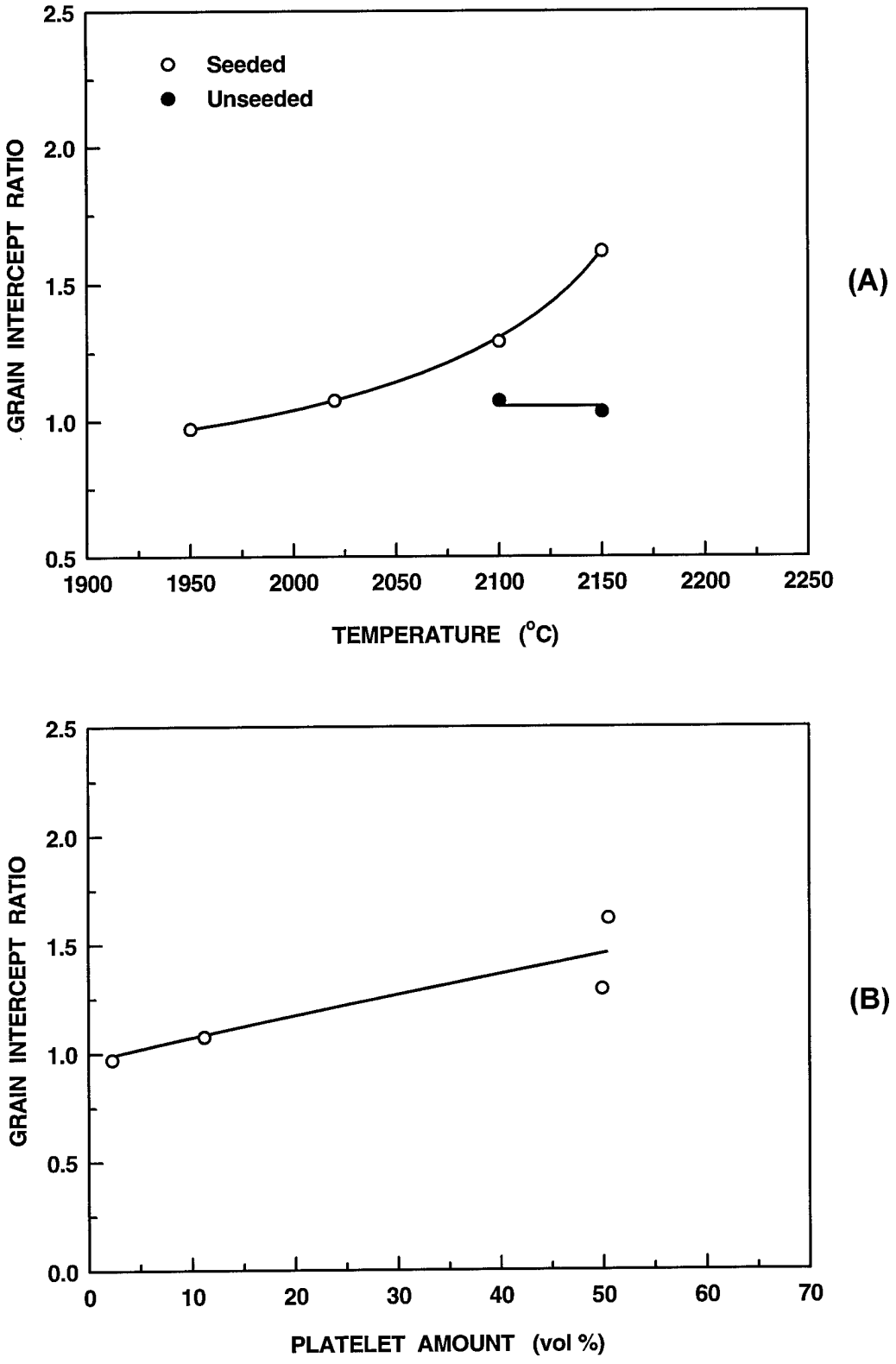

Figure 17. (A) Plot of the matrix grain intercept ratio as a function of the heat treatment temperature for both seeded (2% platelets) and unseeded SiC samples. (B) Plot of the matrix grain intercept ratio as a function of the platelet concentration for the seeded (2% platelets) SiC samples.

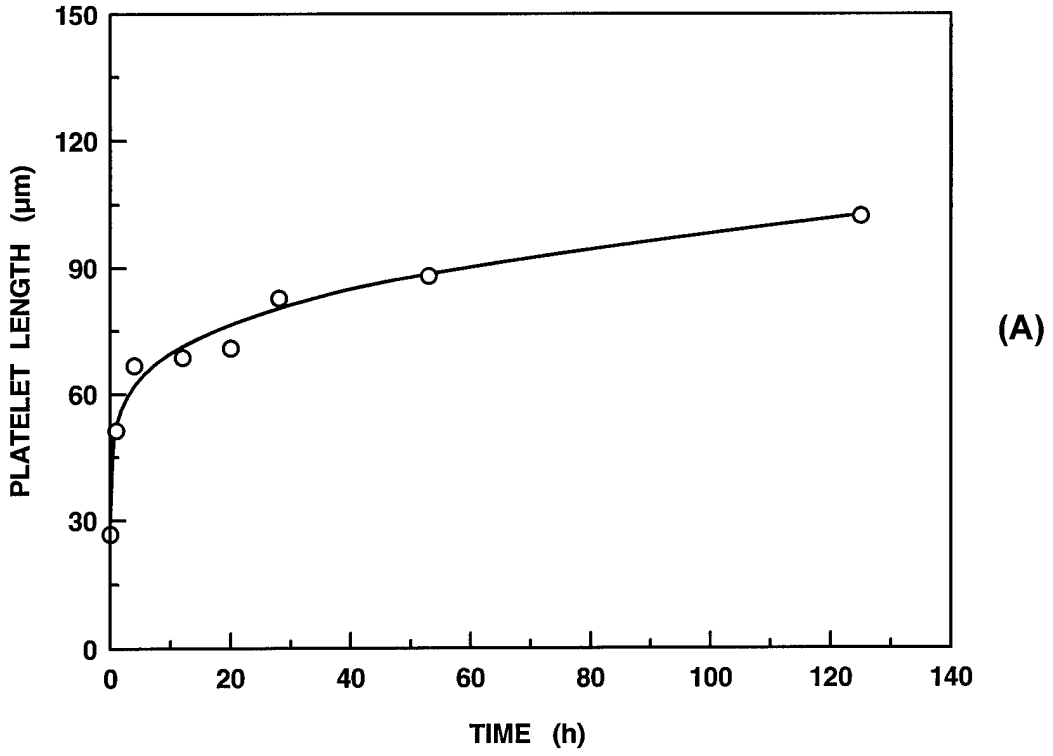

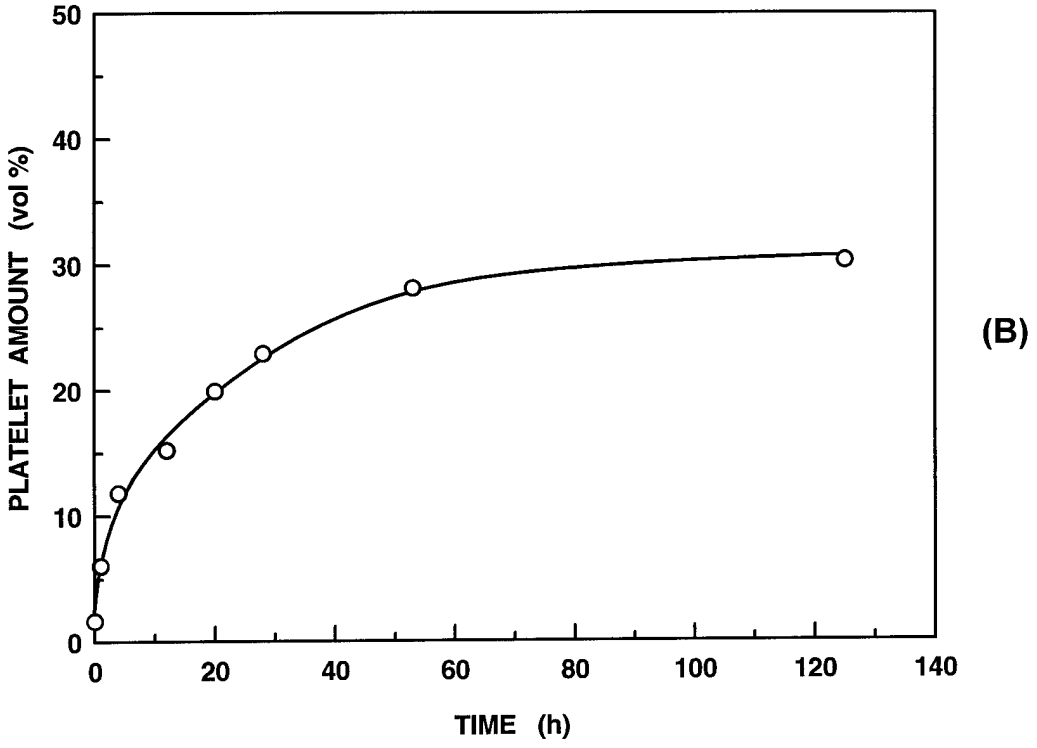

Figure 18. Plots of the (A) platelet length and (B) platelet concentration as a function of the heat treatment time at 1950°C for seeded (2% platelet) SiC samples.

at 1950°C. The rapid decrease in growth rate at longer times (i.e., more rapid than a $G \sim t^{1/2}$ law) may reflect the initial impingement of the growing platelike grains (see Fig. 19), although more data is required before a definitive conclusion can be drawn.

The platelet growth kinetics is dependent upon the matrix grain size. The driving force for growth of the platelet seeds increases with decreasing matrix size. Figure 20 shows the platelet concentration as a function of heat treatment temperature for samples prepared from SiC matrix powders with average particle sizes of 0.2 μm and 0.45 μm. The initial concentration of seed platelets was 2%. It is evident that platelet growth was significantly enhanced at lower temperatures by using the finer matrix particle size. Figures 21A and 21B show optical micrographs of seeded SiC samples which were prepared from the 0.2 μm and 0.45 μm powders, respectively, and were heat treated at 2050°C.

Platelet growth can also be controlled by modifying the initial seed concentration. Figure 22 shows that higher platelet concentrations can be achieved for a given heat treatment temperature by using higher seed concentrations. It is noted, however, that the platelet length increases more rapidly with increasing heat treatment temperature as the seed particle concentration decreases (Fig. 23). This is attributed to less rapid impingement of the growing seed grains. (The average distance separating the seed particles is initially larger in green bodies with smaller seed concentration. Hence, seed platelets can grow to longer lengths before impinging upon other grains.) Figure 24 shows plots of the platelet length/thickness ratios vs. the overall platelet concentration for samples with different seed concentrations. The length/thickness ratio increases with increasing platelet concentration in all the samples. (This was also shown for the sample in Fig. 9B. As noted earlier, this behavior occurs due to the

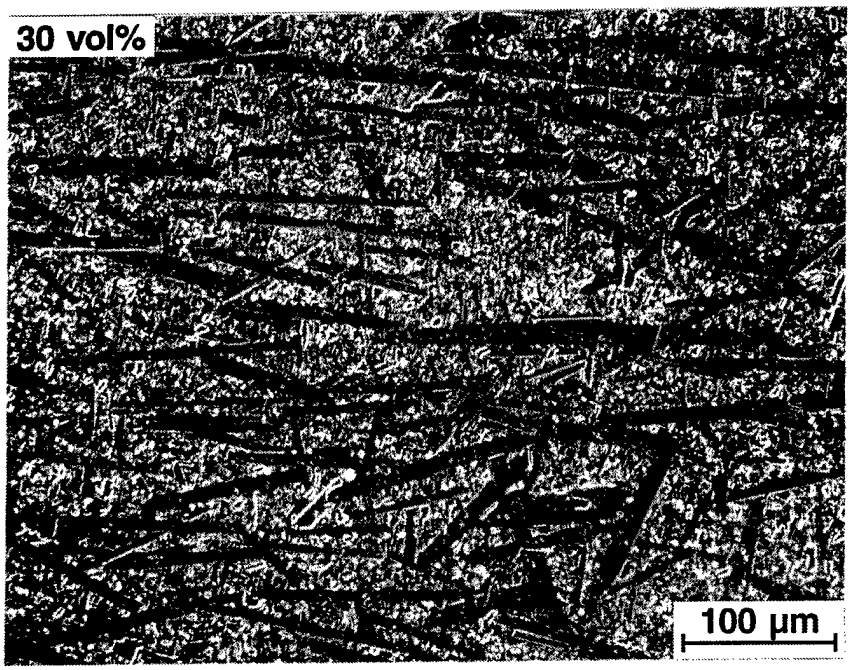

Figure 19. Optical micrograph of a polished section (taken perpendicular to the casting surface) in a seeded (2% platelets) SiC sample which has ~30 vol% platelike grains after heat treatment at ~1950°C for 125 h.

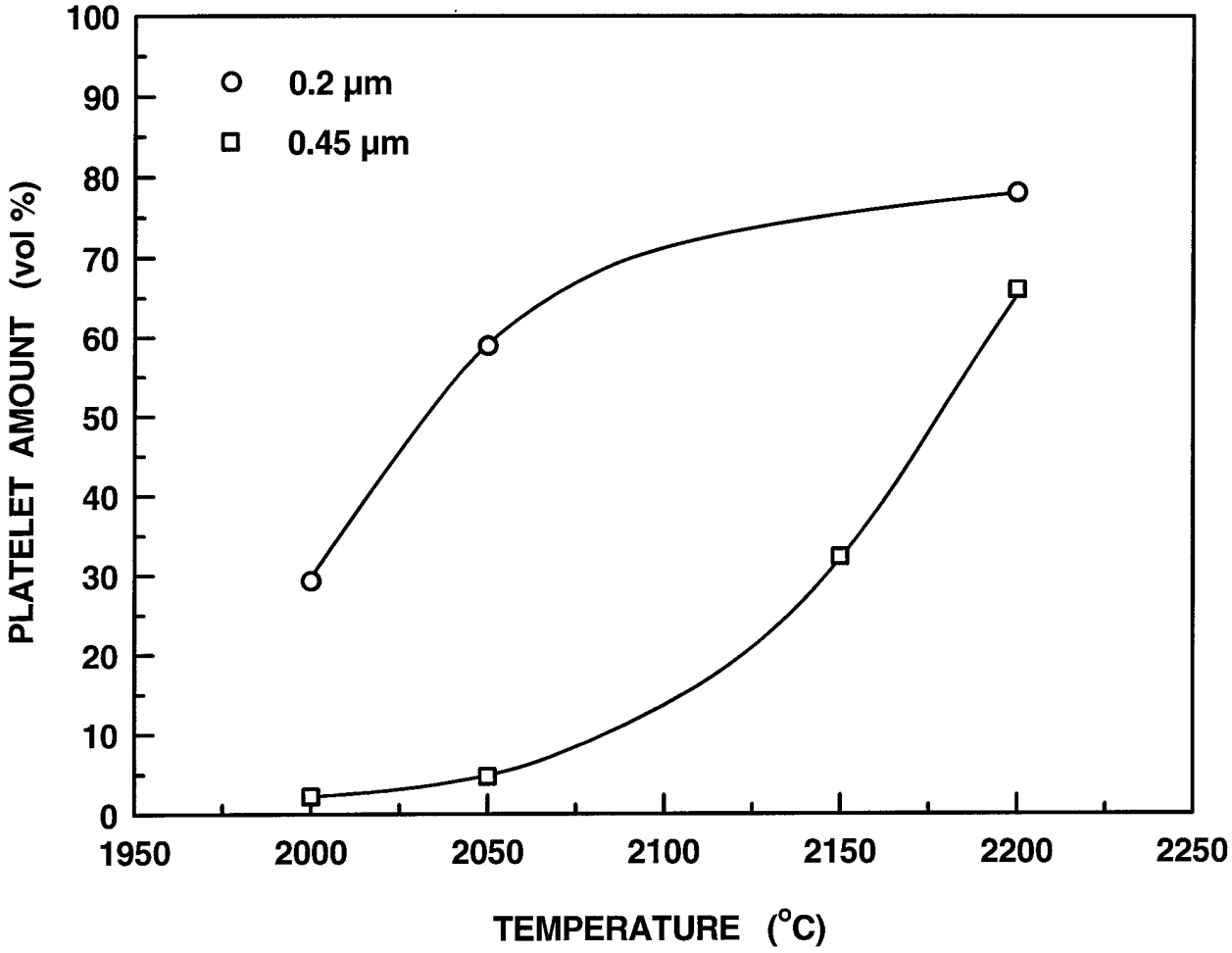

Figure 20. Plots of the platelet concentration vs. heat treatment temperature for seeded (2% platelets) SiC samples prepared with matrix powders with different average particle sizes (0.2 and 0.45 μm).

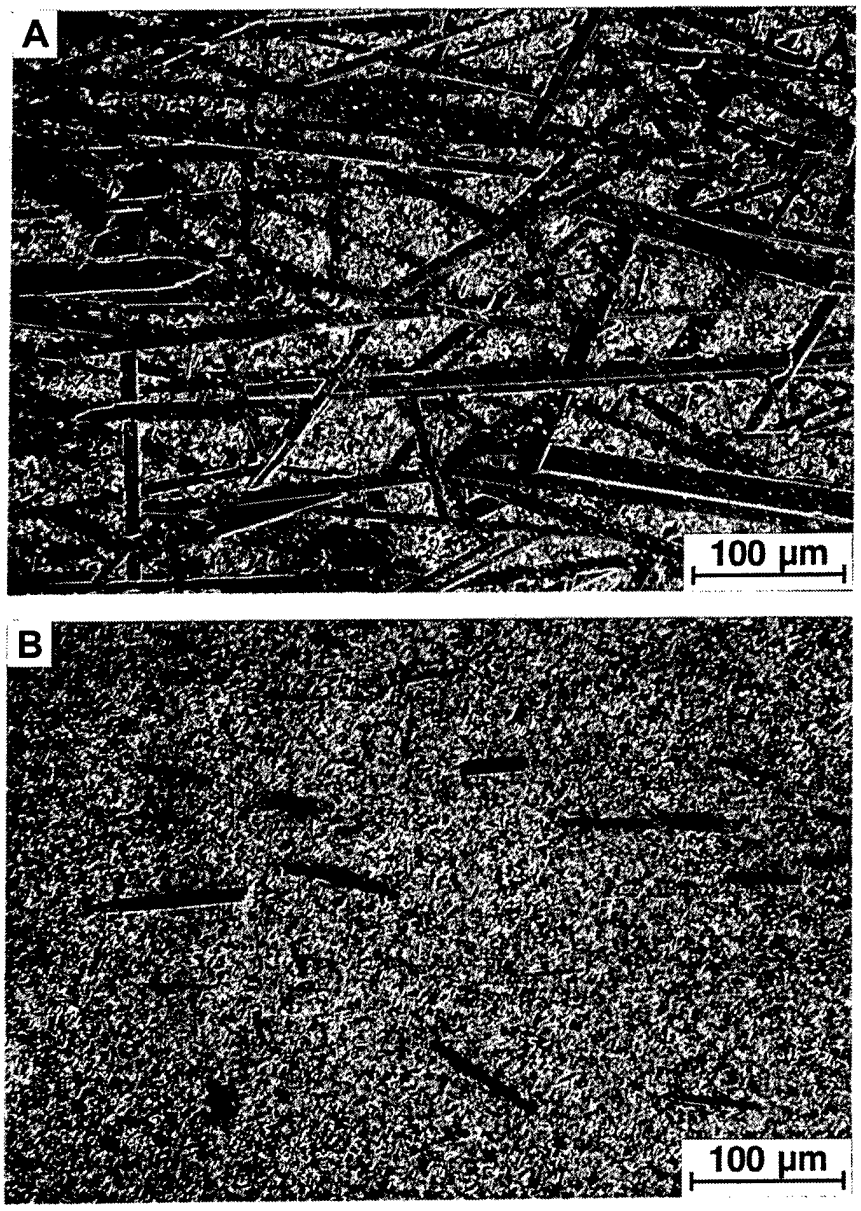

Figure 21. Optical micrographs of polished sections (taken perpendicular to the casting surface) in seeded (2% platelets) SiC samples prepared with matrix powders with (A) 0.2 mm and (B) 0.45 mm average particle sizes.

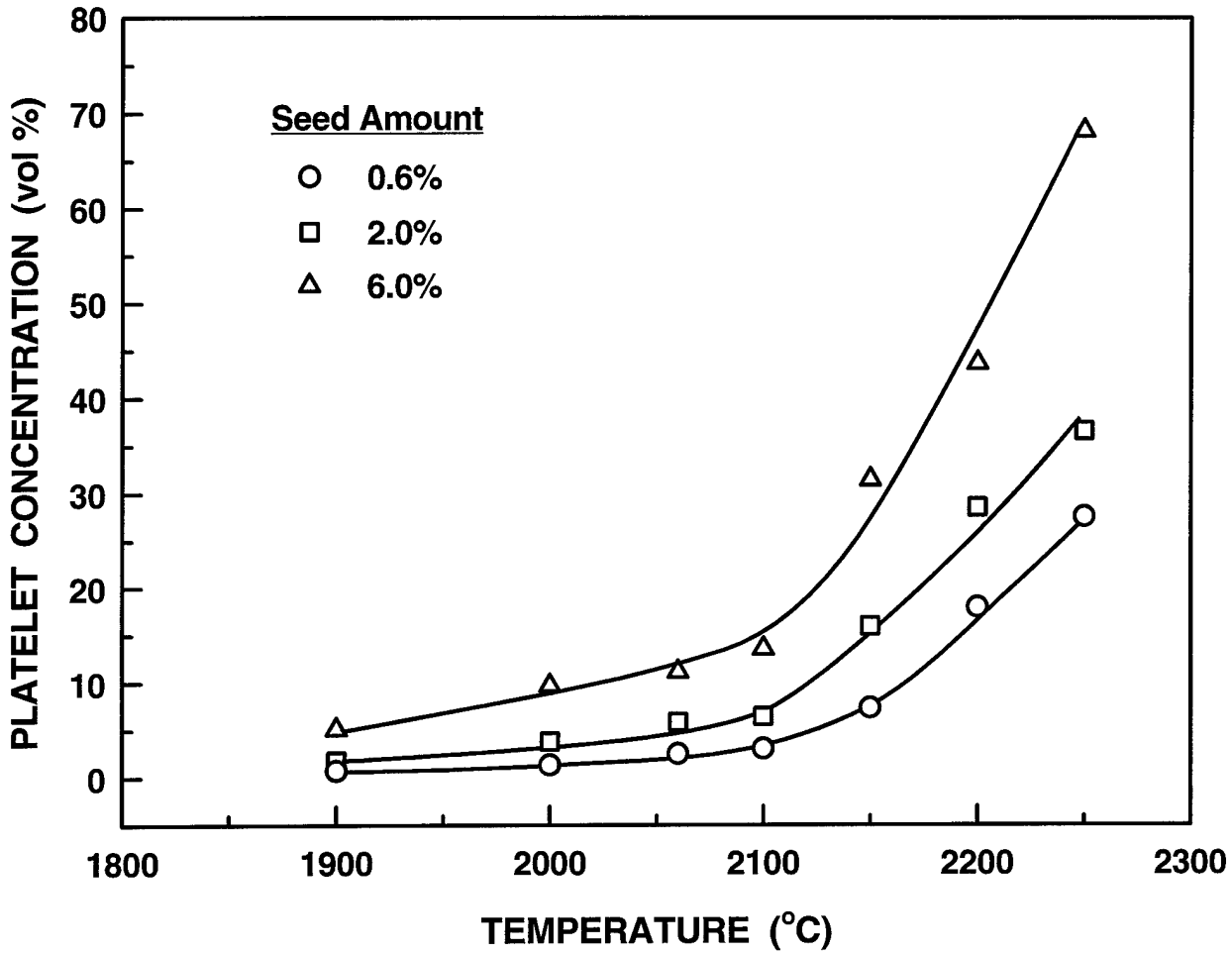

Figure 22. Plots of the platelet concentration vs. heat treatment temperature for SiC samples prepared with varying amount of seeds.

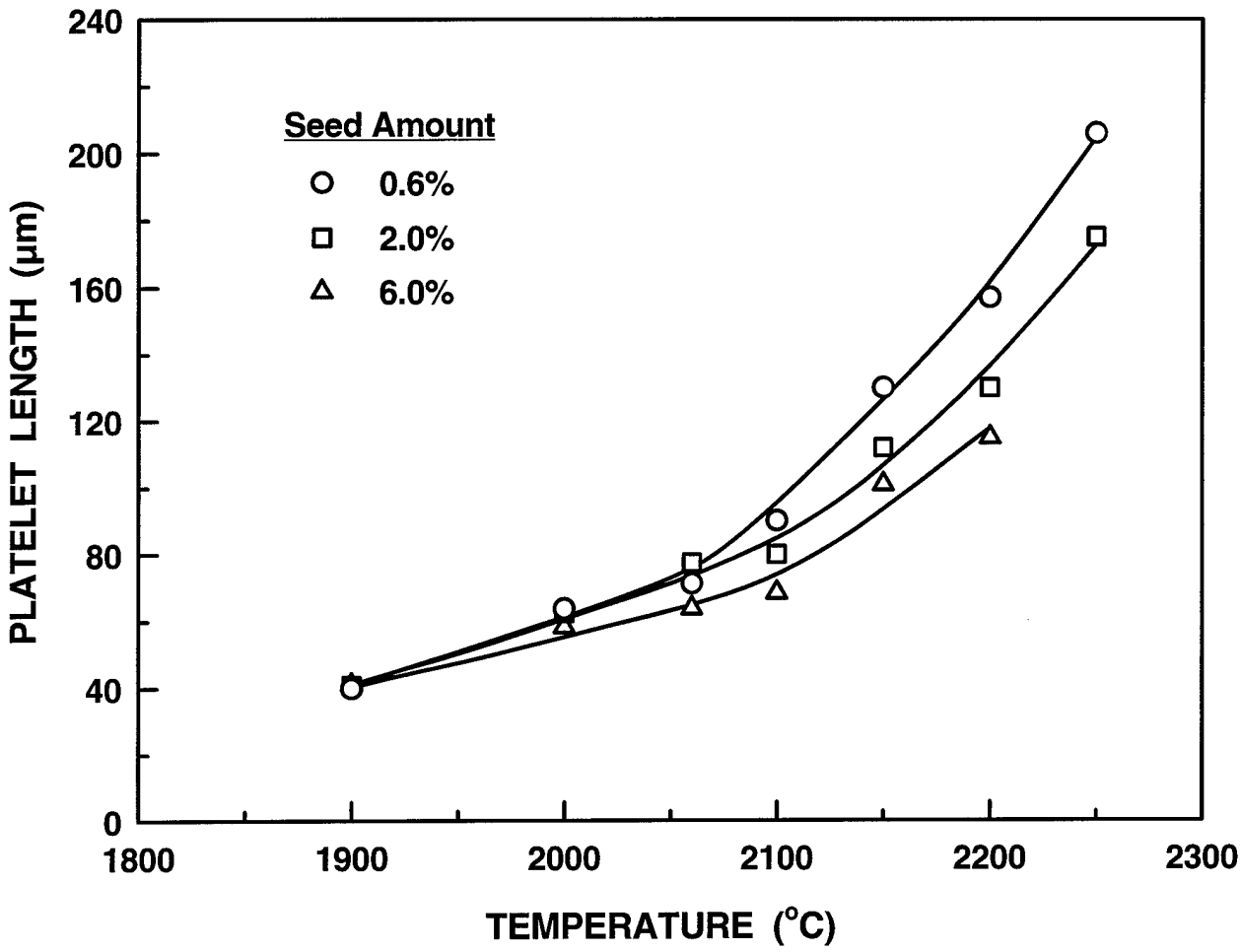

Figure 23. Plots of the platelet length vs. heat treatment temperature for SiC samples prepared with varying amount of seeds.

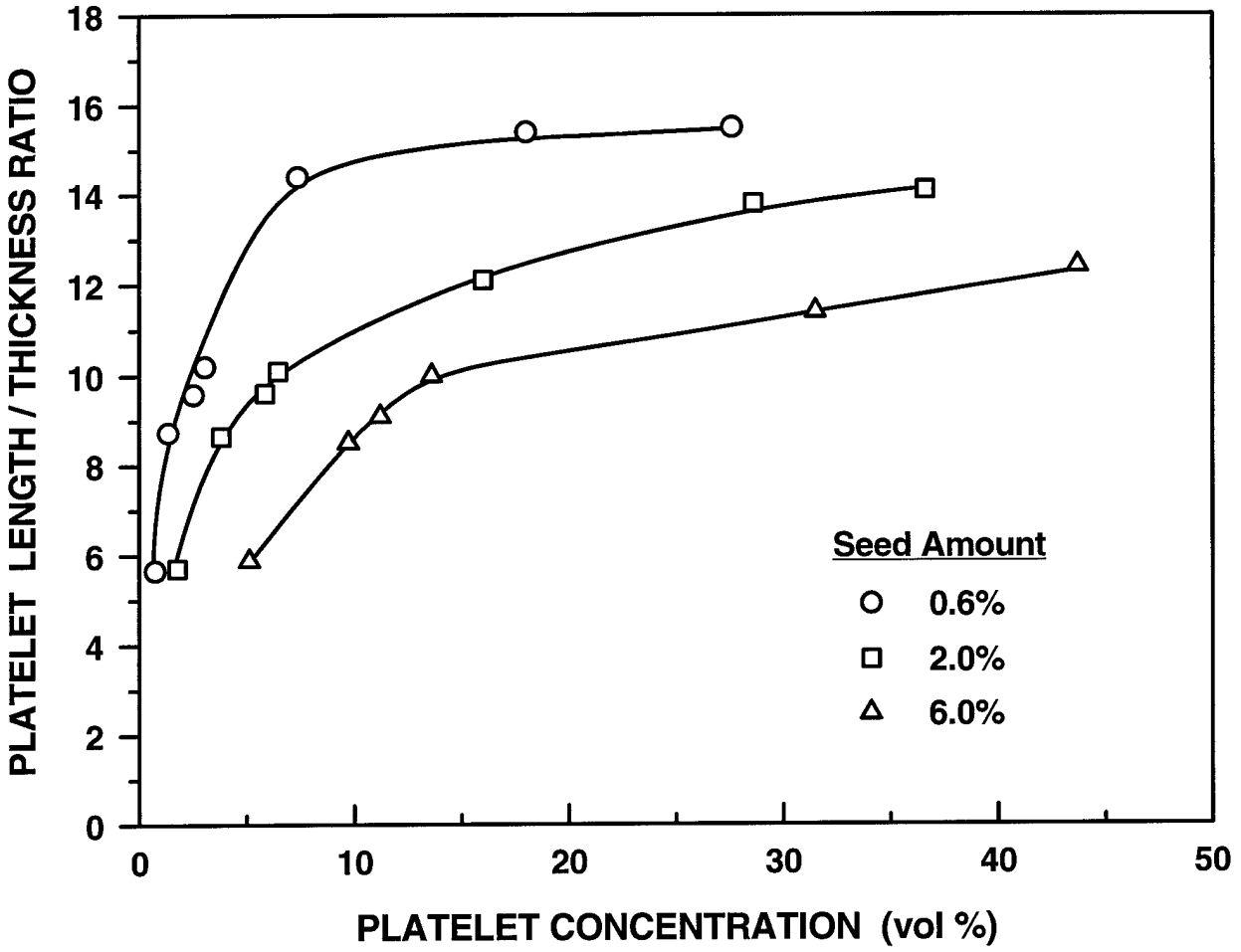

Figure 24. Plots of the length/thickness ratio of the platelet grains vs. platelet concentration for SiC samples prepared with varying amount of seeds.

preferential growth of the close-packed basal planes of the platelets.) In the early stages of platelet growth, the larger length/thickness ratios (at a fixed platelet concentration) for the samples with lower seed concentration reflect the fact that the latter samples have undergone a proportionally greater amount of volumetric growth. The length/thickness ratios also appear to level off at lower values for the samples with 2.0 and 6.0 vol% seeds, although additional data at higher platelet concentrations are needed to confirm this observation. This result is attributed to earlier impingement (i.e., at shorter platelet lengths) of the growing grains.

Bulk samples were characterized for fracture toughness by the microindentation technique. Toughness values with and without platelets were low (~2-2.5 MPa•$m^{1/2}$) which is typical of solid-state sintered SiC. The lack improvement in toughness with the platelet additions is attributed to the lack of a suitable matrix/platelet interface. A variety of studies in recent years have shown that the fracture toughness of SiC can be improved significantly by using liquid-phase sintering additives.[35-37] Hence, a study was initiated to determine if platelet-seeded grain growth could be used to fabricate highly textured, liquid-phase sintered SiC. This initial work is described in the next section.

Platelet-Seeded Liquid-Phase Grain Growth

Alumina and yttria are common additives for liquid-phase sintering of SiC.[35-37] In this study, 6 wt% alumina and 4 wt% yttria were added to tape casting suspensions which contained 2% SiC platelet seeds. Densification was enhanced by the liquid-phase forming additives, such that relative densities ≥96% were reached at ~1900°C, (i.e., ~50-100°C lower than temperatures used for sintering the samples prepared with conventional boron and carbon additives). Platelet growth was observed after heat treatment at higher temperature, as illustrated

in Figs. 25 and 26. (Most of the apparent porosity shown in the SEM micrographs in Fig. 25 is due to removal of second phase upon chemical etching.)

The platelet growth behavior in the samples prepared with alumina and yttria clearly differs from that described in the previous section for the samples doped with boron and carbon. Although the volume fraction of platelets increases (Fig. 26), the platelets retain a more blocky, lower-aspect-ratio morphology. Figure 27 shows the platelet length and platelet thickness as a function of heat treatment temperature. Fig. 28 shows that the platelet length/thickness ratio remains approximately constant with increasing heat treatment temperature. In the boron/carbon - doped samples discussed in the previous section, growth of the low energy basal planes of the hexagonal SiC was favored and, consequently, a large increase in the platelet length/thickness ratio was observed (Figs. 7-9). In contrast, the liquid phase that forms in the alumina/yttria - doped samples apparently reduces interfacial energy anisotropy, thereby favoring isotropic growth. The growth mechanism is apparently one involving solution-precipitation (i.e., dissolution of the fine SiC matrix grains and reprecipitation of SiC on the large seed platelets). This is indicated by the development of "core-rim" structures similar to those commonly observed in liquid-phase sintered Si_3N_4 and which have also been reported previously in liquid-phase sintered SiC.[38] Figure 29 shows examples of large platelike grains platelets which are comprised of the original platelet seed ("core") surrounded by the new growth ("rim") layer of SiC.

Although the platelets grow isotropically, the sample still develops a strong preferred orientation because of the initial orientation of the seed particles. Figure 30 shows the average and median orientation angles as a function of the heat treatment temperature. The results are

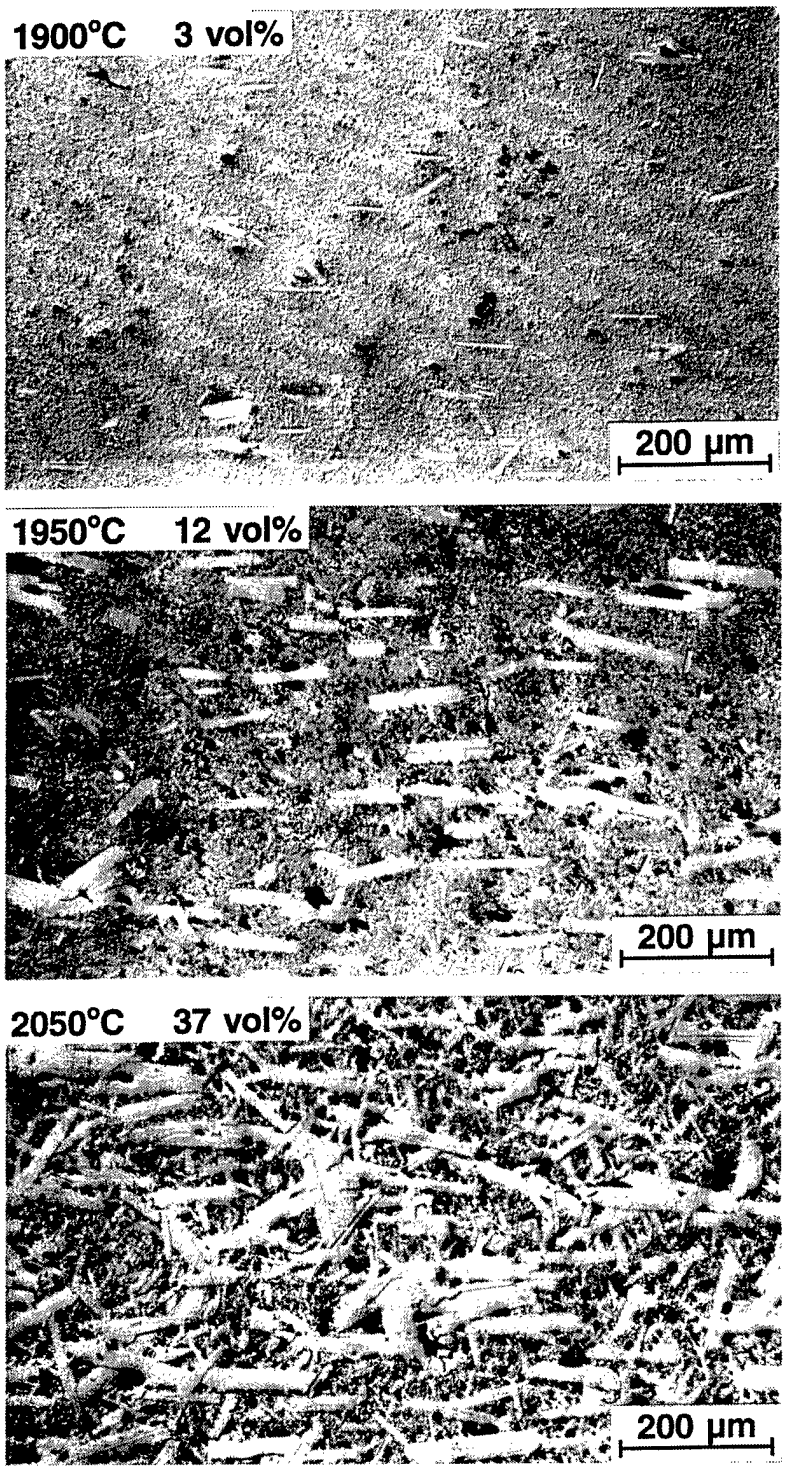

Figure 25. Optical micrographs of polished sections (taken perpendicular to the casting surface) for seeded (2% platelets) SiC samples prepared with alumina/yttria additives and heat treated at the indicated temperatures.

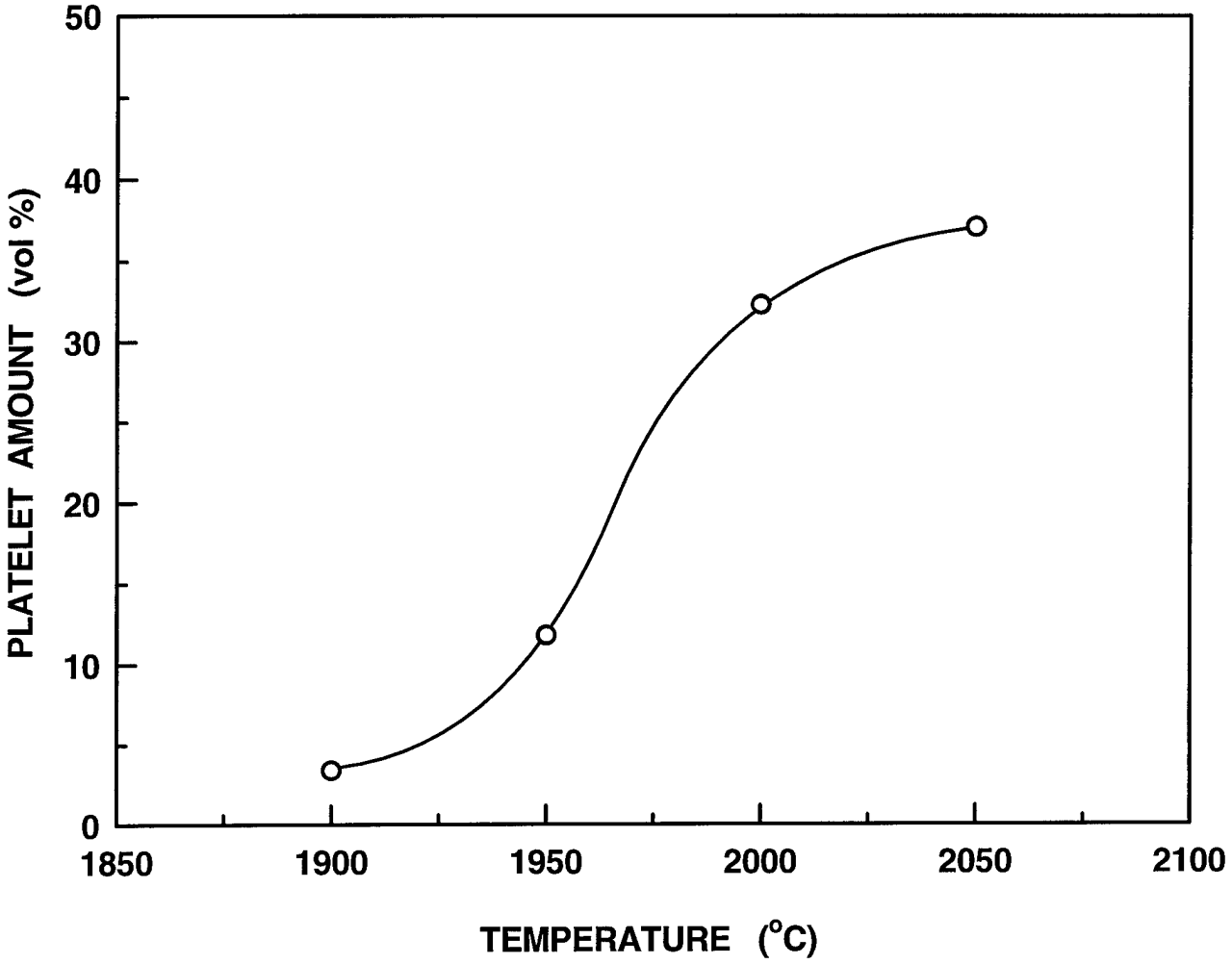

Figure 26. Plot of the volume percentage of platelet grains in the microstructure as a function of the heat treatment temperature for seeded (2% platelets) SiC samples prepared with alumina/yttria additives.

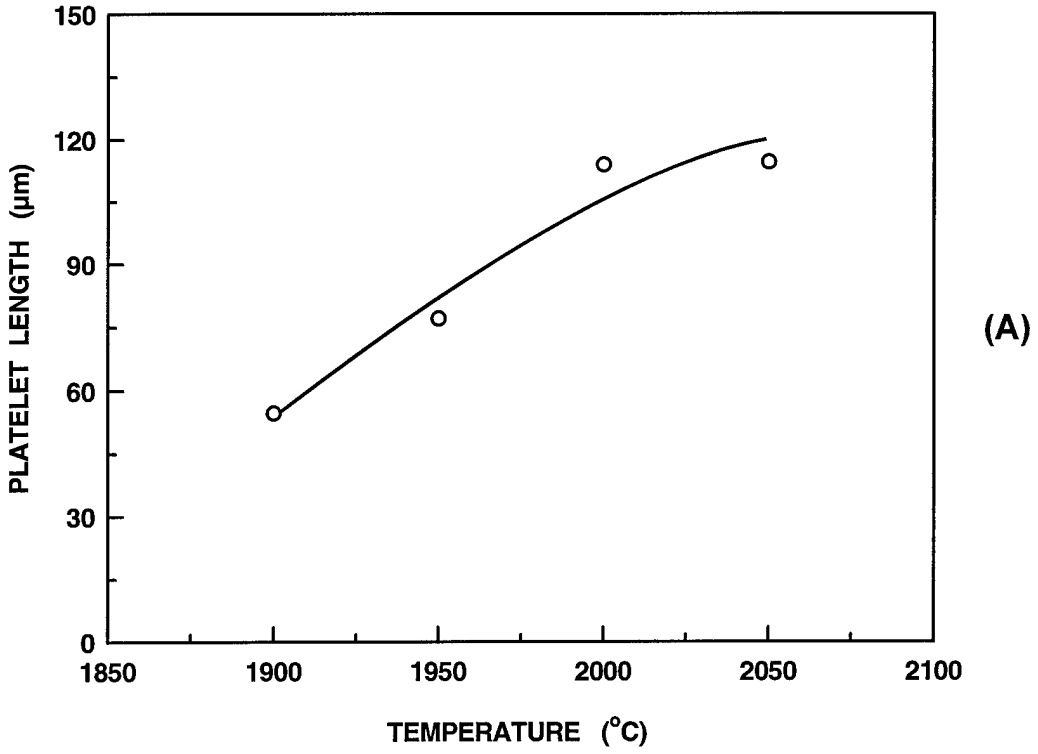

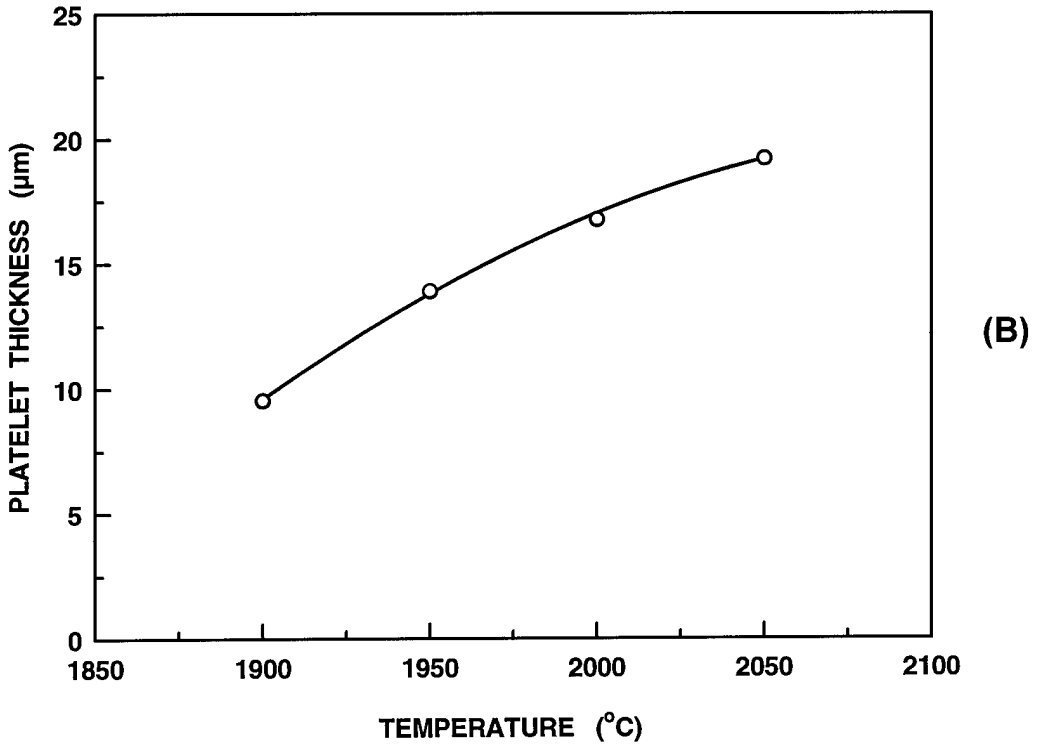

Figure 27. Plots of the (A) length and (B) thickness of the platelet grains as a function of the heat treatment temperature for seeded (2% platelets) SiC samples prepared with alumina/yttria additives.

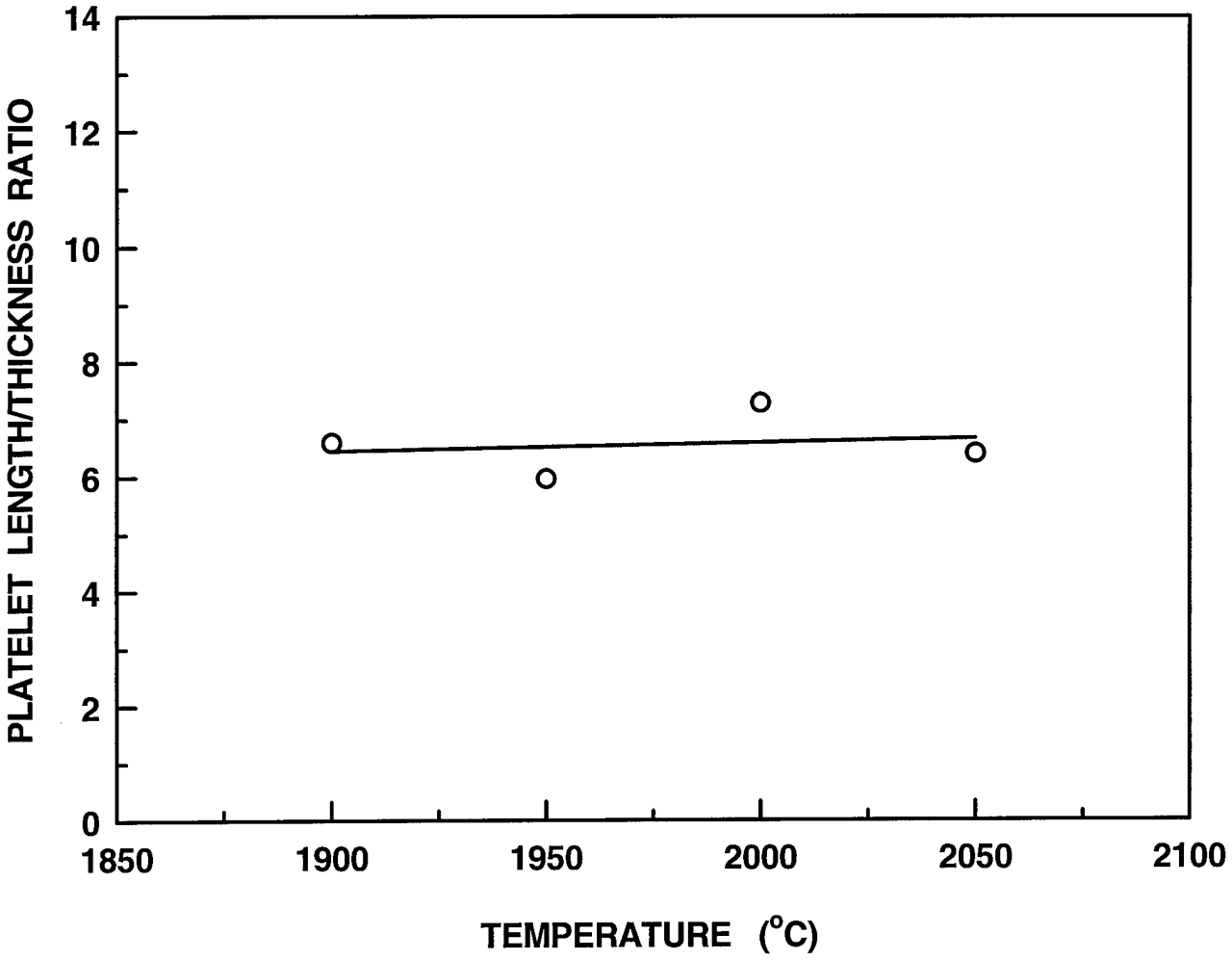

Figure 28. Plot of the length/thickness ratio of the platelet grains as a function of the (A) heat treatment temperature and (B) platelet concentration for seeded (2% platelets) SiC samples prepared with alumina/yttria additives.

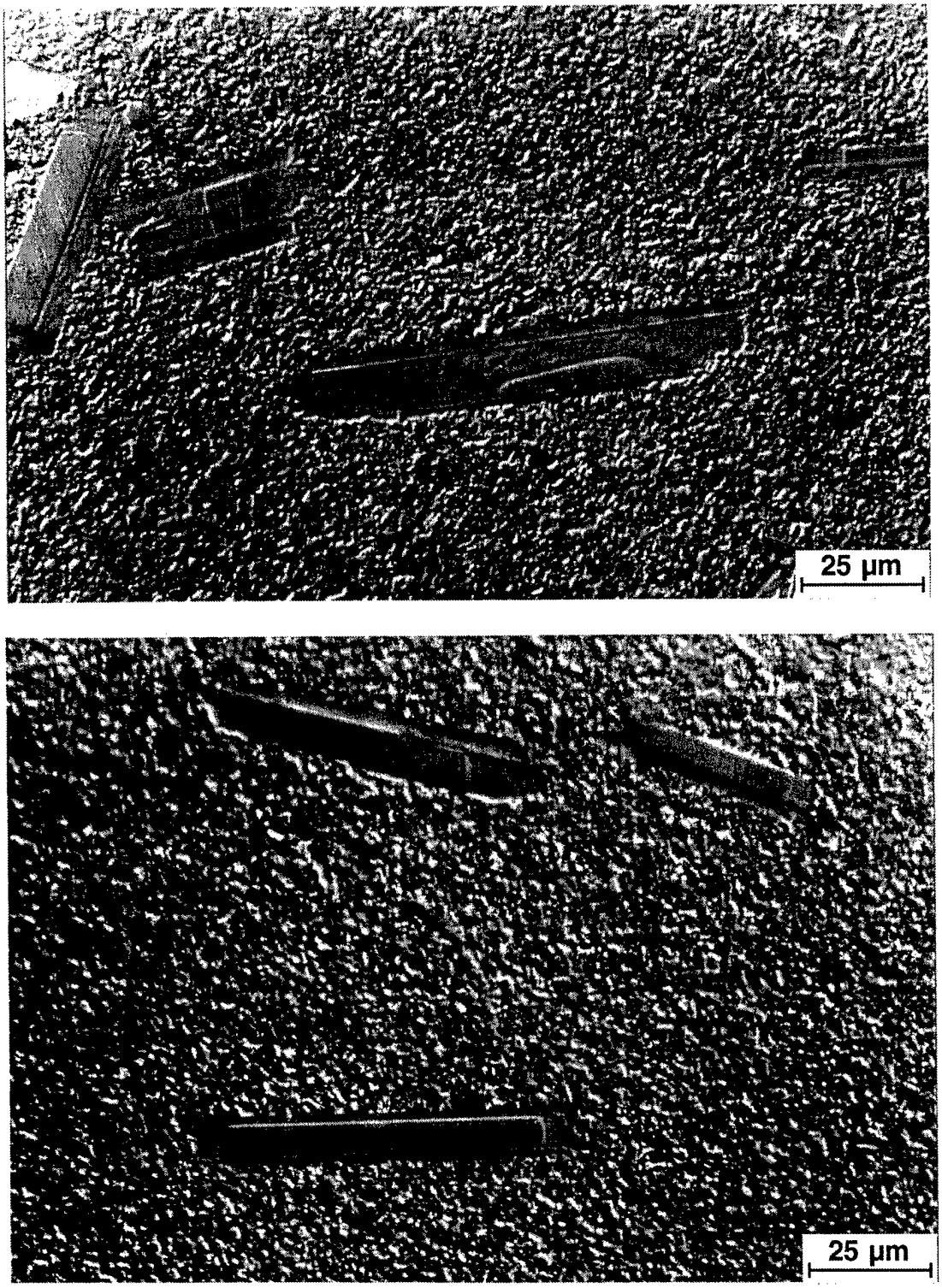

Figure 29. Optical micrographs showing the "core-rim" structure that develops during growth of the platelets in seeded (2% platelets) SiC samples prepared with alumina/yttria additives.

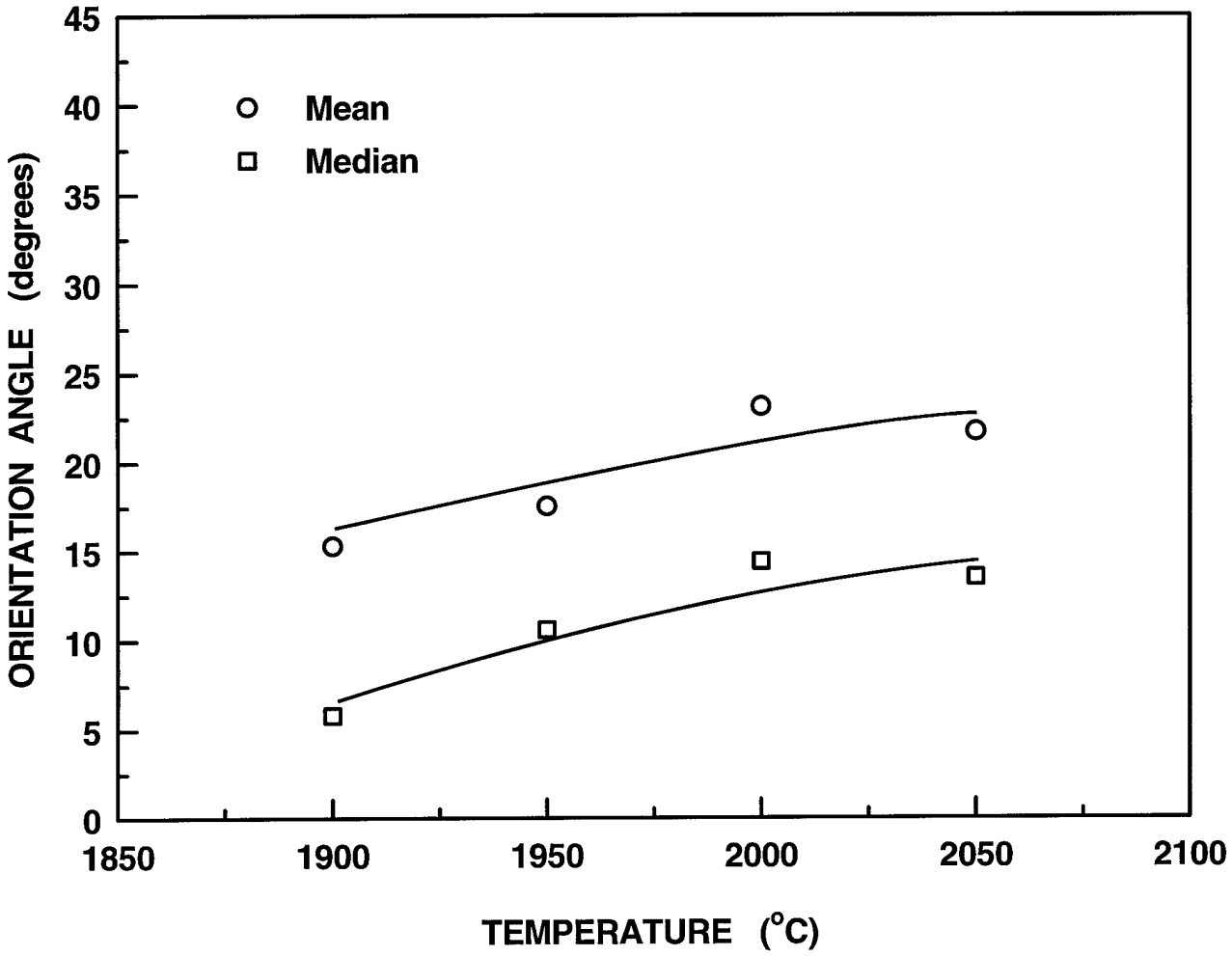

Figure 30. Plots of the median and average orientation angles for the platelet grains as a function of the heat treatment temperature for seeded (2% platelets) SiC samples prepared with alumina/yttria additives.

similar to that obtained with the boron/carbon - doped samples (Figs. 10 and 11).

As expected, the fracture toughness increased in samples prepared with the alumina and yttria additions. Toughness values in the range of ~3-5 MPa•m$^{1/2}$ were obtained using the indentation technique. This increase in toughness is attributed to increases in crack deflection and bridging due to modification of the SiC interfaces. Figure 31 shows the increase in crack path tortuosity for an alumina/yttria - doped sample compared to a boron/carbon - doped sample.

3.1.b Silicon Carbide Fibers

Whisker-Seeded and Platelet-Seeded Silicon Carbide Fibers

The feasibility of preparing textured SiC fibers by seeded grain growth has been investigated. Fine-diameter (typically ~8-14 μm) SiC fibers were processed by dry spinning of a concentrated pre-ceramic polymer solution. SiC whiskers were used as seed particles which were mixed into the polymer solution prior to fiber spinning. The spinning process involves extrusion of the viscous polymer solution through a spinneret. As schematically illustrated in Fig. 32, this process can result in alignment of whiskers along the fiber length and, indeed, such alignment of whiskers in the green state was experimentally realized. After heat treatment, however, seeded growth in fibers with 2% whiskers resulted in a textured microstructure consisting of stacked, platelike grains in which the long dimension of the grains was perpendicular to the long axis of the fibers (Fig. 33). This structure developed because the crystallographic planes for preferred growth in the seed whiskers were aligned perpendicular to their long axis (and, therefore, perpendicular to the long axis of the fibers). The SiC whiskers used in the study (Tateho) were mostly comprised of the cubic (beta) phase which has a structure generated from packing of SiC coordination tetrahedra in close-packed sheets (i.e., (111) planes)

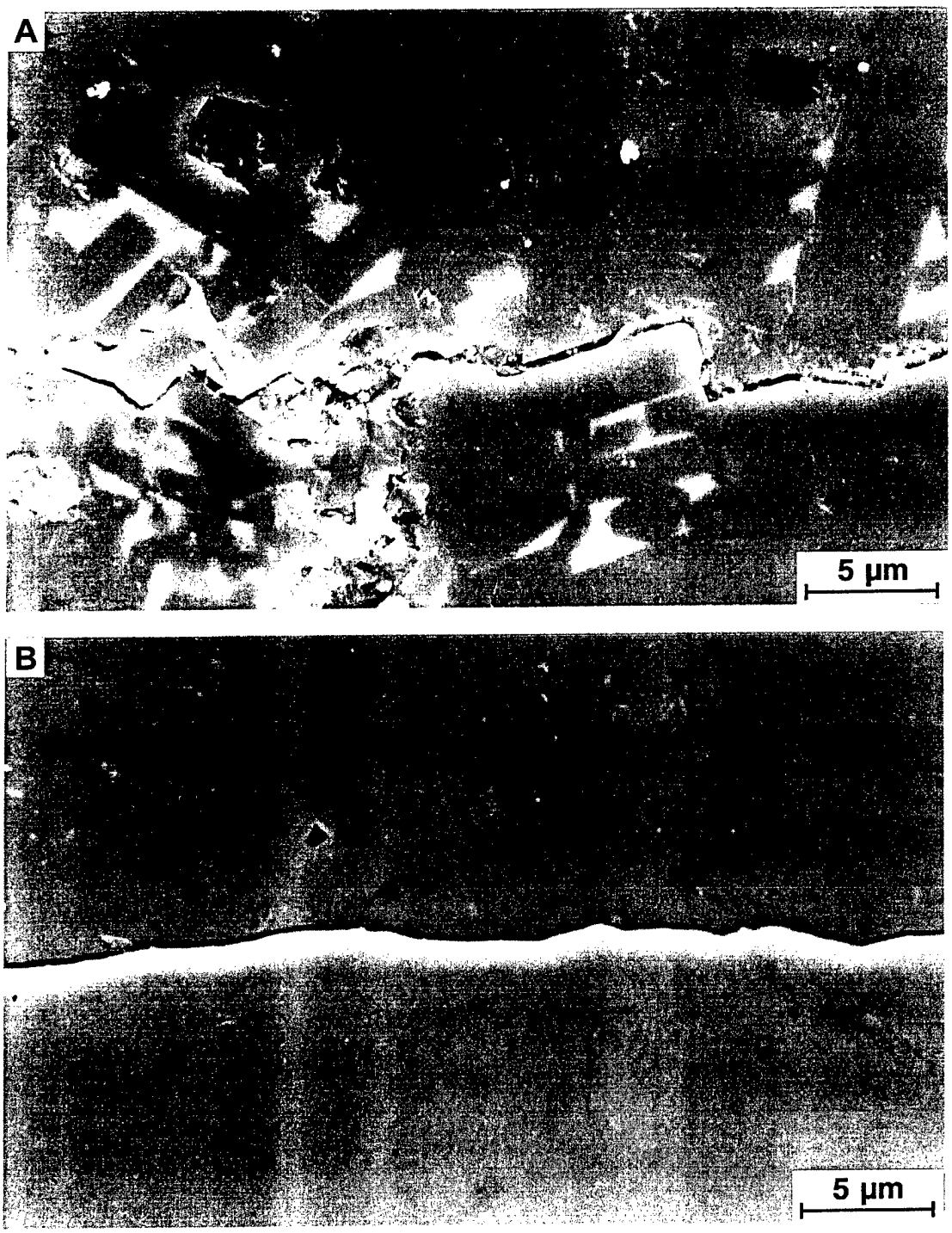

Figure 31. SEM micrographs showing the crack paths for seeded (2% platelets) SiC samples prepared with (A) alumina and yttria additives and (B) boron and carbon additives.

Fiber with Oriented Seeds

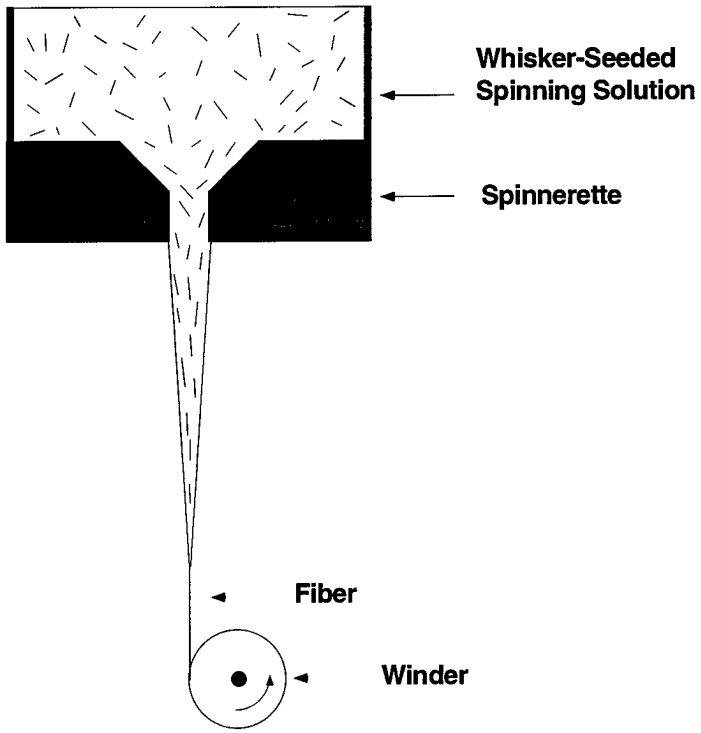

Figure 32. Schematic illustration of whisker alignment during fiber spinning.

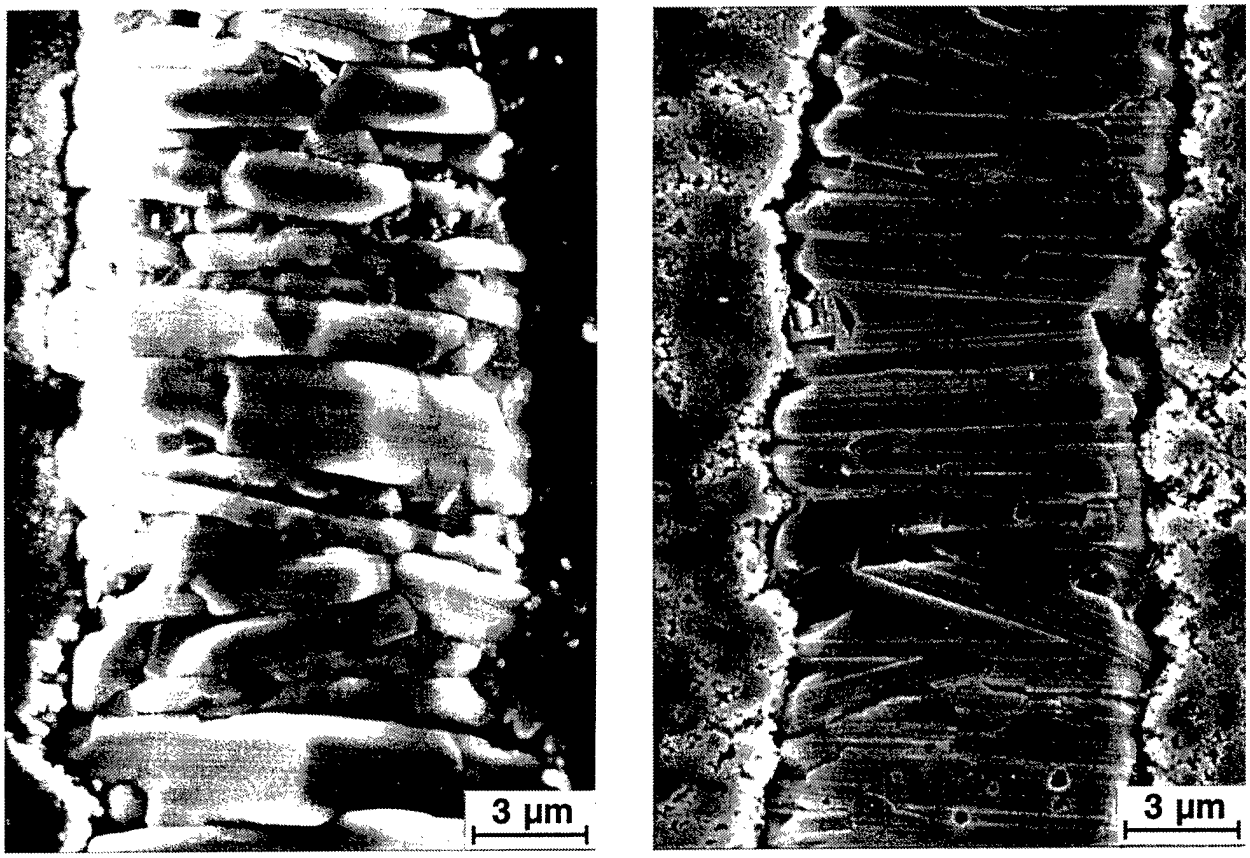

Figure 33. SEM micrographs showing the "stacked plate" grain structure of SiC fibers prepared with 2% whisker seeds and heat treated at ~2250°C.

in the <111> direction. The whiskers have a lamellar structure due to a high density of stacking faults and narrow twins on the close-packed planes. This structure is shown by SEM and TEM in Figs. 34A and 34B, respectively. (Figure 34A shows a whisker protruding from a polished section of a pyrolyzed fiber, while Fig. 34B shows an isolated as-received whisker.) At high temperatures (>2000°C), the whiskers will transform to the alpha phase, but retain the lamellar structure. The transformed whiskers act as seeds for the growth of the stacked, alpha phase, platelike grains observed in fibers processed at high temperatures (Fig. 33). The growth process is schematically illustrated in Fig. 35.

In order to develop fibers in which the long axes of the grains are oriented along the lengths of the fibers, it is necessary to utilize seeds in which the close-packed crystallographic planes are oriented parallel to the fiber axis. We examined by TEM another commercial source of whiskers (i.e., Tokai), but the structure was similar to the Tateho whiskers. Therefore, another approach investigated was to use SiC platelets as seed particles. As noted earlier, the major faces of the platelets are comprised primarily of the close-packed basal planes of the 6H polytype. During the fiber extrusion process, it was expected that the platelet seeds could be substantially aligned with the major faces parallel with the long axis on the fibers. To test the concept, experiments were carried out using 0.2% platelet seeds. (A low concentration was used because prior work with the whisker-seeded fibers showed that the fiber tensile strength decreased significantly as the size and the amount of whisker seeds increased. Unfortunately, the platelets were only available in relatively large sizes and, therefore, a low concentration was used. As discussed below, however, the seeds still acted as major strength-degrading flaws and the sintered fibers were too weak to even make tensile strength measurements.)

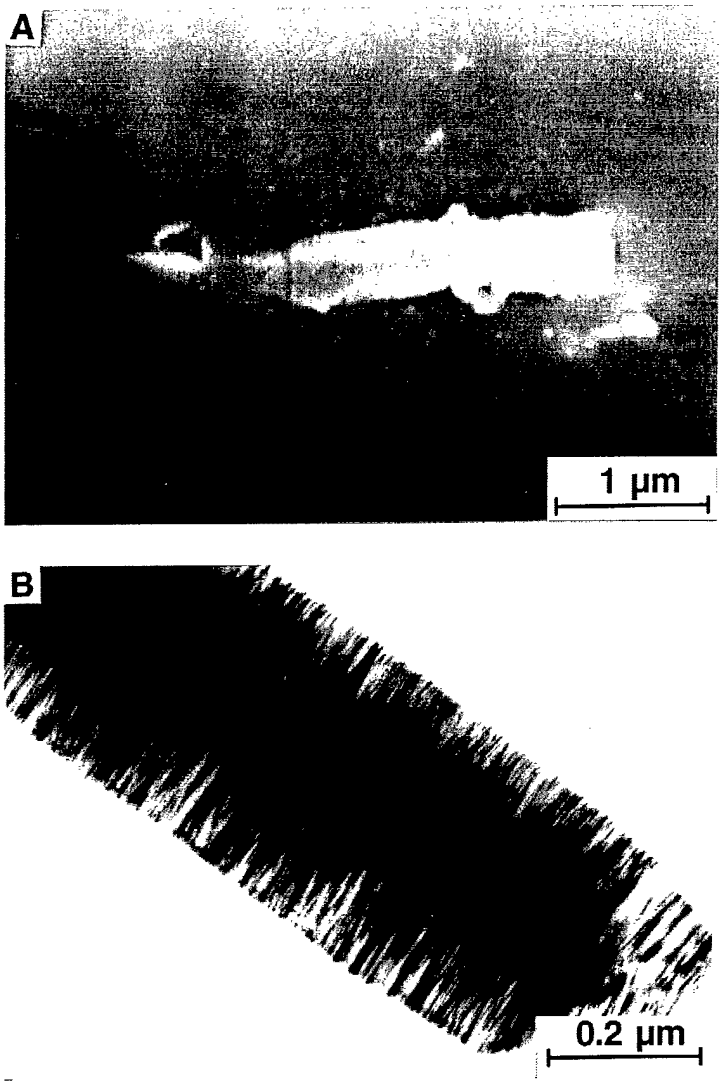

Figure 34. (A) SEM and (B) TEM micrographs showing the lamellar structure of the SiC whisker seeds.

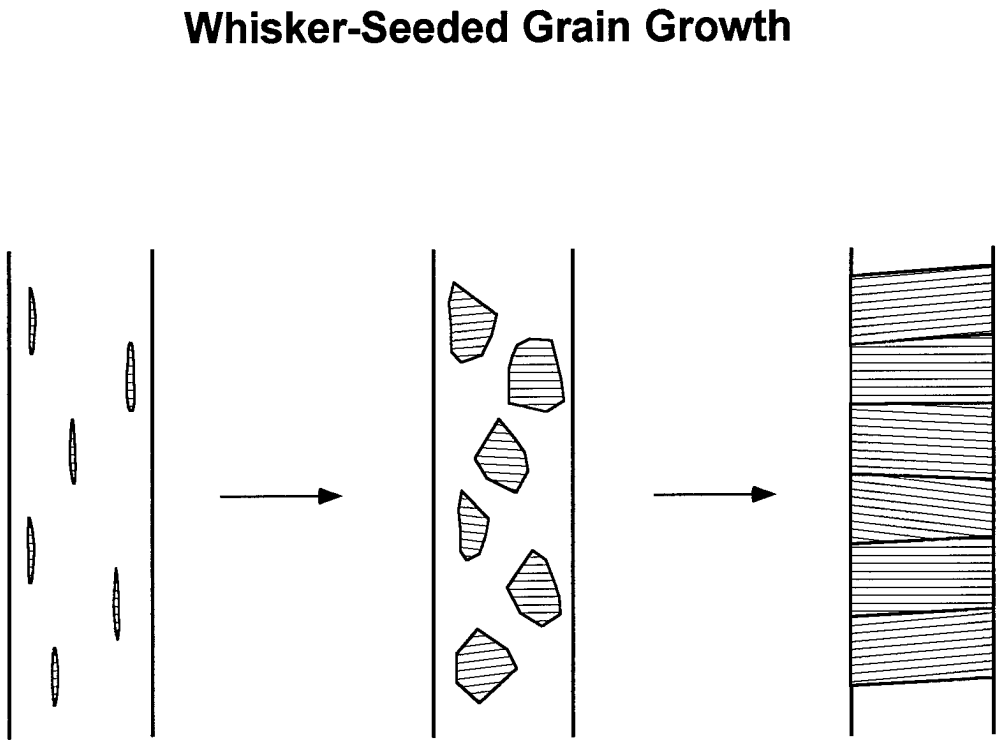

Figure 35. Schematic illustration of the grain growth process in whisker-seeded SiC fibers.

Previous observations by TEM have shown that unseeded fibers have a dense, fine-grained ($\sim$0.1-0.2 μm) structure after sintering at $\sim$1800°C. Fibers with seed platelets were heat treated at higher temperatures (i.e., $\sim$1950-2200°C) to promote platelet growth. Figure 36 show polished sections of fibers heat treated at $\sim$1950°C. The optical micrograph in Fig. 36A shows a single seed platelet (in the middle of the micrograph) which is aligned with the long dimension parallel to the long axis of the fiber. The SEM micrograph in Fig. 36B shows a seed platelet at higher magnification. The seed resulted in the formation of a large defect (porosity). Hence, it is not surprising that fiber strengths were very low. Despite the fine size of the matrix grains, platelet growth was sluggish. Figure 36B shows that only minimal extension of the platelet occurred after heat treatment at $\sim$1950°C.

Figures 37A and 37B show that additional platelet growth occurred after heat treatment at $\sim$2150°C and $\sim$2200°C, respectively. Some large platelets have grown along the length of the fibers, but the seed-derived platelet volume fraction is still relatively low compared to the platelet-seeded powder compacts discussed in the previous section. In addition, exaggerated grain growth was observed in the matrix grain regions of the 2200°C sample. This resulted in many large platelike grains which were not aligned along the fiber long axis.

Although the results to date demonstrate that the concept of fabricating textured fibers via seeding is valid, there are clearly several problems that must be addressed in order for this approach to have practical application. Alternate seeding methods need to be developed to overcome the problem of seeds introducing large, strength-degrading flaws in the fibers. In addition, the texturing growth process needs to be promoted with finer seeds and at lower temperatures to avoid coarse-grained microstructures which result in low-strength fibers.

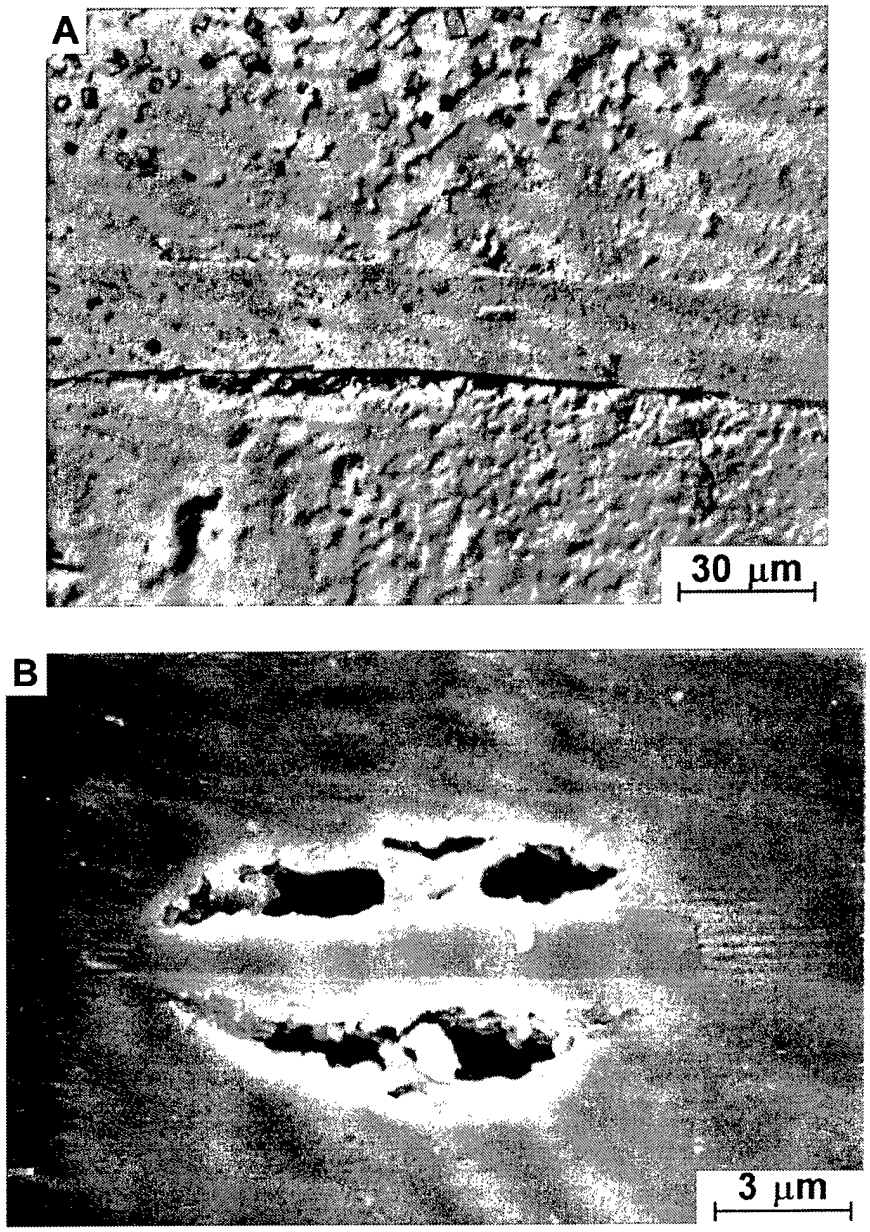

Figure 36. (A) Optical and (B) SEM micrographs of a polished section of an SiC fiber with ~0.2% platelet seeds which was heat treated at ~1950°C.

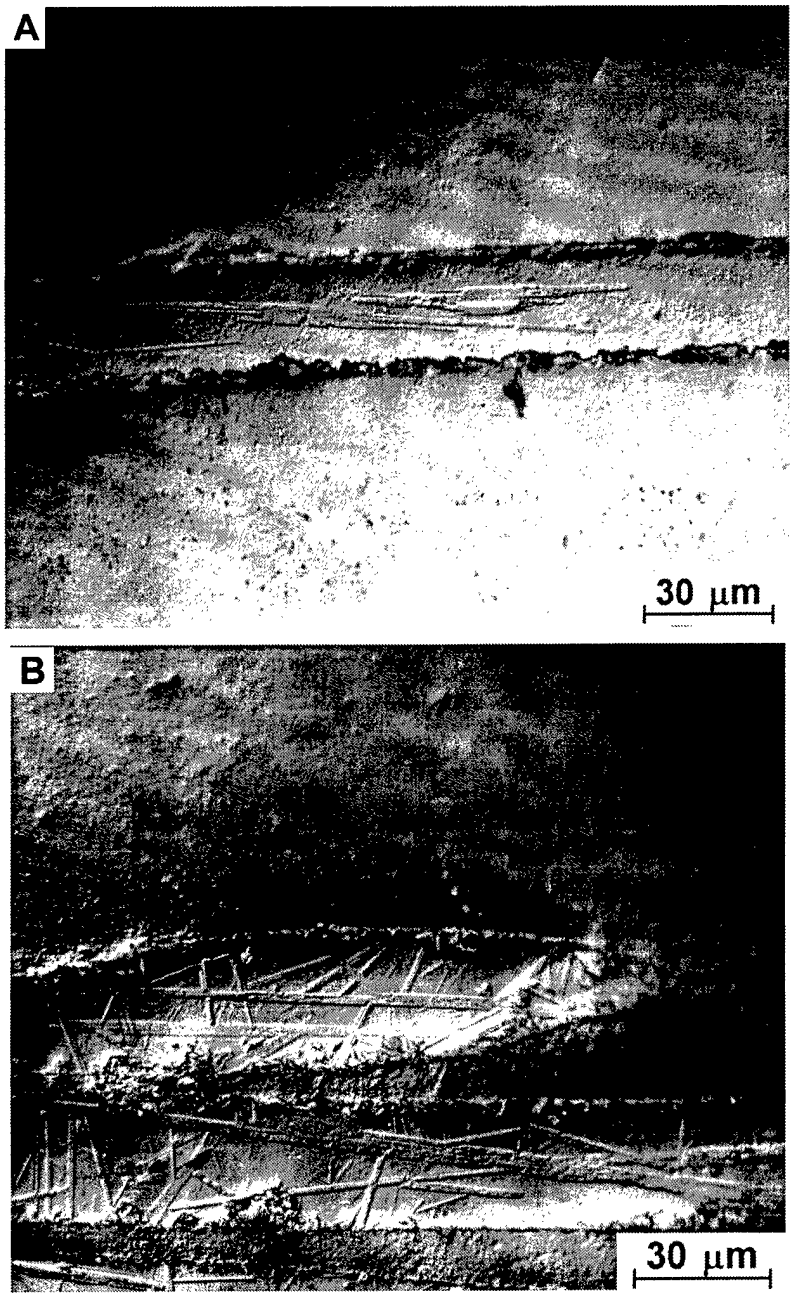

Figure 37. Optical micrographs of polished sections of SiC fibers with ~0.2% platelet seeds which were heat treated at (A) ~2150°C and (B) ~2200°C.

SiC Fibers with In-Situ Processed BN Coatings

SiC fibers with BN surface coatings were prepared by an in-situ process which is schematically illustrated in Fig. 38. Boron-doped fibers were heat treated in a nitrogen-containing atmosphere. BN forms by reaction of boron at the surface with nitrogen in the atmosphere. After the initial reaction at the original SiC fiber surface, it is presumed that the increases in thickness of the coating occur by diffusion of boron from the interior of the fiber to the reaction layer, followed by chemical interdiffusion of boron and nitrogen through the growing BN layer.

Figure 39 shows a TEM micrograph of the BN coatings formed on the SiC fibers. Typical coating thicknesses were $\sim$0.1-0.2 μm, although it may be possible to increase the thickness by using SiC fibers with higher initial boron content. Figure 40 shows an HRTEM micrograph of the BN layer. Electron diffraction analysis and lattice spacing measurements showed that the coating layer is hexagonal BN. The HRTEM micrograph indicates that the BN coating is textured. The coating grows such that the hexagonal BN basal planes are oriented mostly perpendicular to the long axis of the SiC fibers.

SiC fibers prepared with the textured BN coatings retained high strength ($\sim$3 GPa) and excellent creep resistance (see the third paper in the Appendix). The effectiveness of the BN coatings for developing weak fiber/matrix interfaces in CMC's has not yet been evaluated.

IN-SITU FIBER COATING

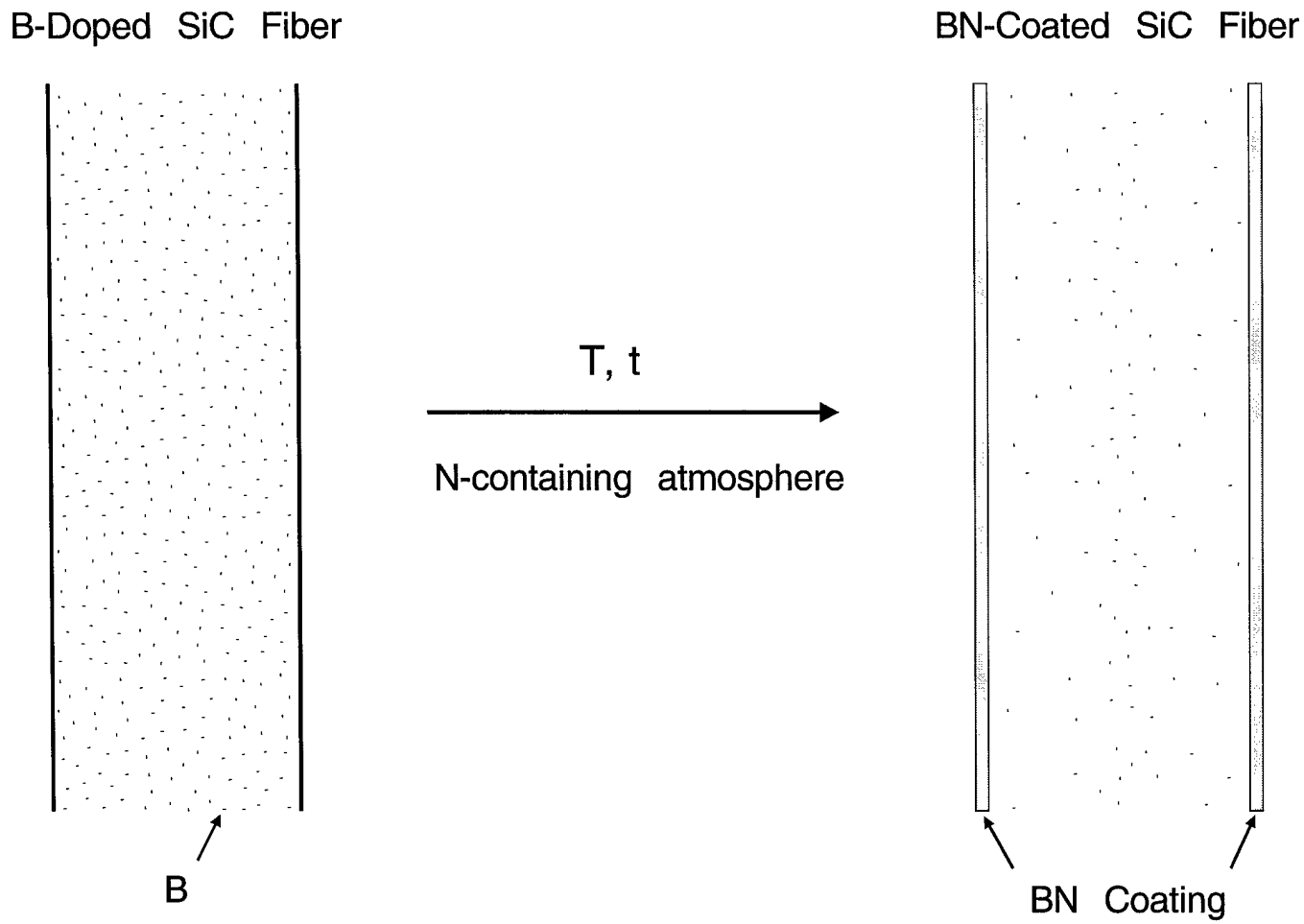

Figure 38. **Schematic illustration of the formation of a BN coating on a SiC fiber by in-situ processing.**

Figure 39. **TEM micrograph showing BN coatings and SiC fiber grains.**

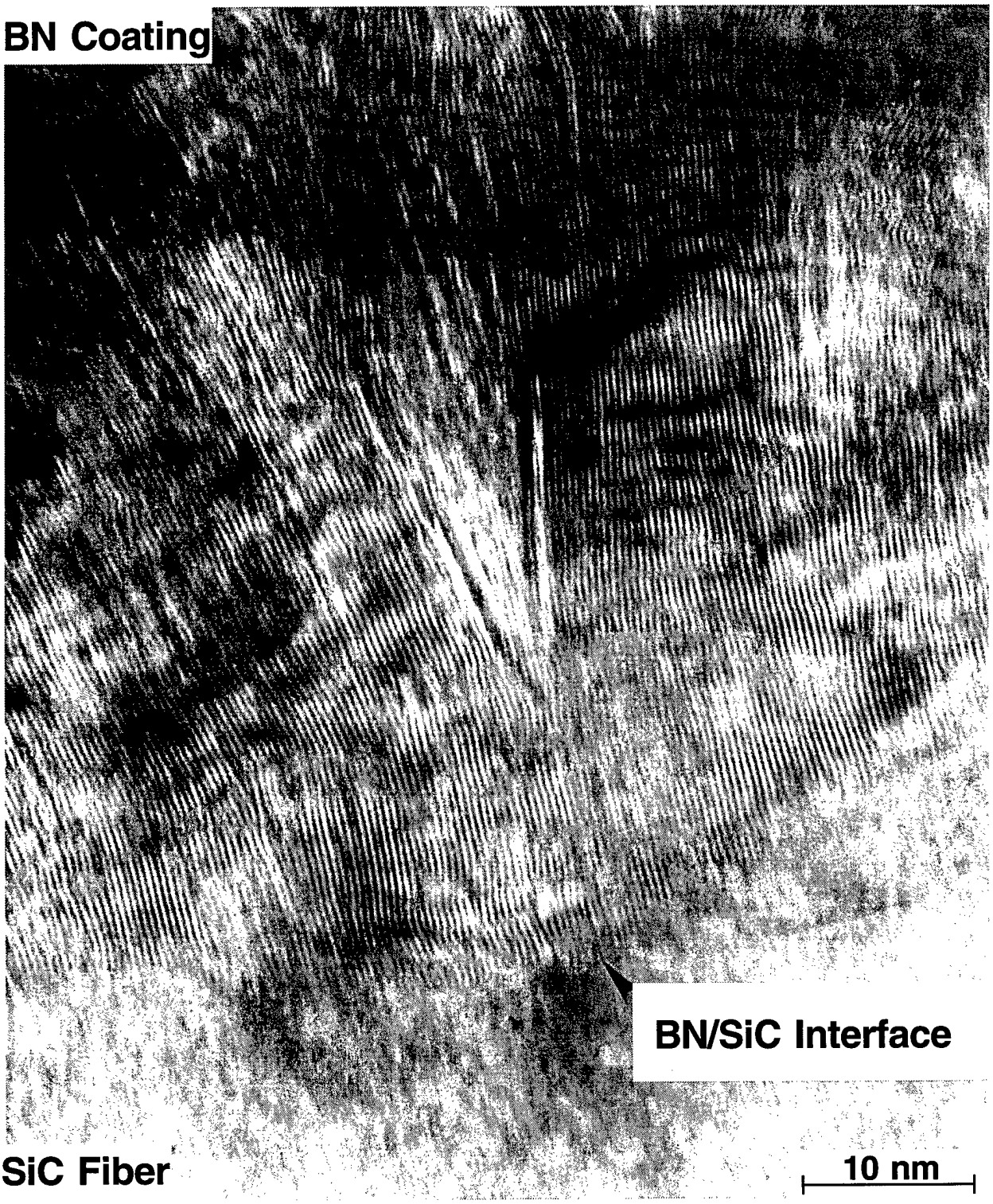

Figure 40. HRTEM micrograph showing the BN coating/SiC fiber interface and the lattice planes of the BN coating. The BN basal planes grow with an orientation that is mostly perpendicular to the long axis of the SiC fiber.

3.2. Textured Silicon Nitride

Studies have demonstrated the feasibility of producing textured Si_3N_4 via anisotropic grain growth. This work was carried out in collaboration with Professor J. Halloran of the University of Michigan. Si_3N_4 powders (with yttria and alumina sintering additives) were formed into fine rods by extrusion. Samples were prepared with and without 1% β-Si_3N_4 whisker seeds. During the extrusion process, the whiskers to become aligned along the long axis of the extruded rods. The extruded rods were bundled together (in an aligned manner) and hot pressed (at $\sim$1750°C) to form dense Si_3N_4 billets, as illustrated schematically in Fig. 41.

Figure 42 shows SEM micrographs of polished sections (taken perpendicular to the hot pressing direction and parallel to the fiber extrusion direction) of hot pressed samples prepared without (top) and with (bottom) 1% Si_3N_4 seeds. The oriented Si_3N_4 grains in the seeded sample are evident. Figure 43 shows the same samples after heat treatment at $\sim$1950°C. Significant growth of the large, well-aligned, rodlike β-Si_3N_4 grains has occurred. In contrast, the rodlike Si_3N_4 grains in the unseeded sample do not show any obvious preferred orientation. In addition, the size and volume fraction of the rodlike grains in the unseeded sample are much smaller. Figure 44 shows SEM micrographs of the seeded 1950°C sample in which a direction comparison is made of polished surfaces taken parallel and perpendicular to the extrusion direction. The latter section shows mostly the ends of the rodlike Si_3N_4 grains. (Note that all the samples in this study were etched with molten sodium hydroxide in order to show the Si_3N_4 grains clearly. This resulted in pore formation due to leaching of second phase(s) which had formed from yttria and alumina sintering additives.)

XRD characterization confirmed the enhanced growth of oriented, rodlike Si_3N_4 grains

Fibrous Monolith with Oriented Seeds

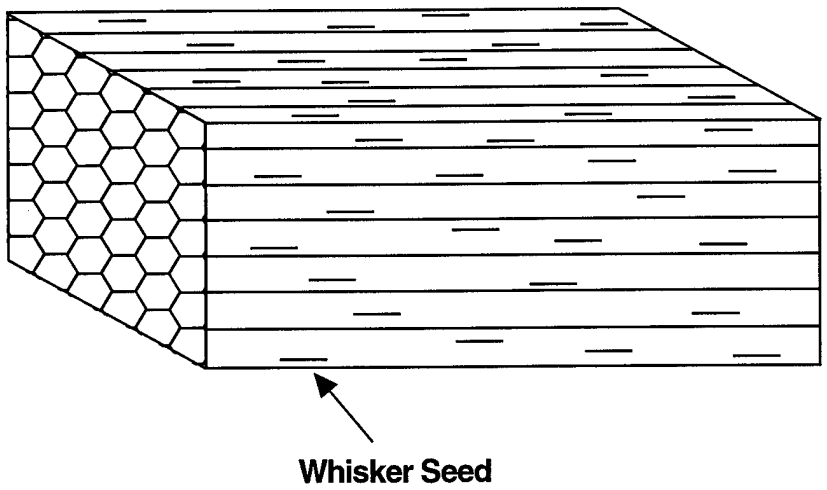

Figure 41. Schematic illustration of the formation of fibrous monoliths with aligned whisker seeds.

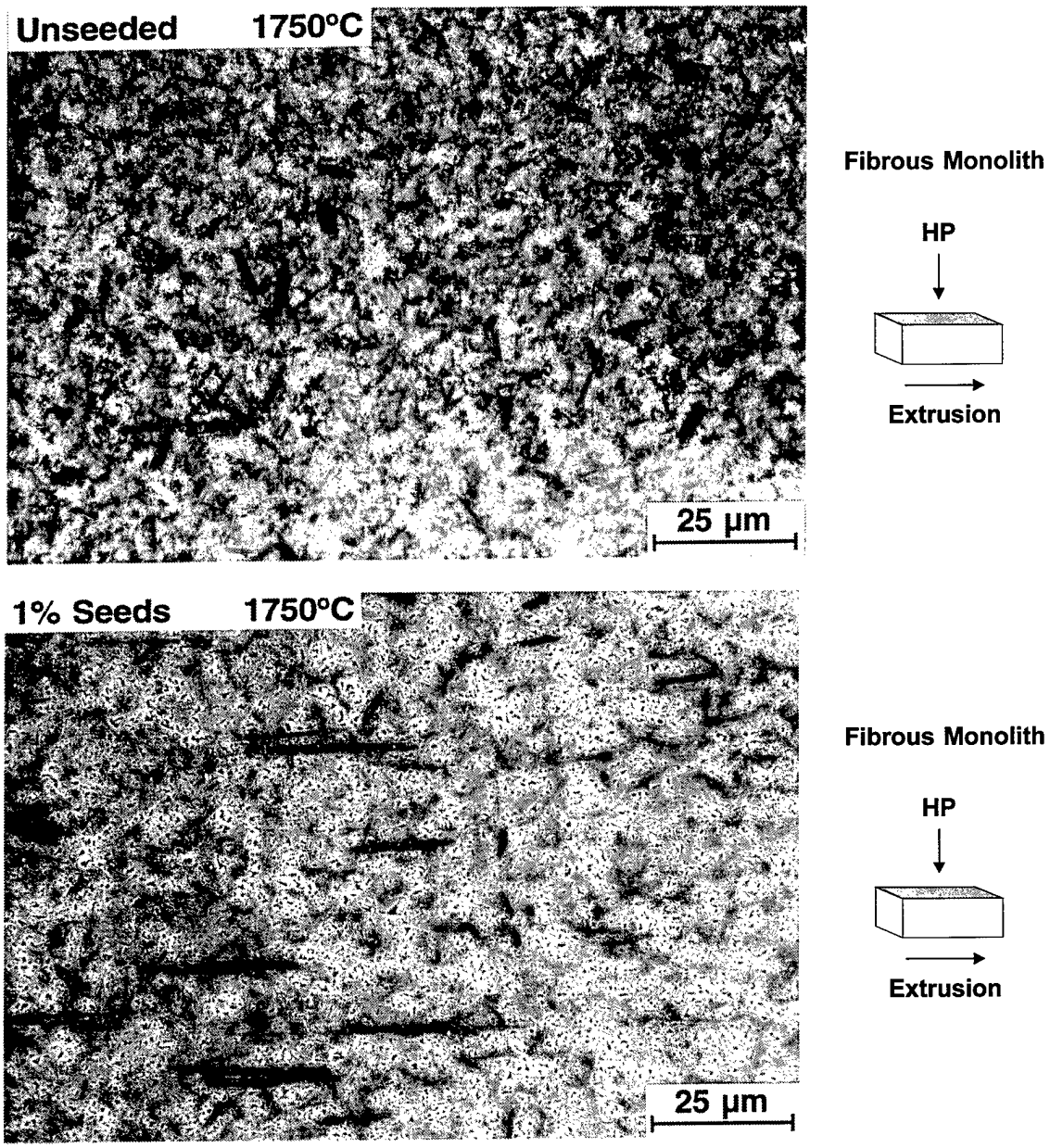

Figure 42. SEM micrographs of polished sections (taken perpendicular to the hot pressing direction and parallel to the fiber extrusion direction) of hot pressed (~1750°C) samples prepared without (top) and with (bottom) 1% Si_3N_4 seeds.

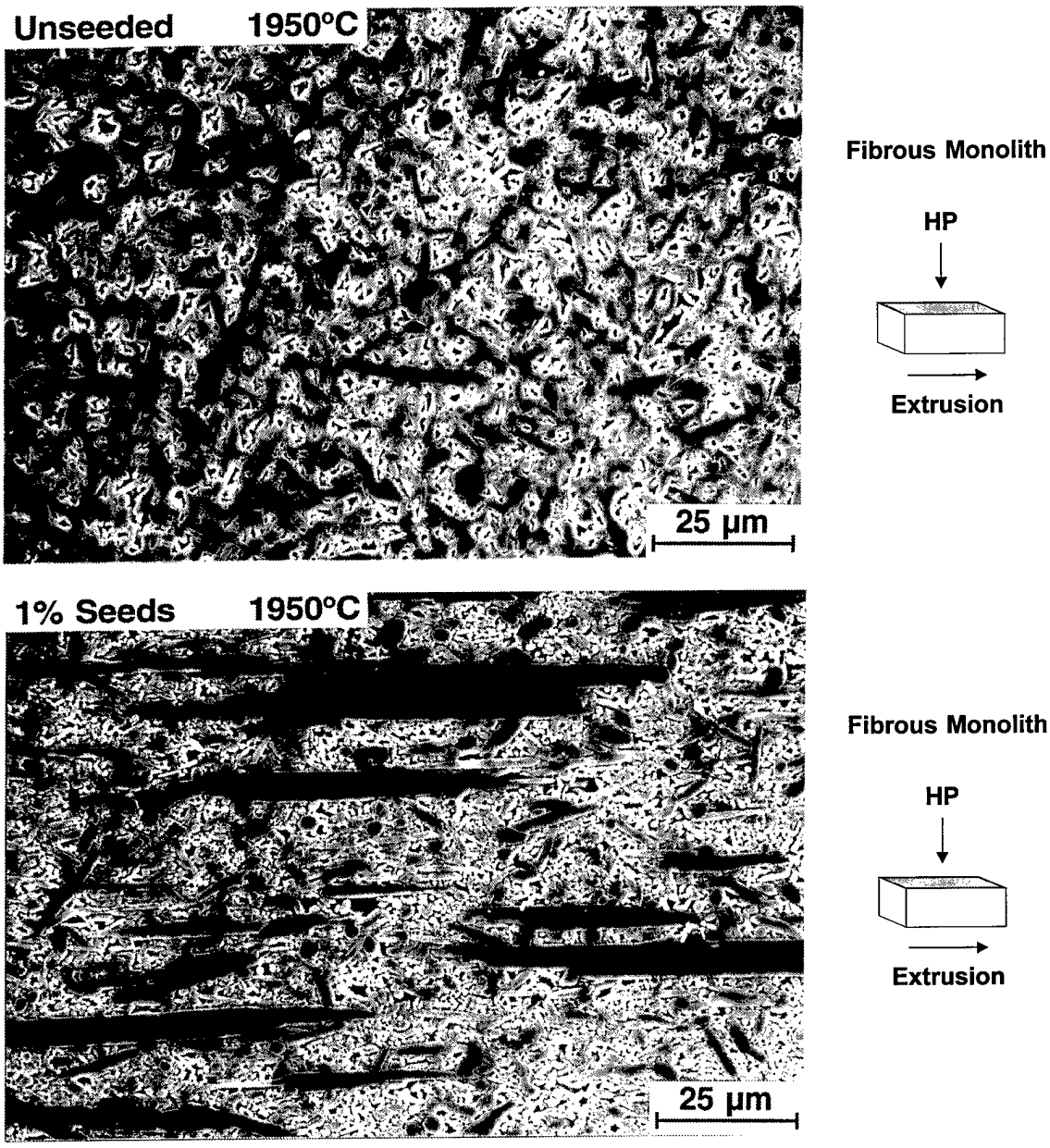

Figure 43. SEM micrographs of polished sections (taken perpendicular to the hot pressing direction and parallel to the fiber extrusion direction) of hot pressed samples prepared without (top) and with (bottom) 1% Si_3N_4 seeds after further heat treatment at 1950°C.

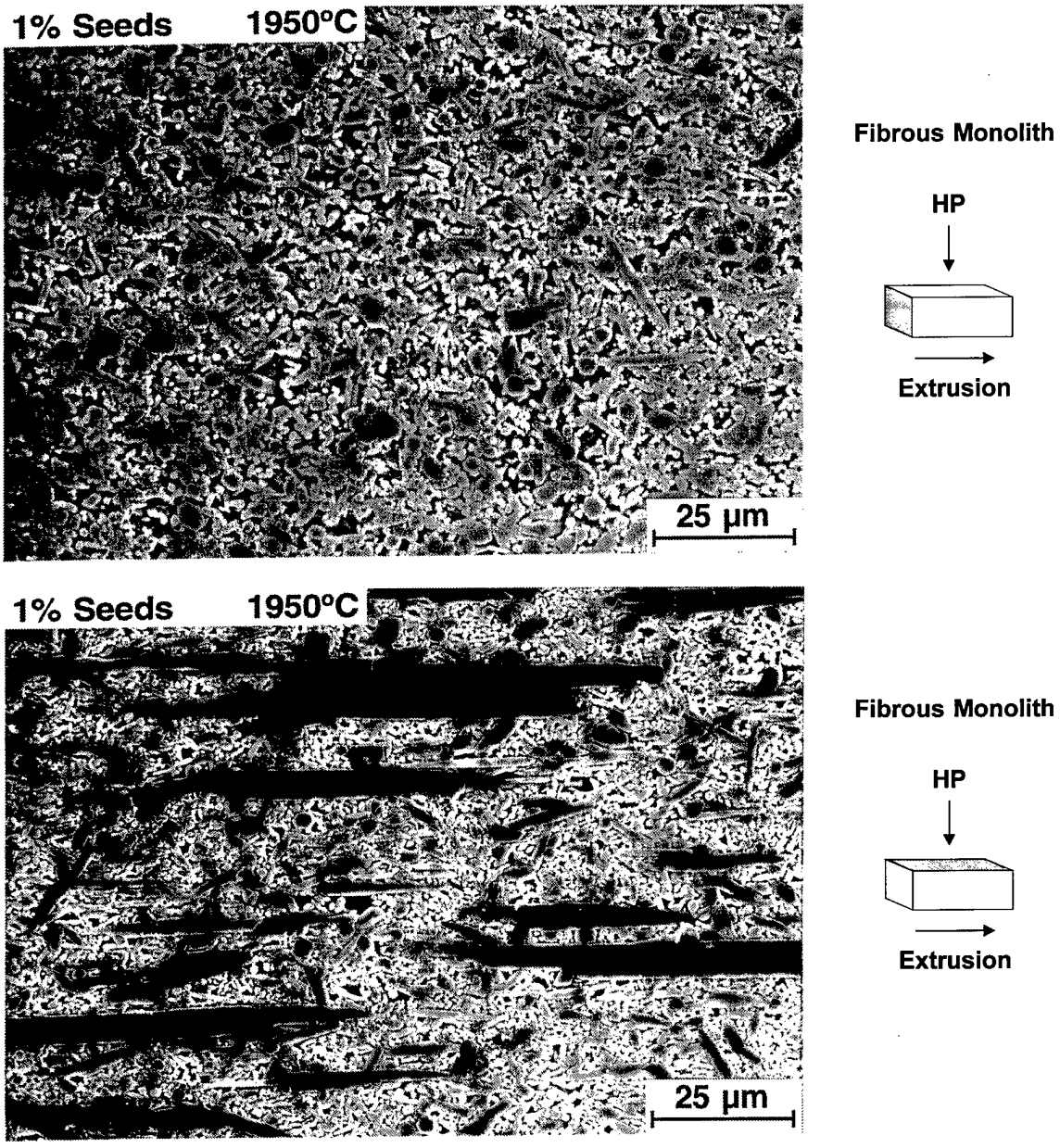

Figure 44. SEM micrographs of the same seeded 1950°C sample in Fig. 37 showing a comparison of polished surfaces taken perpendicular (top) and parallel (bottom) to the extrusion direction.

in the seeded samples. This growth results in an increase in the (210)/(110) peak intensity ratio for XRD measurements taken perpendicular to the extrusion direction and parallel to the hot pressing direction. This is illustrated in Figure 45 which shows a comparison of the XRD spectra for the 1750°C and 1950°C samples with 1% whisker seeds and in Figure 46 which shows a comparison of the XRD spectra for 1950°C samples with and without the 1% whisker seeds. Figure 47 shows the sharp decrease in the (210)/(110) peak intensity ratio that occurs when XRD measurements are taken from the surface parallel to the ends of the large, well-aligned, rodlike Si_3N_4 grains in the seeded 1950°C sample.

The oriented grain structure in the seeded 1950°C samples results in considerable fracture toughness anisotropy. This is illustrated by the crack extension anisotropy shown in the optical micrograph in Fig. 48A. The cracks formed by the microindentor extended to longer distances parallel to the extrusion direction, i.e., parallel to the long dimension of the oriented, rodlike grains. The indentation fracture toughness values calculated from cracks extending parallel and perpendicular to the extrusion direction were in the ranges of ~4-6 $MPa \cdot m^{1/2}$ and ~6-8 $MPa \cdot m^{1/2}$, respectively.

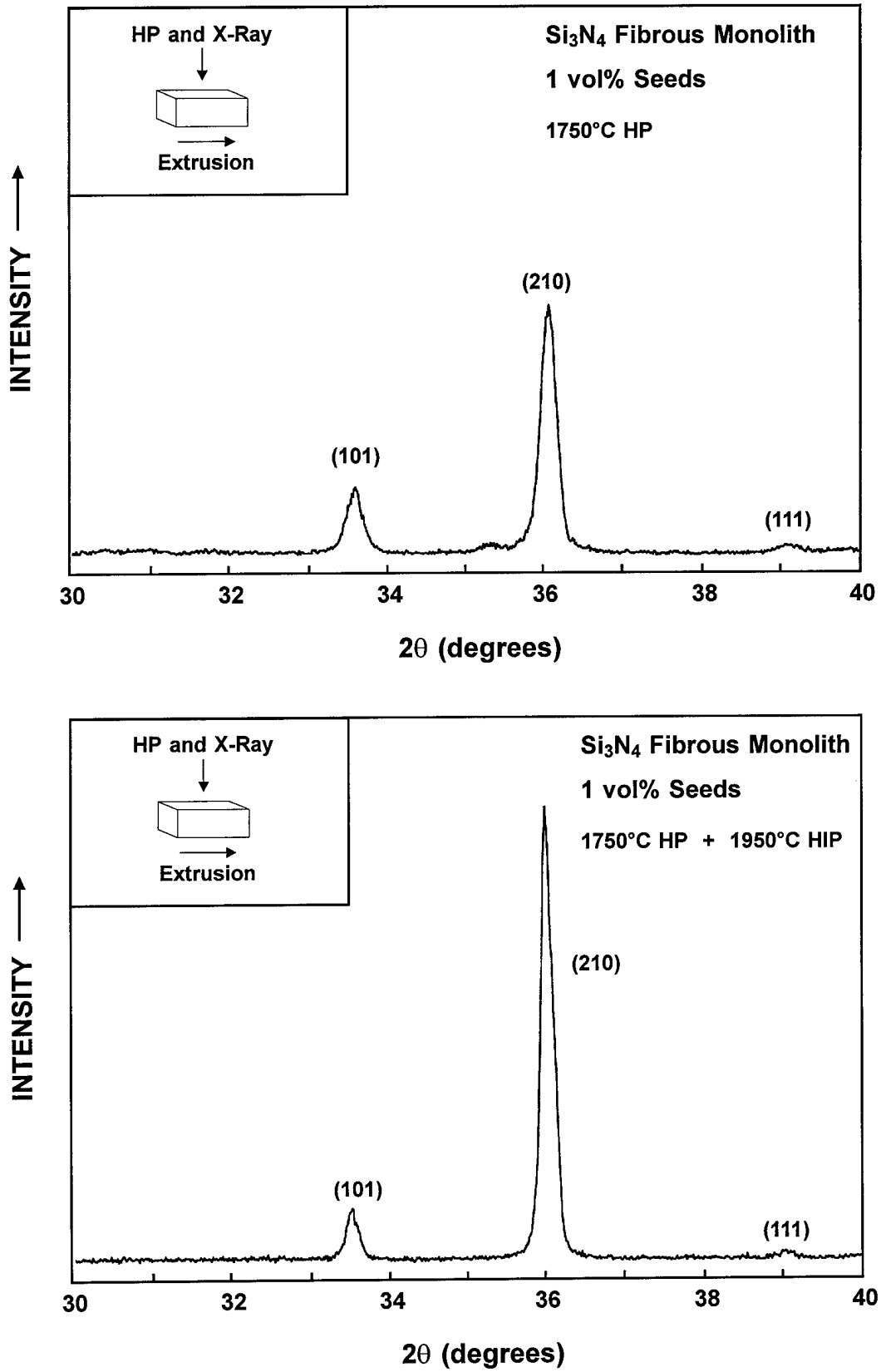

Figure 45. XRD spectra for 1750°C (top) and 1950°C (bottom) samples prepared with 1% Si_3N_4 whisker seeds. Measurements were made from the surface parallel to the extrusion direction and perpendicular to the hot pressing direction.

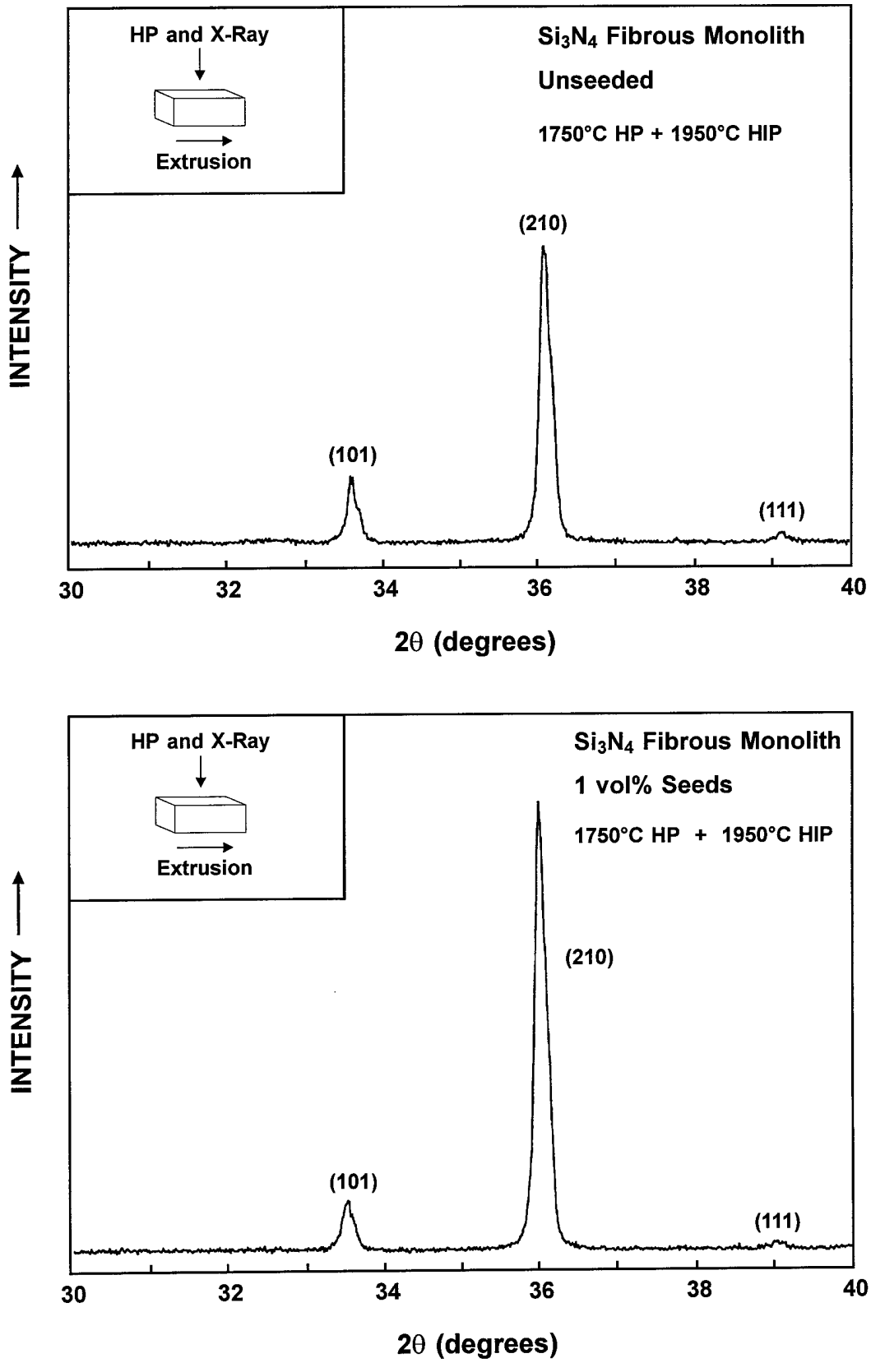

Figure 46. XRD spectra for 1950°C samples without (top) and with (bottom) 1% Si_3N_4 whisker seeds. Measurements were made from the surface parallel to the extrusion direction and perpendicular to the hot pressing direction.

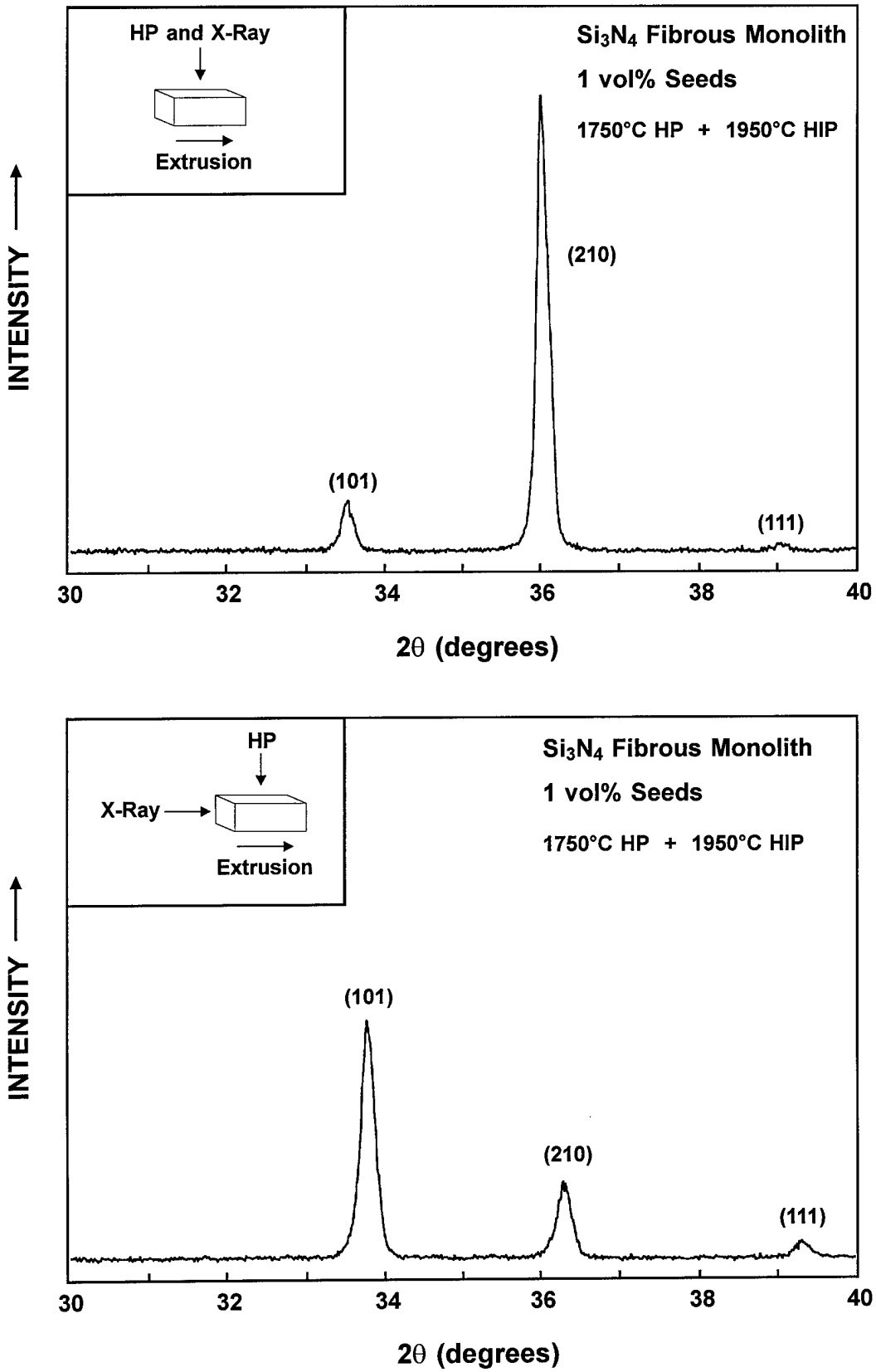

Figure 47. XRD spectra for the seeded (1% Si_3N_4 whiskers) 1950°C sample. Measurements were made from the surface parallel to the extrusion direction and perpendicular to the hot pressing direction (top) and the surface perpendicular to the extrusion direction and parallel to the hot pressing direction (bottom).

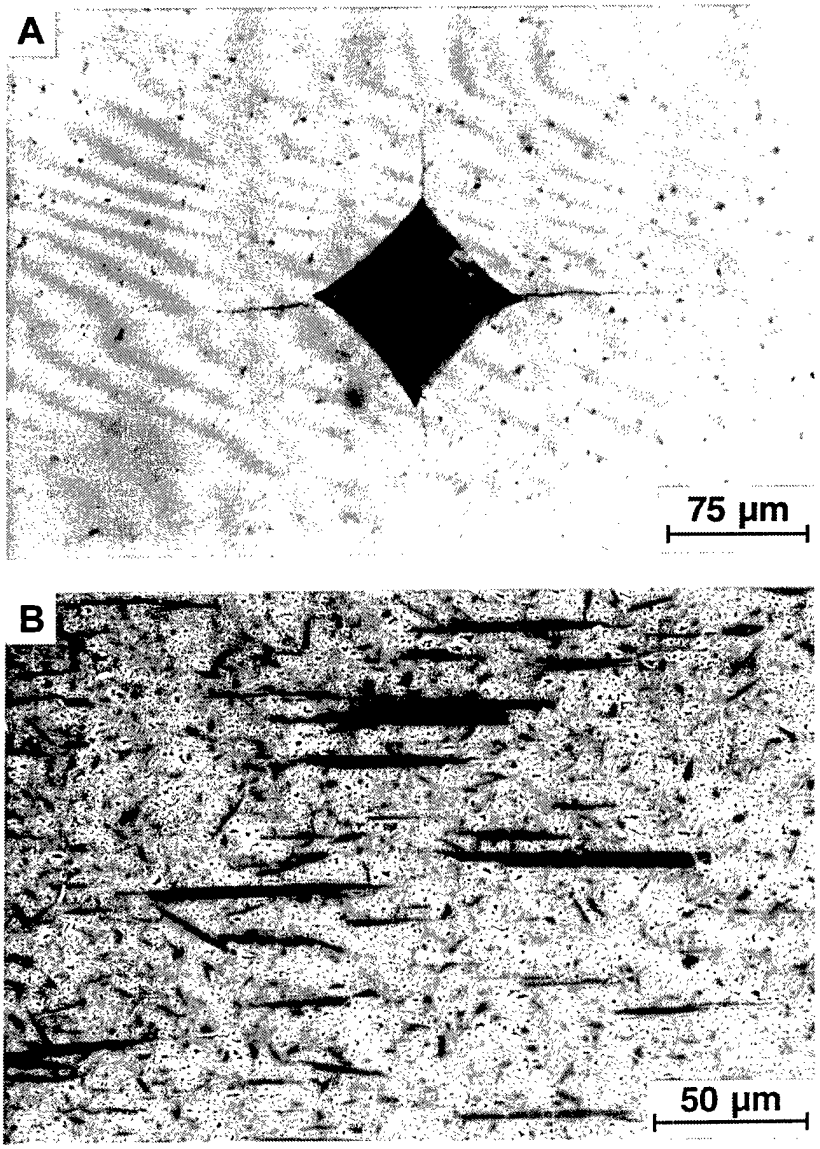

Figure 48. (A) Unetched optical micrograph of a polished section showing the crack extension anisotropy from an indentation in the seeded (1% Si_3N_4 whiskers) 1950°C sample. (B) Etched SEM micrograph of the same polished section in (A) showing the large, oriented, rodlike Si_3N_4 grains in the seeded 1950°C.

4.0 REFERENCES

1. P.F. Becher, "Microstructural Design of Toughened Ceramics," J. Am. Ceram. Soc., 74 [2] 255-269 (1991).

2. P.F. Becher and G.C. Wei, Toughening Behavior in SiC-Whisker-Reinforced Alumina," J. Am. Ceram. Soc., 67 [12] C-267 - C-269 (1984).

3. F.F. Lange, "Relation Between Strength, Fracture Energy, and Microstructure of Hot-Pressed Si_3N_4," Journal of the American Ceramic Society, 56 (10) 518-522 (1973).

4. A.J. Pyzik, and D.R. Beaman, "Microstructure and Properties of Self-Reinforced Silicon Nitride," J. Am. Ceram. Soc. 76 (11) 2737-2744 (1993).

5. C.W. Li, and J. Yamanis, "Super-Tough Silicon Nitride with R-Curve Behavior" Ceram. Eng. Sci. Proc., 10 [7-8] 632-645 (1989).

6. K. Matsuhiro, and T. Takahashi, "The Effect of Grain Size on the Toughness of Sintered Si_3N_4" Ceram. Eng. Sci. Proc., 10 [7-8] 807-816 (1989).

7. N. Hirosaki, and Y. Akimune, "Effect of Grain Growth of β-Silicon Nitride on Strength, Weibull Modulus, and Fracture Toughness," J. Am. Ceram. Soc., 76 (7) 1892-1894 (1993).

8. C.J. Hwang, S.M. Fuller, and D.R. Beaman, "Development of a High-Performance Si_3N_4 Material: Using Transient-Liquid-Phase and Self-Reinforcing Technology," Ceram. Eng. Sci. Proc., 15 [5] 685-693 (1994).

9. K. Hirao, T. Nagaoka, M. Brito, and S. Kanzaki, "Microstructure Control of Silicon Nitride by Seeding with Rodlike β-Silicon Nitride Particles," J. Am. Ceram. Soc., 77 [7] 1857-1862 (1994).

10. K. Hirao, M. Ohashi, M.E. Brito, and S. Kanzaki, "A Processing Strategy for Producing High Anisotropic Silicon Nitride," J. Am. Ceram. Soc., 78 (6) 1687-1690 (1995).

11. D. Muscat, M.D. Pugh, and R.A.L. Drew, "Pressureless Sintering of an Extruded Si_3N_4 Whisker-Reinforced Composite"; pp. 137-143 in Advanced Composite Materials, Ceramic Transactions, Vol. 19. Edited by M.D. Sacks. American Ceramic Society, Westerville, OH, 1991.

12. D.A. Warner, K.A. Warner, D.J. Jensen, and O.T. Sorensen, "Orientation of Platelet Reinforcements in Ceramic Matrix Composites Produced by Pressure Filtration," Ceram. Eng. Sci. Proc. 13 [7-8] 172-179 (1992).

13. Y. Goto, and A. Tsuge, "Mechanical Properties of Unidirectionally Oriented SiC-Whisker-Reinforced Si_3N_4 Fabricated by Extrusion and Hot-Pressing," J. Am. Ceram. Soc., 76 [6] 1420-1424 (1993).

14. M. Farkash, N. Shafry, and D.G. Brandon, "SiC-Whisker-Reinforced Ceramics with Modulated Microstructures," Mater. Sci. Eng. A, 177 277-281 (1994).

15. D. Kragness, M.F. Amateau, and G.L. Messing, "Processing and Characterization of Laminated SiC Whisker Reinforced Al_2O_3," J. Composite Mater., 25 417-432 (1991).

16. Y.S. Chou, and D.J. Green, "Silicon Carbide Platelet/Alumina Composites: I, Effect of Forming Technique on Platelet Orientation," J. A. Ceram. Soc., 75 (12) 3346-3352 (1992).

17. T. Hansson, R. Warren, and J. Wasén, "Fracture Toughness Anisotropy and Toughening Mechanisms of a Hot-pressed Alumina Reinforced with Silicon Carbide Whiskers," J. Am. Ceram. Soc., 76 (4) 841-848 (1993).

18. Y. Zhou, J. Vleugels, and O. Van der Biest, "Toughening ox X-Sialon with Al_2O_3 Platelets"; pp. 294-297 in 5th International Symposium on Ceramic Materials and Components for Engines. Edited by D.S Yan, X.R. Fu, and S.X. Shi. World Scientific Publishing Co., Singapore, 1995.

19. H. Igarashi, K. Matsunaga, T. Taniai, and K. Okazaki, "Dielectric and Piezoelectric Properties of Grain-Oriented $PbBi_2Nb_2O_9$ Ceramics," Am. Ceram. Soc. Bull., 57 (9) 815-817 (1978).

20. F. Lee, and K.J. Bowman, "Texture and Anisotropy in Silicon Nitride," J. Am. Ceram. Soc., 75 (7) 1748-1755 (1992).

21. L.M. Russell, L.F. Johnson, D.P.H. Hasselman, and R. Ruh, "Thermal Conductivity/Diffusivity of Silicon Carbide Whisker Reinforced Mullite," J. Am. Ceram. Soc., 70 [10] C-226 - C-229 (1987).

22. T. Takenaka, and K. Sakata, "Grain Orientation and Electrical Properties of Hot-Forged $Bi_4Ti_3O_{12}$ Ceramics," Jap. J. Applied Phys., 19 (1) 31-39 (1980).

23. H. Kukamura, K. Togano, H. Maeda, J. Kase, and T. Morimoto, "Anisotropy of Critical Current Density in Textured $Bi_2Sr_2Ca_1Cu_2O_x$ Tapes," Appl. Phys. Lett., 58 [24] 2830-2832 (1991).

24. M. Granahan, M. Holmes, and W.A. Schulze, and R.E. Newnham, "Grain-Oriented $PbNb_2O_6$ Ceramics," J. Am. Ceram. Soc., 64 (4) C-68 - C-69 (1981).

25. H. Watanabe, T. Kimura, and T. Yamaguchi, "Particle Orientation During Tape Casting in the Fabrication of Grain-Oriented Bismuth Titanate," J. Am. Ceram. Soc., 72 [2] 289-293 (1989).

26. H. Watanabe, T. Kimura, and T. Yamaguchi, "Sintering of Platelike Bismuth Titanate Powder Compacts with Preferred Orientation," J. Am. Ceram. Soc., 74 [1] 139-147 (1991).

27. J.L. Pentecost, and C.H. Wright, "Preferred Orientation in Ceramic Materials Due to Forming Techniques"; pp. 174-181 in Advances in Xray Analysis, Vol. 7. Edited by W.M. Mueller, G.R. Mallett, and M. Fay. Plenum Press, New York, NY, 1964.

28. M.S. Sandlin, and K.J. Bowman, "Textures in AlN-SiC Composite Ceramics"; pp. 263-269 in Mat. Res. Soc. Symp. Proc., Vol. 327, Materials Research Society, 1994.

29. M.S. Sandlin and K.J. Bowman, "Green Body Processing Effects on SiC Whisker Textures in Alumina Matrix Composites," Ceram. Eng. Sci. Proc., 13 [9-10] 661-668 1992.

30. M. Wu and G.L. Messing, "Fabrication of Oriented SiC-Whisker-Reinforced Mullite Matrix Composites by Tape Casting," J. Am. Ceram. Soc., 77 (10) 2586-2592 (1994).

31. D. Brandon, D. Chen, and H. Chan, "Control of Texture in Monolithic Alumina," Mat. Sci. Eng. A, 195 189-196 (1995).

32. M. Farkash and D.G. Brandon, "Whisker Alignment by Slip Extrusion," Mat. Sci. Eng. A, 177 269-275 (1994).

33. T. Yamaguchi and H. Kosha, "Sintering of Acicular Iron Oxide," J. Am. Ceram. Soc., 65 [5] C-84 - C-85 (1981).

34. D. Muscat, M.D. Pugh, and R.A.L. Drew, "Microstructure of an Extruded β-Silicon Nitride Whisker-Reinforced Silicon Nitride Composite," J. Am. Ceram. Soc., 75 [10] 2713-2718 (1992).

35. R.A. Cutler and T.B. Jackson, "Liquid Phase Sintered Silicon Carbide," pp. 309-318 in Third International Symposium on Ceramic Materials and Components for Engines. Edited by V.J. Tennery. American Ceramic Society, Westerville, OH, 1989.

36. D. Kim and C.H. Kim, "Toughening Behavior of Silicon Carbide with Additions of Yttria and Alumina," J. Am. Ceram. Soc., 73 [5] 1431-1434 (1990).

37. N.P. Padture, "In Situ-Toughened Silicon Carbide," J. Am. Ceram. Soc., 77 [2] 519-523 (1994).

38. L.S. Sigl and H.-J. Kleebe, "Core/Rim Structure of Liquid-Phase-Sintered Silicon Carbide," J. Am. Ceram. Soc., 76 [3] 773-776 (1993).

5.0 PUBLICATIONS/PATENTS

Publications

M.D. Sacks, G.W. Scheiffele, G.A. Staab, "Fabrication of Textured Silicon Carbide Via Seeded Anisotropic Grain Growth," J. Am. Ceram. Soc., 79 [6] 1611-1616 (1996).

M.D. Sacks, "In-Situ Processing of Silicon Carbide Fibers and Bulk Materials," to be published in the proceedings of the 6th International Symposium on Ceramic Materials & Components for Engines, October 19-22, 1997, Arita, Japan.

M.D. Sacks, G.W. Scheiffele, L. Zhang, Y. Yang, and J.J. Brennan, "Polymer-Derived SiC-Based Fibers with High Tensile Strength and Improved Creep Resistance," to be published in Ceram. Eng. Sci. Proc., Vol. 19 (1998).

Manuscripts in Preparation

G.A. Staab and M.D. Sacks, "Microstructure Evolution in Textured SiC Fabricated by Seeded Anisotropic Grain Growth," manuscript in preparation.

G.A. Staab, "Effect of Processing Variables on Microstructure Development in Textured SiC Fabricated by Seeded Anisotropic Grain Growth," M.S. thesis in preparation.

Inventions Disclosures/Patents

"Method for Preparing Textured Silicon Carbide Materials," Invention disclosure (May 1995), UF #1382.

"Method for Preparing Textured Silicon Carbide Fibers," Invention disclosure (May 1995), UF #1383.

"Silicon Carbide Fibers with Boron Nitride Coatings," Invention disclosure (December 1996), UF #1656; Patent application filed in August, 1997.

"Creep-Resistant, High-Strength Silicon Carbide Fibers," Invention disclosure (March 1997), UF #1686; Patent application filed in August, 1997.

6.0 APPENDIX

Reprint: "Fabrication of Textured Silicon Carbide Via Seeded Anisotropic Grain Growth," J. Am. Ceram. Soc., 79 [6] 1611-1616 (1996).

Preprint: M.D. Sacks, "In-Situ Processing of Silicon Carbide Fibers and Bulk Materials," to be published in the proceedings of the 6th International Symposium on Ceramic Materials & Components for Engines, October 19-22, 1997, Arita, Japan.

Preprint: M.D. Sacks, G.W. Scheiffele, L. Zhang, Y. Yang, and J.J. Brennan, "Polymer-Derived SiC-Based Fibers with High Tensile Strength and Improved Creep Resistance," to be published in Ceram. Eng. Sci. Proc., Vol. 19 (1998).

journal

Reprinted from the Journal of the American Ceramic Society, Vol. 79, No. 6, June 1996

J. Am. Ceram. Soc., 79 [6] 1611–16 (1996)

Fabrication of Textured Silicon Carbide via Seeded Anisotropic Grain Growth

Michael D. Sacks,* Gary W. Scheiffele, and Greg A. Staab

Ceramics Division, Department of Materials Science and Engineering, University of Florida, Gainesville, Florida 32611

Highly textured silicon carbide was fabricated via anisotropic grain growth. Large, platelike grains were grown from a fine-grained sintered matrix which had been seeded with ≤2% SiC platelets. The seeds were initially incorporated with preferred orientation during the green-state forming process and this resulted in oriented growth of the platelike grains. The development of texture in the samples was evident from microstructure observations and X-ray diffraction analysis.

I. Introduction

THE development of anisotropic grain structures in ceramics and composites can result in improved physical properties. For example, increases in fracture toughness have been achieved when ceramic matrices are reinforced with rodlike or platelike grains.[1–21] However, it is often difficult to achieve high relative density (low porosity) by pressureless sintering techniques if the samples are fabricated using powders which contain whisker or platelet additions. This is largely because the anisotropic particles tend to form continuous networks which constrain densification of the matrix phase. Hence, hot pressing is often used to achieve high relative densities. An alternative processing approach involves growing the anisotropic particles *in situ*, i.e., after the sample has been substantially densified by pressureless sintering. This method has been very successful in producing silicon nitride-, SiAlON-, and silicon carbide-based ceramics with high strength and high fracture toughness.[3–13] The morphology of the anisotropic grains produced by *in situ* processing methods depends on many factors, including the characteristics of the starting powder, type and concentration of second-phase additives, heat treatment conditions, etc. In silicon nitride, it has been demonstrated that the incorporation of small amounts of rod-shaped silicon nitride particles in the starting powder promotes the formation of relatively large concentrations of elongated grains in the sintered microstructures.[9,10]

Microstructural texture is often developed in materials with anisotropic grain structures. This results in bulk samples which have orientation-dependent properties (e.g., mechanical, electrical, thermal, etc.).[2–4,14–18,20–27] There are several mechanisms for texture development in materials fabricated from powders which initially contain anisotropic particles. In many cases, the anisotropic particles become oriented in preferred directions due to nonisotropic applied stresses during powder consolidation/shape forming operations such as extrusion, tape casting, slip casting, dry pressing, etc.[10,14–19,27–38] This orientation is usually retained during subsequent sintering operations. Preferred orientation can also develop during heat treatment. For example, textured materials are commonly produced by rotation of the rigid anisotropic particles under applied stresses during high-temperature consolidation and deformation of bulk compacts (e.g., hot pressing, hot forging, etc.).[2–4,17–25,31] It has also been observed that texture can develop via anisotropic grain growth.[14,29,31,34,37,38] Watanabe[29] prepared compacts from platelike bismuth titanate particles which developed a preferred orientation during the initial forming operation (i.e., tape casting and lamination). The degree of orientation showed little change as compacts densified during sintering. However, with additional heat treatment (higher temperatures or longer times), there was a significant increase in the degree of orientation which coincided with observations of anisotropic grain growth. Sandlin and Bowman[31] prepared AlN/15–30 vol% SiC platelets in which the platelets were oriented during the green forming operation. The AlN matrix initially developed some basal plane texture when the composite samples were uniaxially hot-pressed to high relative density. The degree of preferred orientation for the AlN increased substantially during subsequent (pressureless) annealing at higher temperatures, but only in samples which contained the oriented SiC platelets. This suggested that the platelets induced anisotropic grain growth in the AlN matrix. Drew *et al.*[14,37] observed texture development during sintering of β′-SiAlON samples which were processed with 15 vol% β-Si_3N_4 whiskers that were oriented during the green forming (extrusion) operation. During sintering, the matrix grains showed preferential growth in the direction of the whiskers. Brandon *et al.*[34] observed extensive texture development in alumina samples prepared with 5–10 vol% of alumina platelets that were aligned during tape casting. Texture development was associated with the growth of the seed platelets into the surrounding fine-grained matrix during heat treatment. Sabol *et al.*[38] developed textured alumina fibers using boehmite sols which contained 5 wt% acicular α-Fe_2O_3 particles. These particles were aligned during fiber drawing and subsequently acted as seeds for oriented growth of platelike α-Al_2O_3 grains during heat treatment.

In this paper, we report the fabrication of highly textured bulk SiC samples via anisotropic grain growth which was seeded by very low concentrations (≤2%) of SiC platelets. The platelets were initially oriented during the green body forming operation. Similar work has recently been reported for silicon nitride[10] and has been suggested for mullite.[39]

II. Experimental Procedure

Samples were prepared using SiC powder (A-2, Showa Denka K.K., Tokyo, Japan), SiC platelets (C-Axis Technology Co., Scottsdale, AZ), carbon black powder (Special Black 250, Degussa Corp., Ridgefield, Park, NJ), and boron powder (Alfa Aesar/Johnson Matthey Co., Ward Hill, MA). (Carbon and boron are conventional sintering aids for SiC.)

D. J. Green—contributing editor

Manuscript No. 192263. Received October 10, 1995; approved January 23, 1996.
Supported by the Advanced Research Projects Agency through Air Force Office of Scientific Research Grant No. F49620-94-1-0429.
*Member, American Ceramic Society.

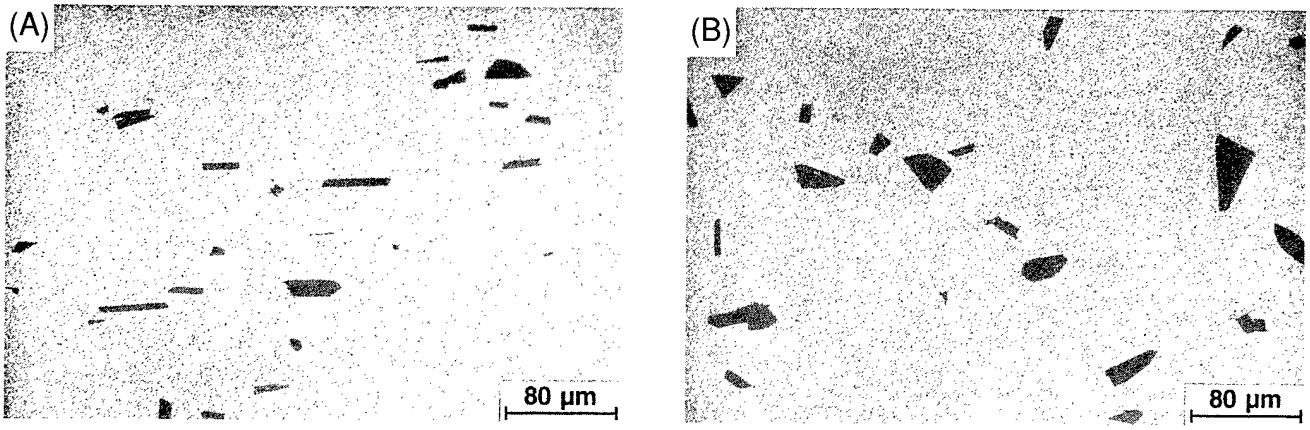

Fig. 1. SEM micrographs of polished sections taken (A) perpendicular and (B) parallel to the casting surface for a presintered (1480°C) sample containing ~2% platelets.

X-ray diffraction (XRD) showed that the SiC powder consisted mostly of the 6H polytype (hexagonal α phase). The SiC powder was used either in the as-received condition or after fractionation by fluid classification (i.e., in order to remove hard aggregates). Particle size analysis by a centrifugal photosedimentation method (Model CAPA-700, Horiba Instruments, Inc., Irvine, CA) showed that the as-received powder had a median Stokes diameter of ~0.4 μm and that ~85% of the particles were less than 1 μm. The fractionated powder had a median Stokes diameter of ~0.3 μm and ~95% of the particles were less than 1 μm.

The as-received carbon black and boron powders were fractionated by fluid classification in order to reduce particle sizes. The median Stokes diameters of the fractionated carbon black and boron powders were ~0.1 and ~0.45 μm, respectively. All powder compacts were processed using carbon and boron additions of 2.0% and 0.75%, respectively, based on the SiC powder weight.

Two grades of SiC platelets—"F" and "M"—were used in the as-received condition. The nominal average diameters were 17 and 24 μm, respectively, according to the manufacturer. XRD showed the platelets were mostly the 6H polytype,

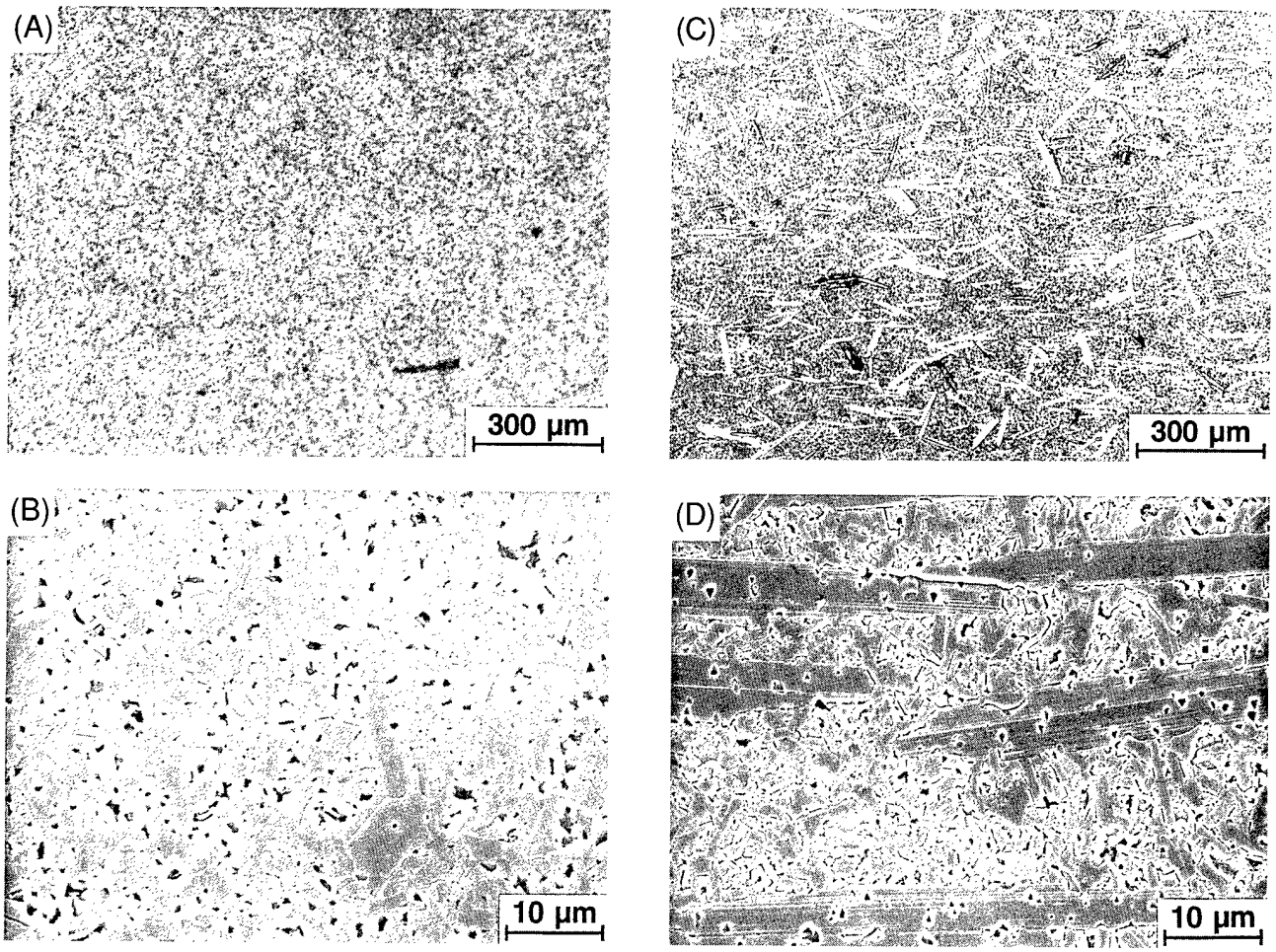

Fig. 2. Optical (top) and SEM (bottom) micrographs of polished and etched sections taken perpendicular to the casting surface for (A,B) unseeded and (C,D) seeded (~2% platelets) samples which were heat-treated at 2040°C.

although the 4H polytype was also present.[40] Electron diffraction showed that the hexagonal, close-packed basal planes were parallel with the plate faces (i.e., parallel with the large area dimension of the platelets).[40] Powder compacts were prepared with platelet additions of either 2.0% "F" grade or 0.2% "M" grade based on the SiC powder weight. (The volume percentages in the compact were 1.9% and 0.19% when the carbon and boron additions are included.) Samples prepared with the "F" platelets were processed using the fractionated SiC powder, while the as-received SiC powder was used for the samples prepared with the "M" platelets.

Powder compacts were prepared by slip casting. Well-dispersed aqueous suspensions were prepared using ultrasonication to break down powder agglomerates and pH adjustment (to ~9–10) to provide electrostatic stabilization against flocculation. The solids loadings of the suspensions were in the range of 25–35%. Disk-shaped compacts were formed by casting the suspension into Teflon rings (~19 mm diameter) set upon plaster blocks. (A 0.22 μm cellulosic filter was placed between each Teflon ring and the plaster.) For samples prepared without platelets, suspension was poured into the mold all at once. In contrast, the samples containing platelets were prepared by sequential slip casting, i.e., each sample was formed by casting six thin layers in succession. This procedure was utilized to enhance the preferred orientation of the platelets in the green compacts. Previous studies have shown that the platelets in disk-shaped compacts prepared by slip casting (and pressure filtration) have a tendency to align with the plate surfaces perpendicular to the casting direction.[15,19,30,31] However, significant deviations from this alignment occur due to the complex fluid flow conditions during casting and consolidation.[15,19] Qualitative microscopy observations were made during the course of this investigation which indicated that platelet alignment was improved by using sequential casting of thin layers. After casting, samples were stored for at least 10 h in a chamber at room temperature (~20–25°C) with an air atmosphere having >90% relative humidity. Samples were subsequently oven-dried in air at ~80°C for at least 10 h. One of the compacts with ~2% platelets was "presintered" at 1480°C (2 h) in flowing argon. This provided a sample with sufficient handling strength for polishing and subsequent observations of the SiC platelets within the powder compact matrix. The other samples were directly heat-treated for 30 min at temperatures in the range of ~2040–2360°C in flowing argon using a graphite element furnace.

Densities of sintered samples were determined using the Archimedes method with ethanol as the liquid medium. The samples were polished by conventional ceramographic techniques to a 0.25 μm finish. Samples were subsequently etched using boiling Murakami's solution (1:1:2.5 weight ratio of $K_3Fe(CN)_6$:NaOH:H_2O). Microstructures were observed using optical and scanning electron microscopies. The lengths, widths, and volume fraction of the SiC platelets were measured for selected heat-treated samples. (The platelet volume fraction was determined by the point count method.[41])

X-ray diffraction (XRD) measurements were carried out on the heat-treated bulk samples. The bottom surfaces of the samples were ground to a 30 μm finish prior to the analysis.

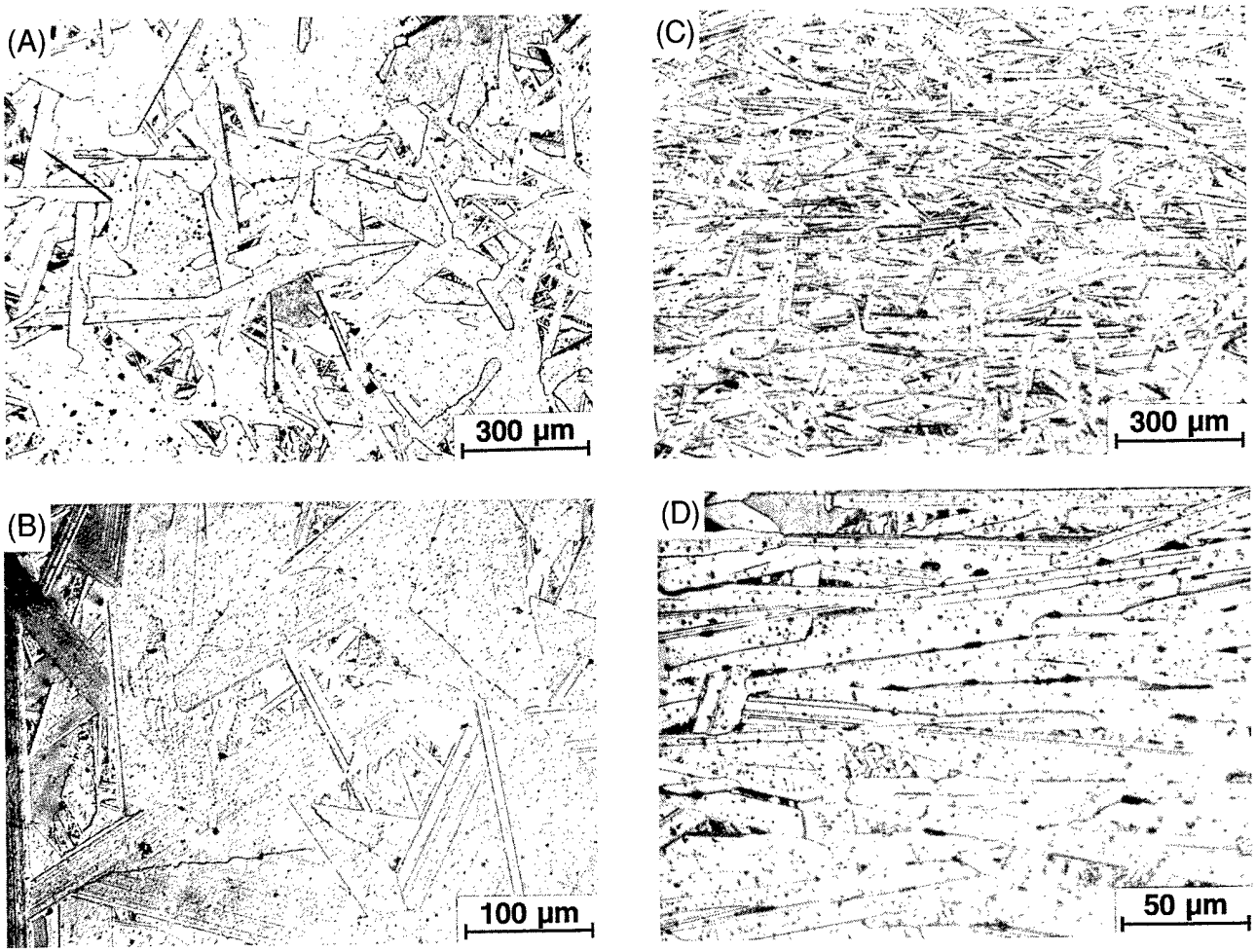

Fig. 3. Optical micrographs of polished and etched sections taken perpendicular to the casting surface for (A,B) unseeded and (C,D) seeded (~2% platelets) samples which were heat-treated at 2360°C.

Measurements were made using Ni-filtered Cu$K\alpha$ radiation and a scanning rate of 3°/min.

III. Results and Discussion

Figure 1 shows SEM micrographs which illustrate alignment of platelets ("F" grade) in a compact which was "presintered" at 1480°C (2 h). A polished section taken perpendicular to the casting surface (Fig. 1(A)) shows mostly platelet edges, while a section taken parallel to the casting surface (Fig. 1(B)) shows mostly platelet faces.

Stereological measurements were carried out on the 1480°C sample using the polished section taken perpendicular to the casting surface. (Eight randomly selected fields were used for analyses.) The measured volume fraction of platelets was 1.9%, which is in excellent agreement with the expected amount from the starting powder composition. The average length and width of the platelets were 16.0 and 5.5 μm, respectively, based on ~250 measurements. (Standard deviations were 8.0 and 2.4 μm, respectively.)

Platelet additions had no significant effect on the sintered densities. Samples prepared with and without ~2% "F" platelets were initially sintered at ~2040°C. The measured bulk densities were 3.13 and 3.10 g/cm^3, respectively. A portion of each sample was subsequently heat-treated at ~2360°C. The measured bulk densities were 3.09 and 3.11 g/cm^3 for the samples with and without platelets, respectively. The calculated relative densities for these samples are all in the range of ~96–98% if the solid density is taken as the theoretical density for SiC (i.e., 3.21 g/cm^3). However, the actual solid densities are expected to be lower (and, hence, the relative densities would be higher) because the samples contain carbon and boron. (The precise relative densities could not be calculated because the residual amounts of carbon and boron after heat treatment were not determined.)

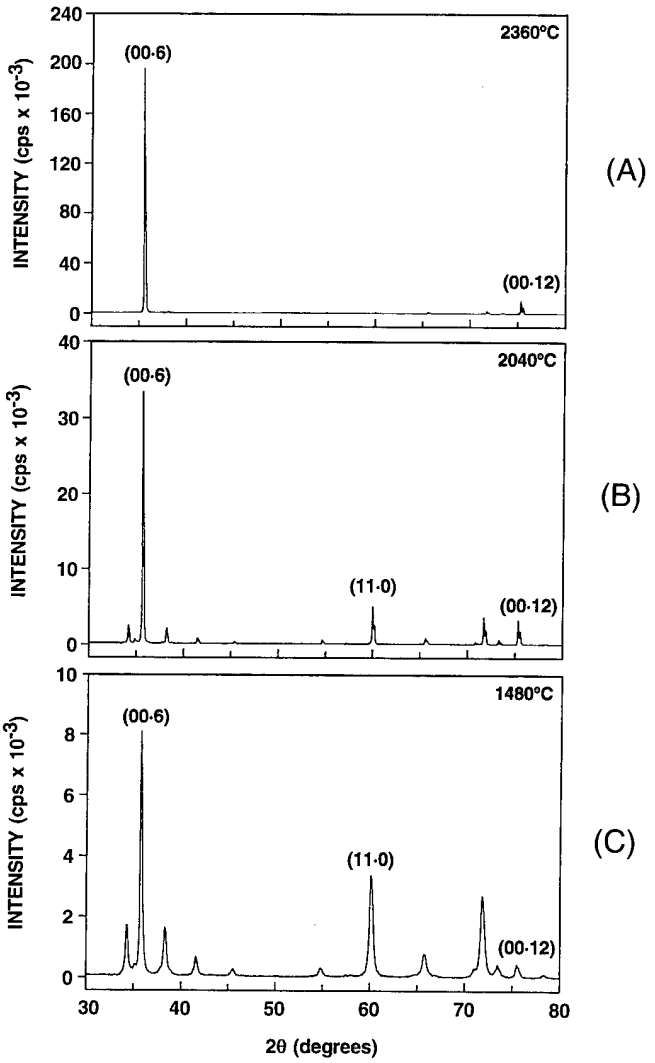

Fig. 4. XRD patterns for seeded (~2% platelets) samples which were heat-treated at (A) 2360°, (B) 2040°, and (C) 1480°C.

Figure 2 shows optical micrographs (lower magnification, Figs. 2(A) and (C)) and scanning electron micrographs (higher magnification, Figs. 2(B) and (D)) of the 2040°C heat-treated samples prepared with and without ~2% platelets. The microstructures are from polished sections taken perpendicular to the casting surface. The 2040°C sample without platelets has a relatively fine grain microstructure (Figs. 2(A) and (B)). Some larger, platelike grains have begun to develop (Fig. 2(B)), but these usually do not exceed 10 μm for any dimension. In addition, qualitative observations do not suggest any preferred orientation for the grains. Much of the porosity observed in this sample (and the other samples in the study) is due to the action of the chemical etchant, as aggressive etching conditions were used in order to show the grain boundaries clearly. The 2040°C sample prepared with ~2% platelets shows a significant increase in the amount and size of platelike grains (Figs. 2(C) and (D)). The volume fraction of these large grains (from stereological measurements) is ~26%. Many of the platelike grains are aligned with the major faces parallel to the casting surface, i.e., similar to that observed in the presintered compacts (Fig. 1(A)). This indicates that the large grains have developed by preferential (seeded) growth of the original platelets, i.e., in which the original platelets "consume" fine grains of the surrounding matrix. The average length and width of the platelets were 52.4 and 5.4 μm, respectively, based on measurements for ~430 particles. (Standard deviations were 31.8 and 3.3 μm, respectively.) From a comparison with the platelet dimensions obtained for the 1480°C sample, it is evident that the dominant growth direction was in the plane of the platelet faces (i.e., the close-packed basal planes of the hexagonal α-SiC). The formation of platelike grains via preferred growth along the basal planes is typical for sintered α-SiC.[42,43]

The 2040°C samples shown in Fig. 2 were given further heat treatment to ~2360°C. Figure 3 shows optical micrographs from polished sections taken perpendicular to the original casting surface. Both samples have undergone extensive growth of the platelike grains. However, the unseeded sample does not show any obvious orientation of the grains, as both the faces and edges of the grains are observed in Figs. 3(A) and (B). In contrast, it is evident that the platelet-seeded sample is highly textured (Figs. 3(C) and (D)). Many of the platelike grains are stacked nearly parallel to the casting surface, i.e., similar to the original orientation of the platelets in the green compacts.

The preferred orientation in the platelet-seeded samples was also shown from XRD measurements. Figure 4 shows XRD patterns for the 1480°, 2040°, and 2360°C samples. The predominant phase in each case is the 6H polytype, although some 4H polytype was evident in the 2040° and 2360°C samples. The XRD pattern for the presintered 1480°C sample (Fig. 4(C)) is

Table I. Effect of Seeding and Heat Treatment Temperature on (00·6)/(11·0) XRD Peak Intensity Ratios

Platelet seeds	Temperature (°C)	$I_{(00\cdot6)}/I_{(11\cdot0)}$
None	1480	1.8
None	2040	1.1
None	2360	0.9
2% "F"	1480	2.3
2% "F"	2040	7.7
2% "F"	2360	191
0.2% "M"	2250	18.3

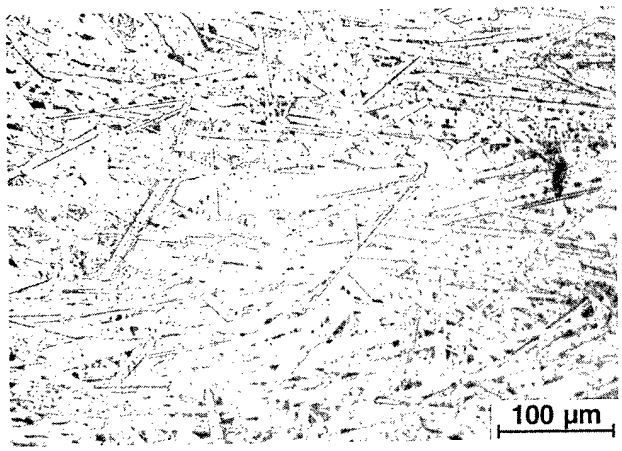

Fig. 5. Optical micrograph of a polished and etched section taken perpendicular to the casting surface for a sample seeded with only ~0.2% platelets and heat-treated at 2250°C.

nearly identical to the pattern for the starting SiC powder (not shown in Fig. 4). In contrast, the pattern for the 2040°C sample (Fig. 4(B)) shows sharp increases in intensities for the (00·*l*) reflections, i.e., the (00·6) and (00·12) close-packed basal planes for the 6H polytype. (Note the changes in the intensity scale in Fig. 4(B).) This result indicates that a significant portion of the faces of the platelike grains are parallel to the XRD measurement surface of the sample. (As indicated earlier, the XRD measurements were taken from bottom surfaces of the samples.) The XRD results show even more pronounced preferred orientation in the platelet-seeded 2360°C sample (Fig. 4(A)). The peak intensities arising from the (00·*l*) reflections again show sharp increases. Only the (00·6) and (00·12) reflections are visible for the scale used in Fig. 4(A). (Again, note the increase in values for the abscissa.) Although not shown in Fig. 4(A), the third most intense peak was from the 00·18 reflection (at $2\theta \approx 134°$).

The differences in preferred orientation between the seeded and unseeded samples can be quantified by comparing ratios of the peak intensities for the 00·6 basal plane/11·0 prism plane. Table I shows that the ratio increases rapidly with heat treatment for the seeded samples, while there is relatively little change for the unseeded samples.

Significant texture also developed for a sample prepared with only 0.2% "M" platelets. This is illustrated in Fig. 5, which shows an optical micrograph of a polished section of a sample sintered at ~2250°C. (The bulk density for this sample was 3.14 g/cm^3. As noted earlier, most of the porosity arises from chemical etching.) The preferred orientation was also confirmed by XRD. Table I shows that the (00·6)/(11·0) peak intensity ratio was 18.3.

IV. Conclusion

Highly textured silicon carbide samples were fabricated via oriented growth of platelike grains. The growth process was seeded using SiC platelets which were initially incorporated with preferred orientation during green-state processing of SiC powder compacts. During heat treatment, the platelet seeds grew rapidly by consuming the fine grains of the surrounding sintered SiC matrix. The dominant growth direction was in the close-packed hexagonal basal planes of the SiC platelets. Although the initial concentration of seeds was only ~0.2–2%, almost the entire sample consisted of large, oriented, platelike grains after heat treatment at temperatures ≥2250°C.

References

[1]P. F. Becher, "Microstructural Design of Toughened Ceramics," *J. Am. Ceram. Soc.*, **74** [2] 255–69 (1991).

[2]P. F. Becher and G. C. Wei, "Toughening Behavior in SiC-Whisker-Reinforced Alumina," *J. Am. Ceram. Soc.*, **67** [12] C-267–C-269 (1984).

[3]F. F. Lange, "Relation Between Strength, Fracture Energy, and Microstructure of Hot-Pressed Si_3N_4," *J. Am. Ceram. Soc.*, **56** [10] 518–22 (1973).

[4]A. J. Pyzik and D. R. Beaman, "Microstructure and Properties of Self-Reinforced Silicon Nitride," *J. Am. Ceram. Soc.*, **76** [11] 2737–44 (1993).

[5]C. W. Li and J. Yamanis, "Super-Tough Silicon Nitride with *R*-Curve Behavior," *Ceram. Eng. Sci. Proc.*, **10** [7–8] 632–45 (1989).

[6]K. Matsuhiro and T. Takahashi, "The Effect of Grain Size on the Toughness of Sintered Si_3N_4," *Ceram. Eng. Sci. Proc.*, **10** [7–8] 807–16 (1989).

[7]N. Hirosaki and Y. Akimune, "Effect of Grain Growth of β-Silicon Nitride on Strength, Weibull Modulus, and Fracture Toughness," *J. Am. Ceram. Soc.*, **76** [7] 1892–94 (1993).

[8]C. J. Hwang, S. M. Fuller, and D. R. Beaman, "Development of a High-Performance Si_3N_4 Material: Using Transient-Liquid-Phase and Self-Reinforcing Technology," *Ceram. Eng. Sci. Proc.*, **15** [5] 685–93 (1994).

[9]K. Hirao, T. Nagaoka, M. Brito, and S. Kanzaki, "Microstructure Control of Silicon Nitride by Seeding with Rodlike β-Silicon Nitride Particles," *J. Am. Ceram. Soc.*, **77** [7] 1857–62 (1994).

[10]K. Hirao, M. Ohashi, M. E. Brito, and S. Kanzaki, "A Processing Strategy for Producing High Anisotropic Silicon Nitride," *J. Am. Ceram. Soc.*, **78** [6] 1687–90 (1995).

[11]S. K. Lee. Y. C. Kim, and C. H. Kim, "Microstructural Development and Mechanical Properties of Pressureless-Sintered SiC with Plate-like Grains Using Al_2O_3–Y_2O_3 Additives," *J. Mater. Sci.*, **29**, 5321–26 (1994).

[12]M. A. Mulla and V. D. Kristic, "Mechanical Properties of β-SiC Pressureless Sintered with Al_2O_3 Additions," *Acta Metall. Mater.*, **42** [1] 303–308 (1994).

[13]N. P. Padture, "*In-Situ*-Toughened Silicon Carbide," *J. Am. Ceram. Soc.*, **77** [2] 519–23 (1994).

[14]D. Muscat, M. D. Pugh, and R. A. L. Drew, "Pressureless Sintering of an Extruded Si_3N_4 Whisker-Reinforced Composite"; pp. 137–43 in Ceramic Transactions, Vol. 19, *Advanced Composite Materials*. Edited by M. D. Sacks. American Ceramic Society, Westerville, OH, 1991.

[15]D. A. Warner, K. A. Warner, D. J. Jensen, and O. T. Sorensen, "Orientation of Platelet Reinforcements in Ceramic Matrix Composites Produced by Pressure Filtration," *Ceram. Eng. Sci. Proc.*, **13** [7-8] 172–79 (1992).

[16]Y. Goto and A. Tsuge, "Mechanical Properties of Unidirectionally Oriented SiC-Whisker-Reinforced Si_3N_4 Fabricated by Extrusion and Hot-Pressing," *J. Am. Ceram. Soc.*, **76** [6] 1420–24 (1993).

[17]M. Farkash, N. Shafry, and D. G. Brandon, "SiC-Whisker-Reinforced Ceramics with Modulated Microstructures," *Mater. Sci. Eng. A*, **177**, 277–81 (1994).

[18]D. Kragness, M. F. Amateau, and G. L. Messing, "Processing and Characterization of Laminated SiC Whisker Reinforced Al_2O_3," *J. Compos. Mater.*, **25**, 417–32 (1991).

[19]Y. S. Chou and D. J. Green, "Silicon Carbide Platelet/Alumina Composites: I, Effect of Forming Technique on Platelet Orientation," *J. Am. Ceram. Soc.*, **75** [12] 3346–52 (1992).

[20]T. Hansson, R. Warren, and J. Wasén, "Fracture Toughness Anisotropy and Toughening Mechanisms of a Hot-Pressed Alumina Reinforced with Silicon Carbide Whiskers," *J. Am. Ceram. Soc.*, **76** [4] 841–48 (1993).

[21]Y. Zhou, J. Vleugels, and O. Van der Biest, "Toughening of X-Sialon with Al_2O_3 Platelets"; pp. 294–97 in *5th International Symposium on Ceramic Materials and Components for Engines*. Edited by D. S. Yan, X. R. Fu, and S. X. Shi. World Scientific Publishing Co., Singapore, 1995.

[22]H. Igarashi, K. Matsunaga, T. Taniai, and K. Okazaki, "Dielectric and Piezoelectric Properties of Grain-Oriented $PbBi_2Nb_2O_9$ Ceramics," *Am. Ceram. Soc. Bull.*, **57** [9] 815–17 (1978).

[23]F. Lee and K. J. Bowman, "Texture and Anisotropy in Silicon Nitride," *J. Am. Ceram. Soc.*, **75** [7] 1748–55 (1992).

[24]L. M. Russell, L. F. Johnson, D. P. H. Hasselman, and R. Ruh, "Thermal Conductivity/Diffusivity of Silicon Carbide Whisker Reinforced Mullite," *J. Am. Ceram. Soc.*, **70** [10] C-226–C-229 (1987).

[25]T. Takenaka and K. Sakata, "Grain Orientation and Electrical Properties of Hot-Forged $Bi_4Ti_3O_{12}$ Ceramics," *Jpn. J. Appl. Phys.*, **19** [1] 31–39 (1980).

[26]H. Kukamura, K. Togano, H. Maeda, J. Kase, and T. Morimoto, "Anisotropy of Critical Current Density in Textured $Bi_2Sr_2Ca_1Cu_2O_x$ Tapes," *Appl. Phys. Lett.*, **58** [24] 2830–32 (1991).

[27]M. Granahan, M. Holmes, W. A. Schulze, and R. E. Newnham, "Grain-Oriented $PbNb_2O_6$ Ceramics," *J. Am. Ceram. Soc.*, **64** [4] C-68–C-69 (1981).

[28]H. Watanabe, T. Kimura, and T. Yamaguchi, "Particle Orientation During Tape Casting in the Fabrication of Grain-Oriented Bismuth Titanate," *J. Am. Ceram. Soc.*, **72** [2] 289–93 (1989).

[29]H. Watanabe, T. Kimura, and T. Yamaguchi, "Sintering of Platelike Bismuth Titanate Powder Compacts with Preferred Orientation," *J. Am. Ceram. Soc.*, **74** [1] 139–47 (1991).

[30]J. L. Pentecost and C. H. Wright, "Preferred Orientation in Ceramic Materials Due to Forming Techniques"; pp. 174–81 in *Advances in X-ray Analysis*, Vol. 7. Edited by W. M. Mueller, G. R. Mallett, and M. Fay. Plenum Press, New York, 1964.

[31]M. S. Sandlin and K. J. Bowman, "Textures in AlN–SiC Composite Ceramics"; pp. 263–69 in Materials Research Society Symposia Proceedings, Vol. 327, *Covalent Ceramics II: Non-Oxides*. Edited by A. R. Barron, G. S. Fischman, M. A. Fury, and A. F. Hepp. Materials Research Society, Pittsburgh, PA, 1994.

[32]M. S. Sandlin and K. J. Bowman, "Green Body Processing Effects on SiC Whisker Textures in Alumina Matrix Composites," *Ceram. Eng. Sci. Proc.*, **13** [9–10] 661–68 (1992).

[33]M. Wu and G. L. Messing, "Fabrication of Oriented SiC-Whisker-Reinforced Mullite Matrix Composites by Tape Casting," *J. Am. Ceram. Soc.*, **77** [10] 2586–92 (1994).

[34]D. Brandon, D. Chen, and H. Chan, "Control of Texture in Monolithic Alumina," *Mater. Sci. Eng. A*, **195**, 189–96 (1995).

[35]M. Farkash and D. G. Brandon, "Whisker Alignment by Slip Extrusion," *Mater. Sci. Eng. A*, **177**, 269–75 (1994).
[36]T. Yamaguchi and H. Kosha, "Sintering of Acicular Iron Oxide," *J. Am. Ceram. Soc.*, **65** [5] C-84–C-85 (1981).
[37]D. Muscat, M. D. Pugh, and R. A. L. Drew, "Microstructure of an Extruded β-Silicon Nitride Whisker-Reinforced Silicon Nitride Composite," *J. Am. Ceram. Soc.*, **75** [10] 2713–18 (1992).
[38]S. M. Sabol, G. L. Messing, and R. E. Tressler, "Textured Alumina Fibers with Elongated Grains"; pp. 21-1–21-14 in NASA Conference Publication 10104, Vol. 1, NASA Hi-Temp Review. National Aeronautics and Space Administration, Cleveland, OH, October 27–28, 1992.
[39]S.-H. Hong, W. Cermignani, and G. L. Messing, "Anisotropic Grain Growth in Seeded and B_2O_3-Doped Diphasic Mullite Gels," *J. Eur. Ceram. Soc.*, in press.
[40]Y.-J. Lin and M. D. Sacks; unpublished results.
[41]E. E. Underwood, *Quantitative Stereology*. Addison Wesley, Reading, MA, 1970.
[42]C. A. Johnson and S. Prochazka, "Microstructures of Sintered SiC"; pp. 366–78 in *Ceramic Microstructures '76*. Edited by R. M. Fulrath and J. A. Pask. Westview Press, Boulder, CO, 1977.
[43]A. H. Heuer, G. A. Fryburg, L. U. Ogbuji, T. E. Mitchell, and S. Shinozaki, "β ⇒ α Transformation in Polycrystalline SiC: I, Microstructural Aspects," *J. Am. Ceram. Soc.*, **61** [9–10] 406–12 (1978). □

To be published in the proceedings of the 6th International Symposium on Ceramic Materials & Components for Engines, October 19-22, 1997, Arita, Japan.

IN-SITU PROCESSING OF SILICON CARBIDE FIBERS AND BULK MATERIALS

Michael D. Sacks

Department of Materials Science and Engineering
University of Florida, Gainesville, Florida 32611, USA

ABSTRACT

Silicon carbide (SiC) fibers and bulk materials were fabricated using *in-situ* processing methods. Highly textured bulk SiC samples were prepared using platelet-seeded grain growth. The seeds were initially incorporated with preferred orientation during green-state processing and this resulted in oriented growth of platelike grains. The grain growth behavior and microstructure development could be controlled using processing variables such as the matrix particle size, seed concentration, liquid-phase forming additives, etc. Fine-diameter SiC fibers with near-stoichiometric composition, low oxygen content, and high tensile strength were fabricated from organosilicon polymers. Fiber composition was controlled by using *in-situ* reactions during processing of the polymer-derived fibers. Fibers showed excellent strength retention and creep resistance after high temperature heat treatments.

INTRODUCTION

Silicon carbide (SiC) is an important material for high temperature applications due to properties such as good strength retention and creep resistance at elevated temperatures, high thermal conductivity, low specific gravity, etc. In this study, novel SiC fibers and bulk materials were fabricated using *in-situ* processing methods. Some of the potential advantages of *in-situ* processing methods (i.e., compared to conventional methods) include (i) improved control over microstructure development (e.g., to control phase development, develop novel microstructures, etc.), (ii) enhanced densification during sintering, and (iii) lower fabrication cost.

The development of anisotropic grain structures in ceramics and composites can result in improved physical properties. For example, increases in fracture toughness have been achieved when ceramic matrices are reinforced with rodlike or platelike grains.[1-12] However, it may be difficult to achieve high relative density (low porosity) by pressureless sintering if samples are fabricated using powders which contain moderate or high volume fractions of whiskers or platelets. Hence, a preferred approach involves growing the anisotropic particles *in-situ*, i.e, after the sample has been substantially densified.[3-12] *In-situ* growth of anisotropic grains can also be used to fabricate textured materials.[8,9,13-15] (Texturing allows the development of materials with anisotropic physical properties.) In the present study, anisotropic seed crystals (i.e., SiC platelets) were initially incorporated with preferred orientation in SiC powder green bodies using the shear forces applied during processing (e.g., during tape casting, slip casting, etc.). The oriented seed crystals were then used to promote controlled grain growth and *in-situ* microstructural texturing during heat treatment.

Ceramic-matrix composites with improved strength and fracture toughness at elevated temperatures have been produced by combining SiC-based continuous fibers with a variety of matrix materials, including glasses, glass-ceramics, and crystalline ceramics. Continuous SiC fibers with fine-diameter and high-strength are generally prepared using organosilicon ("pre-ceramic") polymers.[16-26] However, commercially-available polymer-derived fibers (e.g., Nicalon®, Nippon Carbon Co. and Tyranno®, Ube Industries, Ltd.) are not pure stoichiometric SiC, i.e., the fibers contain relatively high concentrations of excess carbon and oxygen. (In addition, Tyranno® fibers are actually Si-Ti-C-O fibers.) As a consequence, these fibers degrade extensively at high temperatures due to uncontrolled carbothermal reduction reactions between carbon and siliceous materials.[27-29] In order to produce polymer-derived SiC fibers with improved thermomechanical stability, recent investigations have been directed toward the fabrication of fibers with low oxygen content and/or with compositions closer to that of stoichiometric SiC.[18-26] In the present study, *in-situ* reactions were utilized to produced near-stoichiometric, low-oxygen-content SiC fibers with improved thermomechanical properties.

RESULTS AND DISCUSSION

Textured SiC via Platelet-Seeded Grain Growth

SiC seed particles (i.e., platelets) were aligned by casting processes (e.g., tape casting, slip casting) such that the major faces of the platelets were parallel to the casting surface (Fig. 1). Fine SiC powder compacts, doped with conventional boron and carbon sintering additives, were prepared with and without 2 wt% oriented seed platelets. Samples were sintered to ~96-99% of theoretical density at ~1950-2050°C. (The platelets had essentially no effect on densification due to their low concentration.) The platelets underwent only minimal growth during sintering, as porosity effectively pinned grain boundaries. Once the matrix was substantially densified, large grains developed by preferential (seeded) growth of the original platelets, i.e., in which the closed-packed basal planes of the hexagonal platelets grew by "consuming" fine grains of the surrounding matrix. Platelet growth occurred primarily by increases in length (rather than thickness) and the average platelet length/thickness ratio increased as a function of temperature (and platelet concentration) (Fig. 2). (Since the measurements in Fig. 2 were taken from samples which were sectioned perpendicular to the casting surface, the increases in length and aspect ratio are actually representative of two-dimensional growth of the major faces of the platelike grains.) At sufficiently high temperatures, the microstructure consisted almost entirely of large, oriented, platelike grains (Fig. 3B).

The driving force for growth of the platelet seeds increases with decreasing matrix particle size. Hence, experiments showed that the platelet growth kinetics was significantly enhanced by using finer matrix particle size (i.e., 0.2 μm vs. 0.45 μm). Platelet growth also depended on the seed concentration. The volume fraction of platelike grains, after a given heat treatment, increased with increasing seed concentration. It was also observed that the platelet length and platelet length/thickness ratio increased more rapidly with increasing platelet concentration when lower seed concentrations were used. This presumably reflects differences in the rate of impingement of growing grains. At lower seed concentrations, it is expected that seed-initiated platelike grains will grow to larger size prior to having their growth restricted by impingement with other large, growing platelike grains.

Textured bulk SiC was also fabricated by platelet-seeded isotropic grain growth in the presence of a liquid phase. 6 wt% alumina and 4 wt% yttria were used as liquid-phase sintering additives in tape-cast SiC samples prepared with 2% platelet seeds. Densification was enhanced with these additives, such that relative densities ≥96% were reached at ~1900°C, i.e., ~50-100°C lower than temperatures used for solid-state sintered samples prepared with boron and carbon additives. Significant platelet growth occurred with increasing heat treatment temperature (Fig. 4). The platelet length/thickness ratio remained approximately constant with increasing heat treatment temperature (Fig. 4). The liquid phase that forms in the alumina/yttria - doped samples apparently reduces interfacial energy anisotropy, thereby favoring isotropic growth (i.e., in contrast to the anisotropic growth in the solid-state sintered samples prepared with boron/carbon dopants). Platelet growth apparently occurs by solution-precipitation (i.e., dissolution of the fine SiC matrix grains and reprecipitation of SiC on the large seed platelets). This is indicated by the development of "core-rim" structures [30] comprised of the original platelet seed ("core") surrounded by the new growth ("rim") layer of SiC (Fig. 5A). Although the platelets grow isotropically, the sample still develops a strong preferred orientation because of the initial orientation of the seed particles.

As observed in other studies [12,31], higher fracture toughness values (~3-5 MPa•m$^{1/2}$ as determined by an indentation technique) were obtained with the alumina/yttria - doped samples compared to values obtained for the boron/carbon doped samples (~2-2.5 MPa•m$^{1/2}$). The increased toughness is attributed to increases in crack deflection and bridging due to modification of the SiC interfaces. Figure 5B shows the highly tortuous crack path for an alumina/yttria - doped sample.

SiC Fibers with Near-Stoichiometric Composition

The Si/C ratio in SiC fibers can be varied using *in-situ* processing routes. In one method, fibers were prepared using mixtures of polycarbosilane (PCS) and polymethylsilane (PMS). Upon pyrolysis, PCS decomposes to SiC plus excess carbon, while PMS decomposes to SiC plus excess silicon. The excess C and Si can be reacted *in-situ* to form new SiC by heat treating at higher temperatures. Another method for altering the Si/C ratio is based on using oxygenated PCS. Upon pyrolysis, the PCS decomposes to SiC plus excess carbon and siliceous phase (i.e., as silica and/or silicon oxycarbide). With further heat treatment at higher temperatures, additional SiC is formed *in-situ* by carbothermal reduction reactions between the carbon and siliceous phase. These reactions are accompanied by the evolution of volatiles (primarily CO and SiO) and the formation of porosity in the fibers. However, the porosity can be mostly eliminated by carrying out a sintering heat treatment at higher temperature.

Figure 6 shows electron micrographs of SiC fibers with near-stoichiometric composition that were prepared by the second method described above. The

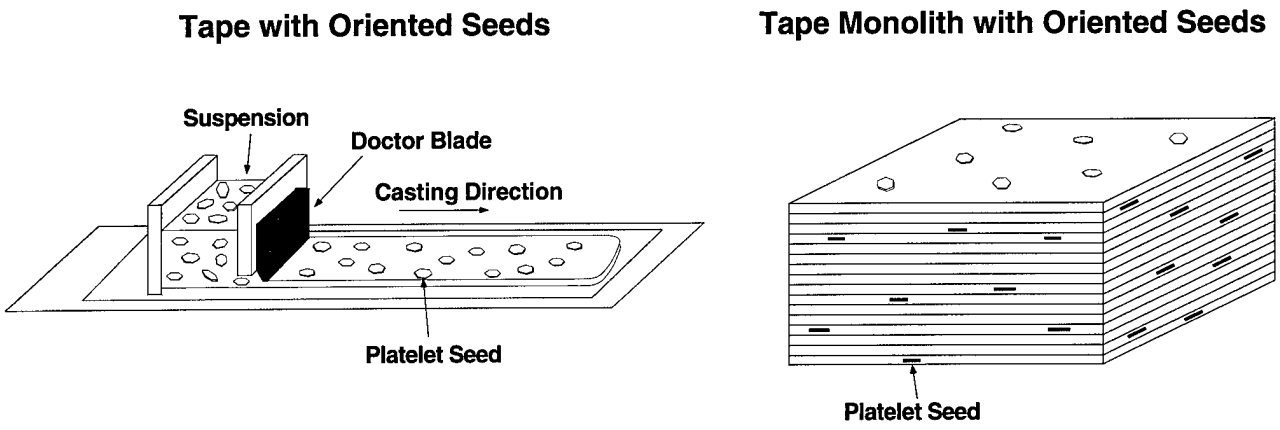

Figure 1. Schematic illustrations of the tape casting method used to prepare green bodies with oriented platelets.

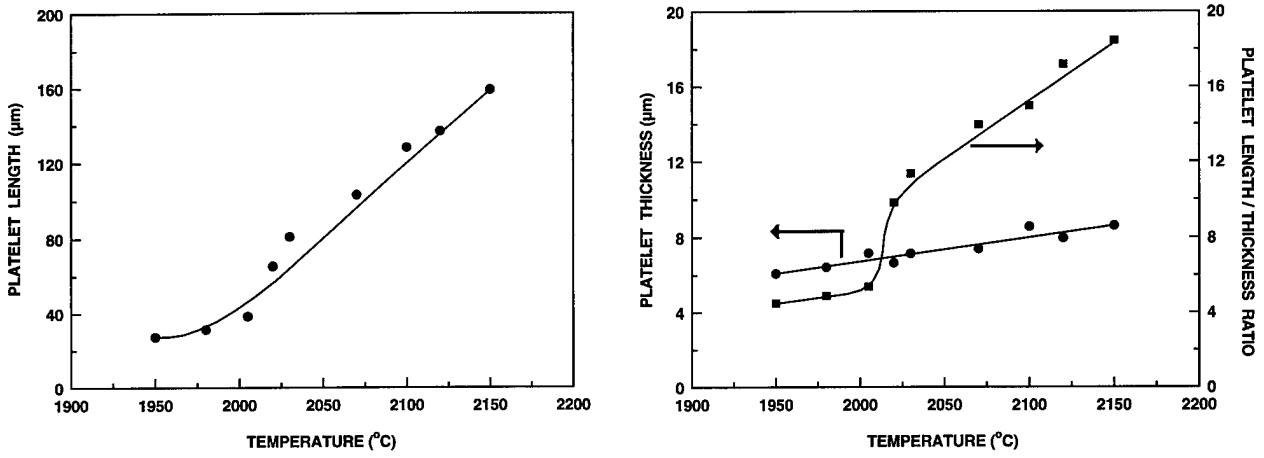

Figure 2. Plots of the length, thickness, and length/thickness ratio of the platelike grains as a function of the heat treatment temperature for seeded (2% platelets) SiC samples.

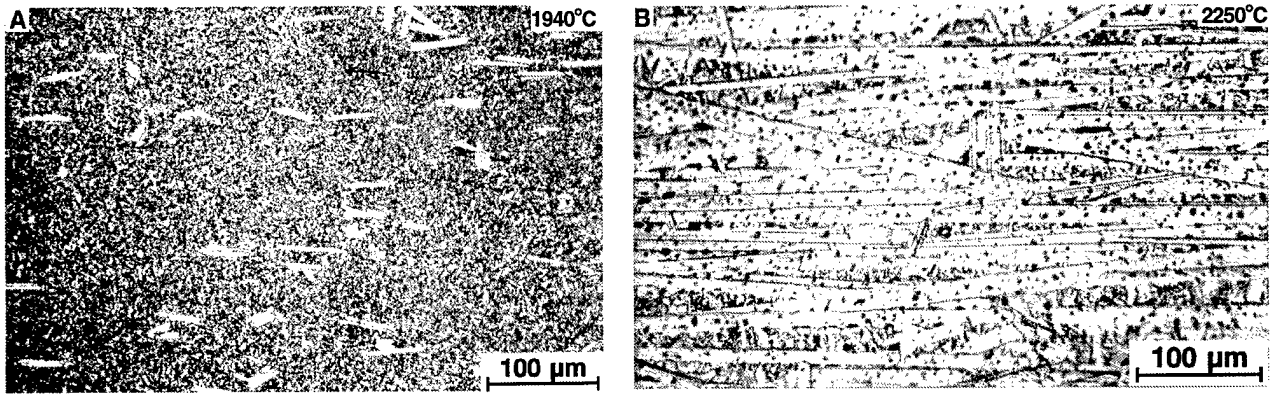

Figure 3. SEM micrographs of polished sections (taken perpendicular to the casting surface) of SiC samples showing the development of large, oriented platelike grains via growth from the oriented platelet seeds.

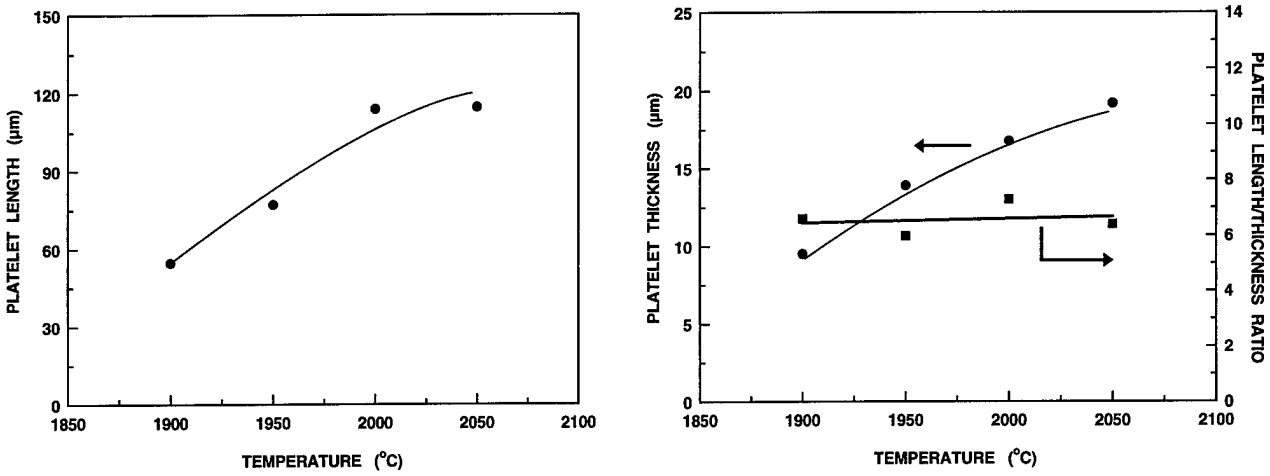

Figure 4. Plots of the length, thickness, and length/thickness ratio of the platelike grains as a function of the heat treatment temperature for seeded (2% platelets) SiC samples prepared with alumina/yttria additives.

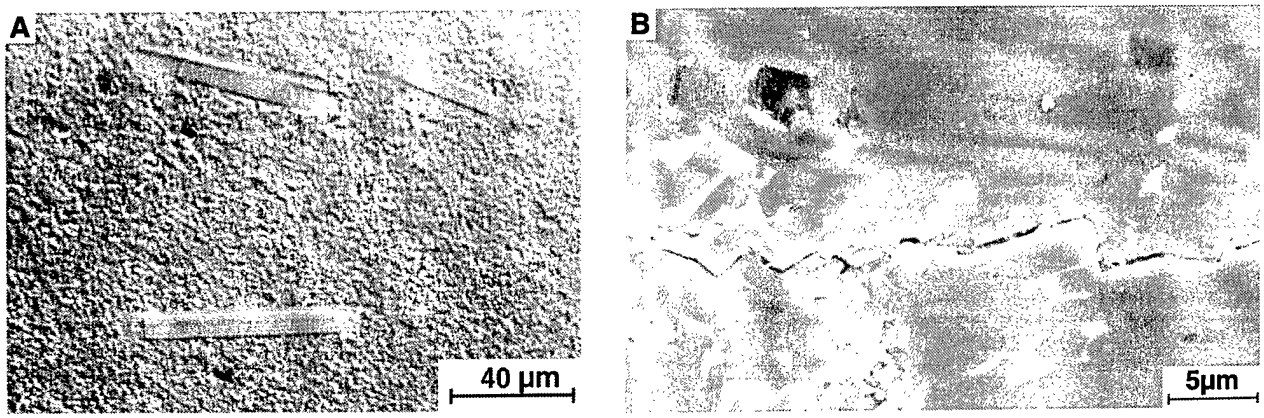

Figure 5. Micrographs of polished sections (taken perpendicular to the casting surface) for seeded (2% platelets) SiC samples prepared with alumina/yttria additives. The optical micrograph (A) shows "core-rim" structures which indicates that growth of the platelike grains occurs by the solution-reprecipitation mechanism. The SEM micrograph (B) shows a highly tortuous crack path which indicates that crack deflection contributes to the increased fracture toughness (i.e., compared to samples prepared with boron and carbon additives).

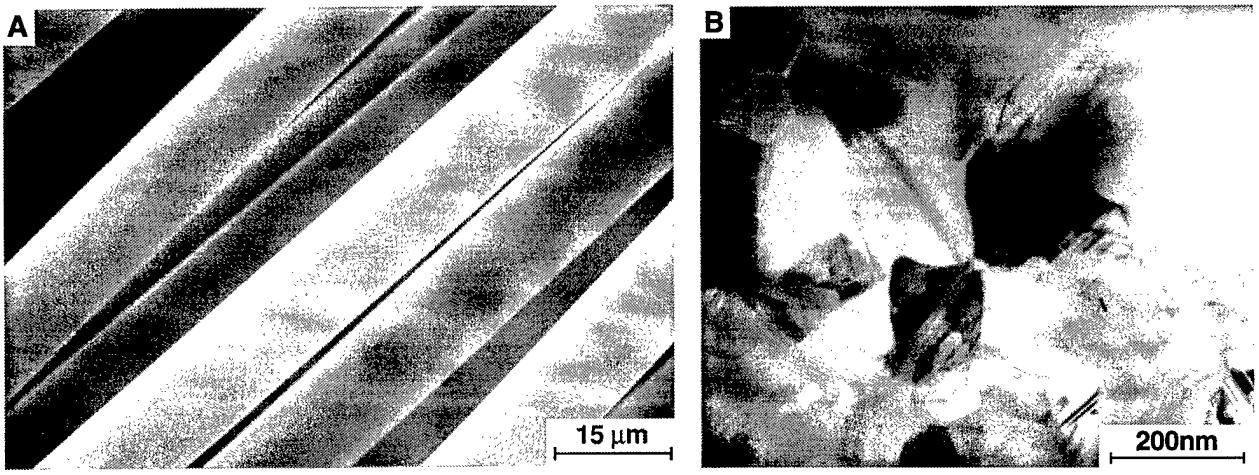

Figure 6. Electron micrographs showing (A) external surfaces and (B) grains of near-stoichiometric SiC fibers.

fibers have relatively smooth surface texture with typical diameters in the range of ~10-15 μm (Fig. 6A). Grain sizes were mostly in the range of ~0.05 - 0.3 μm (Fig. 6B), although some larger grains (i.e., up to ~0.5-1.0 μm) were also be found in the fibers. Fig. 6B also shows that the grains have a high concentration of twins and stacking faults. This is a common observation in SiC, especially in fine-grained samples.[23,32] Electron diffraction and XRD diffraction measurements indicated that β-SiC was by far the predominant phase in the fibers, but a small amount of α-SiC was also detected in some samples.

Fiber apparent densities were measured by the sink-float technique. The average value (for more than 50 samples) was ~3.15 g/cm^3 (standard deviation of ± 0.04 g/cm^3). This is ~98% of the theoretical value of ~3.21 g/cm^3 for fully dense (pore-free), stoichiometric SiC. TEM observations showed that fibers had only small amounts of residual porosity; fine pores (usually <0.1 μm) were occasionally observed at grain junctions. Electron microprobe analysis (EMA) confirmed that fibers had a near-stoichiometric composition. Normalized Si/C weight ratios were typically in the range 67-70 wt% Si/30-33 wt% C, with an average composition (for more than 25 samples) of ~68.5 wt% Si/~31.5 wt% C. This indicated that fibers usually contained a small amount of excess carbon. This was confirmed by high resolution transmission electron microscopy (HRTEM). Figure 7A shows a typical HRTEM micrograph of a carbon-rich region which was identified as a graphitic form based on the measured lattice spacing of 0.34 nm. The carbon-rich regions were invariably located at the SiC grain boundaries (i.e., rather than within the grains). Other than graphitic carbon, no other second phases were detected in the fibers by TEM or XRD. Initial observations by HRTEM show "clean" SiC-SiC grain boundaries, as indicated by the micrograph in Fig. 7B. EMA analyses for oxygen and nitrogen showed that concentrations were less than the resolution limit for the technique (typically ≤0.1 wt%).

The near-stoichiometric, low-oxygen-content SiC fibers prepared in this study had high tensile strengths. Figure 8A shows a histogram plot of the average tensile strengths obtained for 150 separate sets of fibers. The mean tensile strength was 2.85 GPa (413 ksi). (Maximum average tensile strengths were ~3.8 GPa (~550 ksi) and maximum individual filament strengths were ~5 GPa (~725 ksi).) The mean fiber diameter for these test sets was 12.1 μm.

Tensile strengths were also determined after multiple heat treatments in argon for 1 h at successively increasing temperatures in the range of 1400-1950°C. Figure 8B shows a plot of average tensile strength vs. heat treatment temperature for the near-stoichiometric SiC fibers prepared in this study. The average strength of these fibers prior to heat treatment was 2.96 GPa (429 ksi). Fibers retained most of their original strength until the heat treatment temperatures exceeded 1800°C. The gradual decrease in strength with higher temperatures is attributed to grain growth. (The increase in grain size with higher heat treatment temperatures was confirmed by TEM observations.) Fig. 8B also shows that the strength retention upon heat treatment for the near-stoichiometric SiC fibers is much better than that reported for Nicalon® and Hi-Nicalon® fibers.

The creep behavior of fibers was assessed using the bend stress relaxation (BSR) method developed by Morscher and DiCarlo.[33] In this method, stress relaxation values (designated as "M" values) are determined based on the extent of permanent deformation that occurs when fibers are heat treated under an applied bending load. An M value which approaches 1 indicates that no permanent (creep) deformation occurred during the high temperature annealing, while an M value of 0 indicates that the stress completely relaxed. Hence, fibers are considered more thermally stable against creep as the M value increases from 0 to 1.

Figure 9 shows plots of M values as a function of the BSR test temperature (in argon for 1 h) for the near-stoichiometric SiC fibers produced in this study (UF fibers). Figure 9 also shows data measured by other researchers [20,21,34] for three other fibers: Hi-Nicalon® (low-oxygen-content fibers with a large excess of carbon), Hi-Nicalon® Type S (low-oxygen-content fibers with near-stoichiometric composition), and Carborundum (SiC powder-derived fibers). Takeda et al. [20,21] and DiCarlo et al. [34] have shown that M values (at a given test temperature) tend to increase as the grain size of the fiber increases. (This would be expected if creep was controlled by diffusion-accommodated grain boundary sliding.) Hence, Hi-Nicalon® fibers have the lowest M values in Fig. 9 due to their very fine crystallite size. The M values (at a given test temperature) increase in the order Hi-Nicalon® < Hi-Nicalon® Type S < UF < UF - annealed which correlates with increasing grain sizes for these fibers. In contrast, the powder-derived Carborundum fibers have the largest grain sizes, but the M values are not higher than the annealed UF fibers. Furthermore, the Carborundum fibers have relatively low tensile strength (~1.2 GPa). Takeda et al. [21] have shown that Hi-Nicalon® - Type S fibers can be annealed such that the M values increase to similar values as observed for the annealed UF fibers. However, tensile strengths for the Hi-Nicalon® - Type S fibers decrease to ≤1.5 GPa[21] when such annealing heat treatments are carried out. Thus, the UF fibers are unique in that a combination of high tensile strength and excellent creep resistance (as indicated by the M values) are achieved simultaneously.

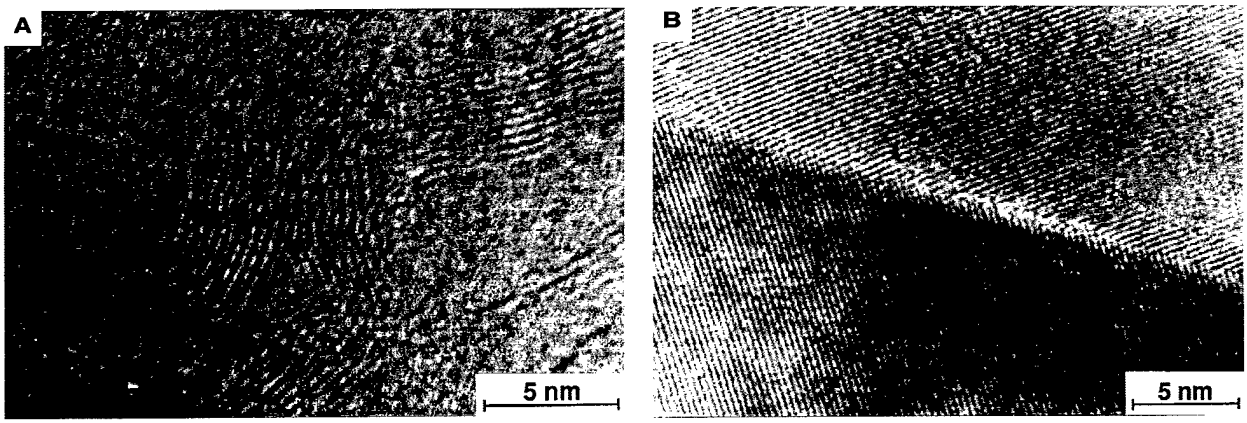

Figure 7. HRTEM micrographs of near-stoichiometric SiC fibers showing (A) graphitic lattice planes for a carbon-rich region and (B) a "clean" SiC-SiC grain boundary.

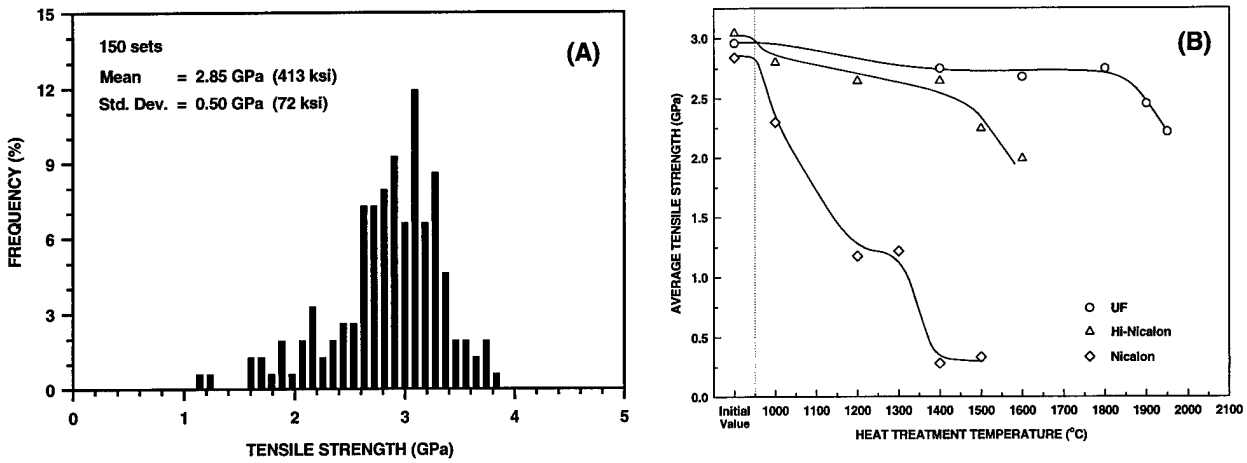

Figure 8. (A) Histogram plot of frequency vs. average tensile strength for 150 sets of near-stoichiometric SiC fibers. (B) Plot of average tensile strength vs. heat treatment temperature for the near-stoichiometric SiC fibers prepared in this study and for Nicalon® and Hi-Nicalon® fibers.

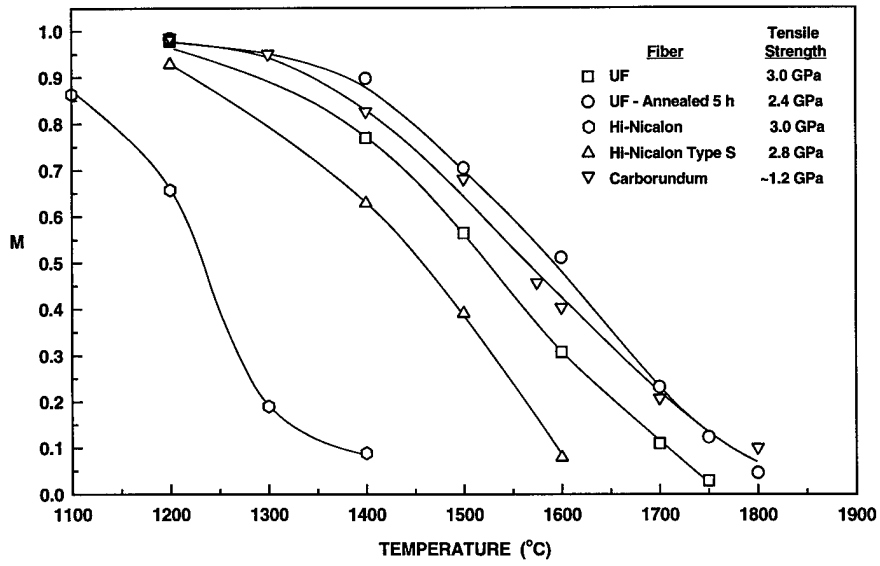

Figure 9. Plots of stress relaxation ratio, M, vs. heat treatment temperature for the near-stoichiometric SiC fibers prepared in this study and for Hi-Nicalon®, Hi-Nicalon® - Type S, and Carborundum fibers.

ACKNOWLEDGEMENT

Experimental contributions by G.A. Staab, G.W. Scheiffele, T.J. Williams, A.A. Morrone, and M. Saleem are gratefully acknowledged. Support for this work by the Advanced Research Projects Agency and the Office of Naval Research (N00014-91-J-4075, N00014-93-1-0853), Air Force Office of Scientific Research, (F49620-94-1-0429, F49620-97-1-0095), and the IHPTET Fiber Development Consortium (IHP-UFLA-93A374-005, IHP-MMM-96A374-011) is also gratefully acknowledged.

REFERENCES

1. P.F. Becher and G.C. Wei, J. Am. Ceram. Soc., 67 [12] C-267 - C-269 (1984).
2. P.F. Becher, J. Am. Ceram. Soc., 74 [2] 255-269 (1991).
3. F.F. Lange, J. Am. Ceram. Soc., 56 (10) 518-522 (1973).
4. C.W. Li and J. Yamanis, Ceram. Eng. Sci. Proc., 10 [7-8] 632-645 (1989).
5. K. Matsuhiro and T. Takahashi, Ceram. Eng. Sci. Proc., 10 [7-8] 807-816 (1989).
6. N. Hirosaki, and Y. Akimune, J. Am. Ceram. Soc., 76 (7) 1892-1894 (1993).
7. C.J. Hwang, S.M. Fuller, and D.R. Beaman, Ceram. Eng. Sci. Proc., 15 [5] 685-693 (1994).
8. K. Hirao, T. Nagaoka, M. Brito, and S. Kanzaki, J. Am. Ceram. Soc., 77 [7] 1857-1862 (1994).
9. K. Hirao, M. Ohashi, M.E. Brito, and S. Kanzaki, J. Am. Ceram. Soc., 78 (6) 1687-1690 (1995).
10. S.K. Lee, Y.C. Kim, and C.H. Kim, J. Mater. Sci., 29 5321-5326 (1994).
11. M.A. Mulla and V.D. Kristic, Acta Metall. Mater., 42 [1] 303-308 (1994).
12. N.P. Padture, J. Am. Ceram. Soc., 77 [2] 519-523 (1994).
13. M.S. Sandlin, and K.J. Bowman, pp. 263-269 in Mat. Res. Soc. Symp. Proc., Vol. 327, Materials Research Society, 1994.
14. D. Muscat, M.D. Pugh, and R.A.L. Drew, J. Am. Ceram. Soc., 75 [10] 2713-2718 (1992).
15. M.D. Sacks, G.W. Scheiffele, and G.A. Staab, J. Am. Ceram. Soc., 79 [6] 1611-1616 (1996).
16. S. Yajima, J. Hayashi, M. Omori, and K. Okamura, Nature, 261 683-685 (1976).
17. S. Yajima, K. Okamura, J. Hayashi, and M. Omori, J. Am. Ceram. Soc., 59 324-327 (1976).
18. T. Ishikawa, Composites Sci. Technol., 51 135-144 (1994).
19. M. Takeda, J. Sakamoto, Y. Imai, H. Ichikawa, and T. Ishikawa, Ceram. Eng. Sci. Proc., 15 133-141 (1994).
20. M. Takeda, J. Sakamoto, A. Saeki, Y. Imai, and H. Ichikawa, Ceram. Eng. Sci. Proc., 16 [4] 37-44 1995.
21. M. Takeda, J. Sakamoto, A. Saeki, and H. Ichikawa, Ceram. Eng. Sci. Proc., 17 [4] 35-43 1996.
22. J. Lipowitz, J.A. Rabe, and G.A. Zank, Ceram. Eng. Sci. Proc., 12 [9-10] 1819-1831 (1991).
23. J. Lipowitz, T. Barnard, D. Bujalski, J.A. Rabe, G.A. Zank, Y. Xu, and A. Zangvil, Composites Sci. Technol., 51 167-171 (1994).
24. Wm. Toreki, G.J. Choi, C.D. Batich, M.D. Sacks, and M. Saleem, Ceram. Eng. Sci. Proc., 13 [7-8] 198-208 (1992).
25. Wm. Toreki, C.D. Batich, M.D. Sacks, M. Saleem, G.J. Choi, and A.A. Morrone, Composites Sci. Technol., 51 145-159 (1994).
26. M.D. Sacks, A.A. Morrone, G.W. Scheiffele, and M. Saleem, Ceram. Eng. Sci. Proc., 16 [4] 25-35 (1995).
27. T. Mah, N.L. Hecht, D.E. McCullum, J.R. Hoenigman, H.M. Kim, A.P. Katz, H. Lipsitt, J. Mater. Sci., 19 [4], 1191-1201 (1984).
28. T.J. Clark, R.M. Arons, J.B. Stamatoff, and J. Rabe, Ceram. Eng. Sci. Proc., 6 [7-8] 576-578 (1985).
29. M.H. Jaskowiak and J.A. DiCarlo, J. Am. Ceram. Soc., 72 [2] 192-197 (1989).
30. L.S. Sigl and H.-J. Kleebe, J. Am. Ceram. Soc., 76 [3] 773-776 (1993).
31. D. Kim and C.H. Kim, J. Am. Ceram. Soc., 73 [5] 1431-1434 (1990).
32. K. Koumoto, S. Takeda, C.H. Pai, T. Sato, and H. Yanagida, J. Am. Ceram. Soc., 72 [10] 1985-1987 (1989).
33. G.N. Morscher and J.A. DiCarlo, J. Am. Ceram. Soc., 75 [1] 136-140 (1992).
34. J.A. DiCarlo, Composites Sci. Technol., 51 213-222 (1994).

Presented at the 22nd Annual Cocoa Beach Conference and Exposition on Composites, Advanced Ceramics, Materials and Structures, Cocoa Beach, FL, January 20-24, 1998 (Paper No. C-132-98). To be published in Ceram. Eng. Sci. Proc., Vol. 19, 1998.

POLYMER-DERIVED SiC-BASED FIBERS WITH HIGH TENSILE STRENGTH AND IMPROVED CREEP RESISTANCE

Michael D. Sacks, Gary W. Scheiffele, Lan Zhang, and Yunpeng Yang
University of Florida, Gainesville, FL 32611

John J. Brennan
United Technologies Research Center, East Hartford, CT 06108

ABSTRACT

Fine-diameter ($\sim$10-15 μm), polymer-derived, SiC-based fibers with carbon-rich and near-stoichiometric compositions were prepared and characterized. Tensile strengths and creep resistance were evaluated for as-fabricated fibers and for fibers given heat treatments at temperatures up to 1950°C. The creep resistance was assessed using the bend stress relaxation (BSR) method developed by Morscher and DiCarlo. Fibers showed excellent strength retention after heat treatments in argon (for 1 h) at temperatures up to 1700°C for the carbon-rich ("UF") fibers and up to 1800°C for the near-stoichiometric ("UF-HM") fibers. Creep resistance of the as-fabricated fibers was greatly improved by high temperature annealing treatments. Heat-treated UF fibers could be prepared with $\sim$3 GPa tensile strengths and BSR creep behavior which was similar to that reported for Hi-Nicalon™ Type S fibers. Heat-treated UF-HM fibers were also prepared with $\sim$3 GPa tensile strengths, while BSR results showed that the creep resistance was significantly better than that reported for Hi-Nicalon™ Type S fibers. It was also shown that the UF-HM fibers could be coated with hexagonal BN using an in-situ processing method.

INTRODUCTION

There has been considerable interest in recent years in producing SiC-based fibers with improved thermomechanical properties. Much of the effort in this area has been directed toward fabrication of fine-diameter, high-strength, polymer-derived fibers which have low oxygen content.[1-14] The development of such fibers with both carbon-rich and near-stoichiometric compositions have been reported by several research groups, including those at Nippon Carbon Co. (Hi-Nicalon™ and Hi-Nicalon™ Type S fibers)[1-6], Dow Corning Co. (Sylramic™ fibers)[7-10], and the University of Florida (UF and

UF-HM fibers).[11-14] All of these fibers show significantly improved thermomechanical properties compared to fibers which contain large amounts of oxygen, such as Nicalon™ and Tyranno™ fibers.

In this study, the tensile strength and creep resistance of carbon-rich UF fibers and near-stoichiometric UF-HM fibers were evaluated before and after heat treatments at temperatures up to 1950°C. The creep resistance was assessed using the bend stress relaxation (BSR) method of Morscher and DiCarlo.[15]

This study also reports the development of boron nitride (BN) coatings on the UF-HM SiC fibers. Well-crystallized hexagonal BN layers were formed by an in-situ processing method.

EXPERIMENTAL

The development of polymer-derived UF and UF-HM fibers has been reported previously.[11-14] Fibers were fabricated using a high-molecular-weight polycarbosilane (PCS) polymer as the primary ceramic precursor. (The infusible PCS polymers were prepared by pressure pyrolysis of polydimethylsilane.) Fine-diameter fibers were formed by dry spinning of concentrated PCS-based polymer solutions. The polymeric fibers were decomposed to SiC-based ceramics by pyrolysis in an inert atmosphere. Carbon-rich fibers (designated "UF fibers") were initially processed at temperatures in range of 1000-1200°C, while the near-stoichiometric fibers (designated "UF-HM fibers") were fabricated at higher temperatures ($\geq$1750°C). Boron additions were used in the latter fibers, both as a sintering aid and as the boron source for the formation of BN coatings by in-situ processing.

Conventional and high resolution transmission electron microscopy (TEM and HRTEM) were used to characterize the fiber microstructure. The phases present were determined by X-ray diffraction (XRD) and electron diffraction. Elemental analyses for Si,C,O, and N were carried out using electron microprobe analysis (EMA). Oxygen concentrations were also determined by neutron activation analysis, NAA, (Nicolet Electron Services, San Diego, CA). NAA was also used to determine boron concentrations (University of Missouri Research Reactor, Columbia, MO). Fiber apparent densities were determined by a sink-float method (ASTM procedure D3800-79).[16]

Single-filament tensile strengths were determined at room temperature according to ASTM procedure D3379.[17] The fiber gage length was 25 mm. The creep behavior of fibers was assessed using the bend stress relaxation (BSR) method.[15] In this method, stress relaxation values (designated as "M" values) are determined based on the extent of permanent deformation that occurs when fibers are heat treated under an applied bending load. An M value which approaches 1 indicates that no permanent (creep) deformation occurred during the high temperature annealing, while an M value of 0 indicates that the stress completely relaxed. Hence, fibers are considered more thermally stable against creep as the M values increase from 0 to 1.

RESULTS AND DISCUSSION

High-Strength, Creep-Resistant UF Fibers and UF-HM Fibers

Table 1 summarizes the characteristics of typical as-fabricated UF fibers (carbon-rich) and UF-HM (near-stoichiometric) fibers.

The as-pyrolyzed UF fibers had normalized Si/C weight ratios in the range of ~59-62 wt% Si/38-41 wt% C, with an average ratio (determined from 8 samples) of ~60.5 wt% Si/~39.5 wt% C. Hence, these fibers are highly carbon-rich relative to stoichiometric SiC (~70 wt% Si/~30 wt% C). Oxygen was present in the fiber as an impurity picked up during various stages of processing.[12] The concentrations usually did not exceed 1.5 wt% and were more typically in the range of ~0.5-1.0 wt%. Some of the fibers were doped with small amounts of boron. The phases present in the UF fibers were β-SiC and XRD-amorphous carbon. TEM and XRD line-broadening measurements indicated that the β-SiC crystallite sizes were less than 5 nm. Fiber apparent densities were in the range of ~2.5-2.7 g/cm^3. The relatively low densities are consistent with the large amount of carbon present in the fibers and the weakly crystalline nature of the SiC grains. (Well-crystallized, high purity SiC has a density of ~3.21 g/cm^3.)

Figure 1A shows a histogram plot of the average room temperature tensile strengths obtained for 43 separate sets of UF fibers. (In most cases, $\geq$15 fibers were tested for each set.) The mean tensile strength was 3.23 GPa (468 ksi). The mean diameter for these test sets was 12.6 μm. Previous fractography studies on similar fibers indicated that the strength-controlling flaw sizes were mostly in the range of ~0.2-0.3 μm.[18] This corresponds closely to the smallest pore sizes of the filters (nominal sizes were 0.1-0.2 μm) that were used to prepare the spinning solutions for fiber fabrication. Hence, it is possible that the tensile strength of the UF fibers is controlled primarily by processing-related particulates (i.e., impurity particles, polymer "microgel" particles, etc.).

The near-stoichiometric UF-HM fibers had normalized Si/C weight ratios mostly in the range of ~67-70 wt% Si/30-33 wt% C, with an average composition (determined from >25 samples) of ~68.5 wt% Si/~31.5 wt% C. This indicates that the fibers usually contained a small amount of excess carbon. X-ray and electron diffraction analyses of the UF-HM fibers showed that β-SiC was the primary phase in the fibers, although traces of the alpha phase were observed in some fibers. The SiC grain sizes were generally in the range of ~0.05 - 0.3 μm, although grains as large as ~0.5-1.0 μm were occasionally observed. Residual carbon was not detected by a standard XRD powder diffraction method, but was observed by TEM. HRTEM analysis showed the stacked hexagonal structural units with interplanar spacing of 0.34 nm that are associated with graphitic carbon. EMA analysis for oxygen and nitrogen showed that concentrations were less than the resolution limit for the technique (typically $\leq$0.2 wt%). The boron concentrations were usually on the order of 1 wt%, although fibers with range of boron concentrations (i.e., ~0.1 - 3.0 wt%) were also prepared.

The apparent densities of the UF-HM fibers were usually in the range of 3.1-3.2

TABLE 1. TYPICAL FIBER CHARACTERISTICS

UF Fibers (Carbon-Rich Composition)		
Elemental Analysis:	Si/C ratio:	~59-62 wt% Si/~38-41 wt% C
	Oxygen:	~0.5 - 1.5 wt%
	Boron:	~0-1 wt%
Phases:		weakly-crystalline β-SiC, XRD-amorphous Carbon
SiC Grain Size:		$\leq$5 nm
Apparent Density:		~2.5-2.7 g/cm^3
Diameter:		~10-15 μm
Tensile Strength:		~400-500 ksi (~2.8-3.5 GPa)
UF-HM Fibers (Near-Stoichiometric Composition)		
Elemental Analysis:	Si/C ratio:	~67-70 wt% Si/~30-33 wt% C
	Boron:	~0.1 - 3.0 wt%
	Oxygen:	$\leq$0.2 wt%
	Nitrogen:	$\leq$0.2 wt%
Phases:		well-crystallized β-SiC trace amounts of graphitic Carbon, α-SiC
SiC Grain Size:		mostly ~0.05-0.3 μm
Apparent Density:		~3.1-3.2 g/cm^3
Diameter:		~10-15 μm
Tensile Strength:		~300-500 ksi (~2.1-3.5 GPa)

g/cm^3, with an average value of ~3.15 g/cm^3. The latter value is 98% of the theoretical value of 3.21 g/cm^3 for fully dense (pore-free), stoichiometric SiC. The density is lower than the theoretical value, at least in part, because of the small amount of residual carbon. In addition, small amounts of fine pores (usually less than 0.1 μm) were occasionally observed (by TEM) at grain junctions.

Figure 1B shows a histogram plot of the average room temperature tensile strengths obtained for 150 separate sets of as-sintered UF-HM fibers. (In most cases, $\geq$15 fibers were tested for each set.) The mean tensile strength was 2.85 GPa (413 ksi). The mean

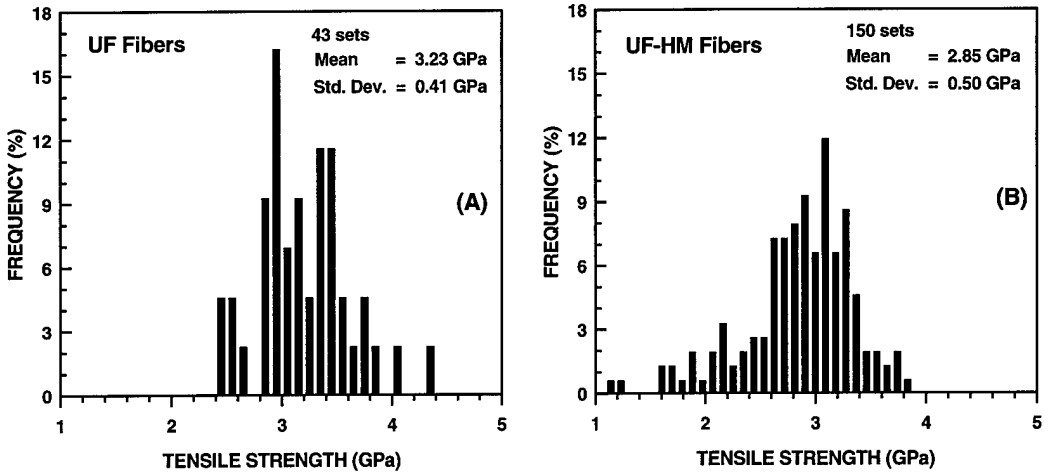

Fig. 1. Histogram plots of frequency vs. tensile strength for (A) UF fibers and (B) UF-HM fibers.

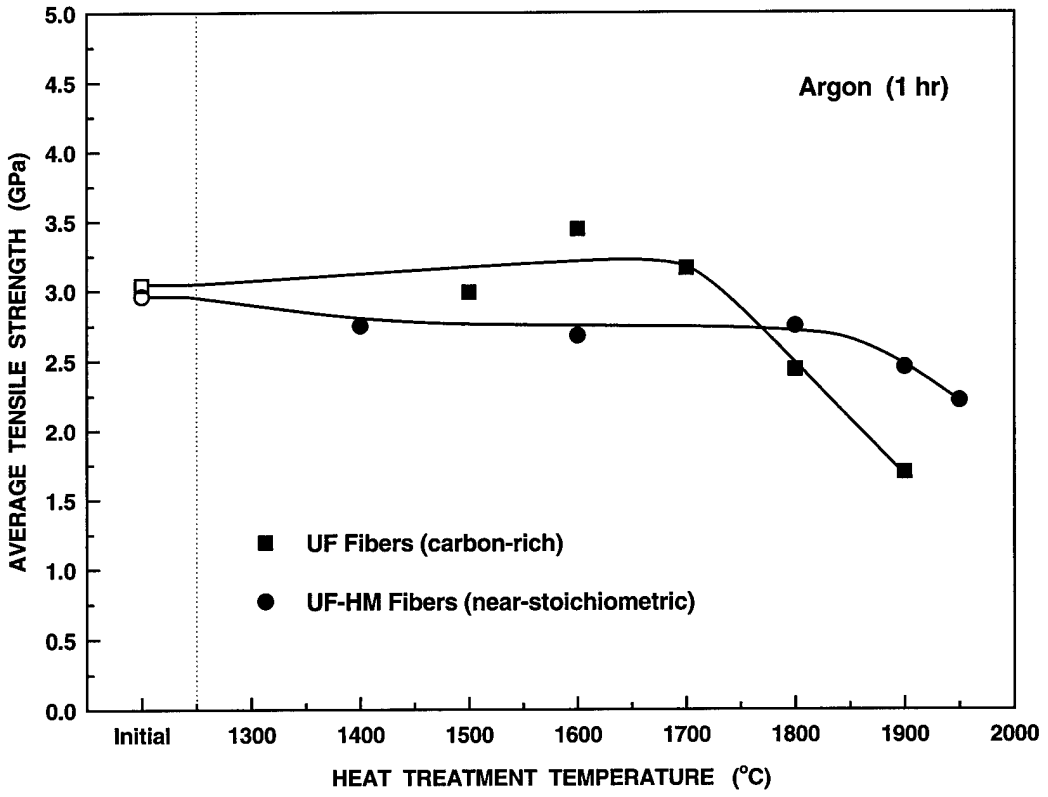

Fig. 2. Plots of average tensile strength vs. heat treatment temperature for UF fibers and UF-HM fibers.

diameter for these test sets was 12.1 μm. The tensile strengths of the UF-HM fibers are probably controlled primarily by larger grains at the fiber surface. (Fracture was generally initiated at the surface, but it was difficult to identify the specific flaws responsible for failure.)

Figure 2 shows room temperature tensile strengths for UF and UF-HM fibers after heat treatments in argon for 1 h at temperatures in the range of 1400-1950°C. The UF-HM fibers retained most of their original strength through heat treatments up to 1800°C and then the strength gradually decreased with heat treatments at higher temperatures (up to 1950°C). The UF fibers showed no loss in strength with heat treatments up to 1700°C and then showed sharper decreases in strength (compared to the UF-HM fibers) with further heat treatments up to 1900°C. Despite these differences, both the UF fibers and the UF-HM fibers show greater retention of their original strengths after high temperature (e.g., $\geq$1600°C) heat treatments in argon compared to the strength retention reported for carbon-rich Hi-Nicalon™ fibers and near-stoichiometric Hi-Nicalon™ Type S fibers, respectively.[4,5,19]

As noted earlier, it is believed that the strength-controlling flaws for the as-prepared UF-HM fibers are larger grains at the fiber surfaces. Therefore, the gradual decrease in tensile strength in the UF-HM fibers after heat treatment in argon at higher temperatures is attributed to grain growth. A small increase in the grain sizes was confirmed by TEM observations on a 1950°C heat-treated sample.[20]

It is not clear why the UF fibers decrease in tensile strength at lower heat treatment temperature (and decrease more sharply with increasing temperature) compared to the UF-HM fibers. For Hi-Nicalon™ fibers, it has been suggested that the strength decreases upon heat treatment in inert atmospheres because of a combination of coarsening of SiC grains and flaw formation resulting from thermochemical degradation reactions.[19] (The presence of small amounts of residual oxygen in the Hi-Nicalon™ fibers is expected to result in the same type of carbothermal reduction reductions that occur in conventional Nicalon™ fibers.[21-24] Such reactions result in weight losses, formation of porosity, and coarsening of SiC grains.[21-24] However, in the case of Hi-Nicalon™ fibers, these effects are much less extensive due to the much lower oxygen content.) Although these strength-degradation mechanisms are not implausible, they do not appear to the likely cause of the strength decay that is observed in Fig. 2 for the UF fibers. This is suggested for the following reasons:

(1) UF fibers undergo SiC grain coarsening during heat treatment which is similar to that observed in Hi-Nicalon[24]; however, the grains remain smaller than the grains observed in the UF-HM fibers. Figures 3A and 3B show TEM micrographs for a UF fiber heat treated for 1 h at 1900°C (in argon) and a UF-HM fiber heat treated for 0.2 h at 1840°C (in argon), respectively. Despite heat treatment at the higher temperature and longer time, the UF fibers have a considerably smaller average grain size compared to the UF-HM fibers. (The relatively slow grain growth in the UF fibers can be attributed to the much larger amount of excess carbon. This is expected to inhibit the Si diffusional transport that is required for SiC grain coarsening.)

(2) The carbothermal degradation reactions arising from the small amounts of residual

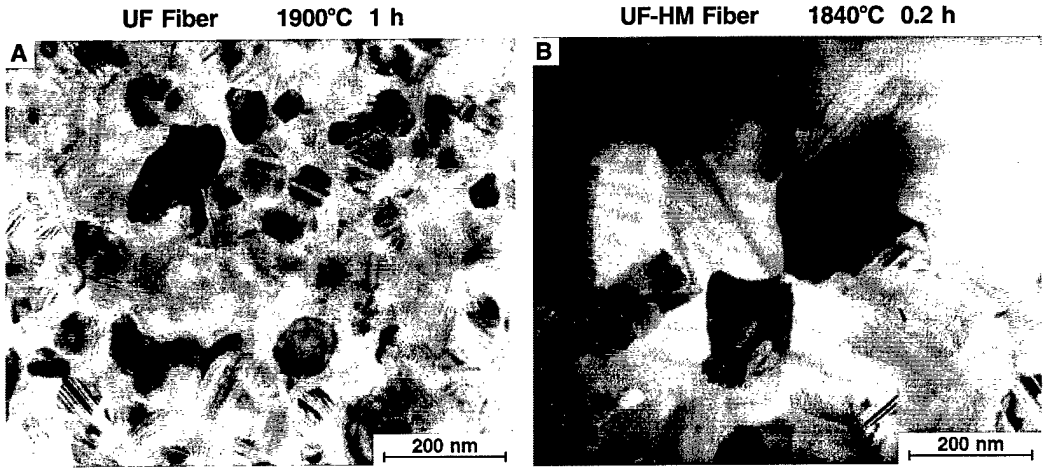

Fig. 3. TEM micrographs for (A) a UF fiber heat treated for 1 h at 1900°C and (B) a UF-HM fiber heat treated for 0.2 h at 1840°C.

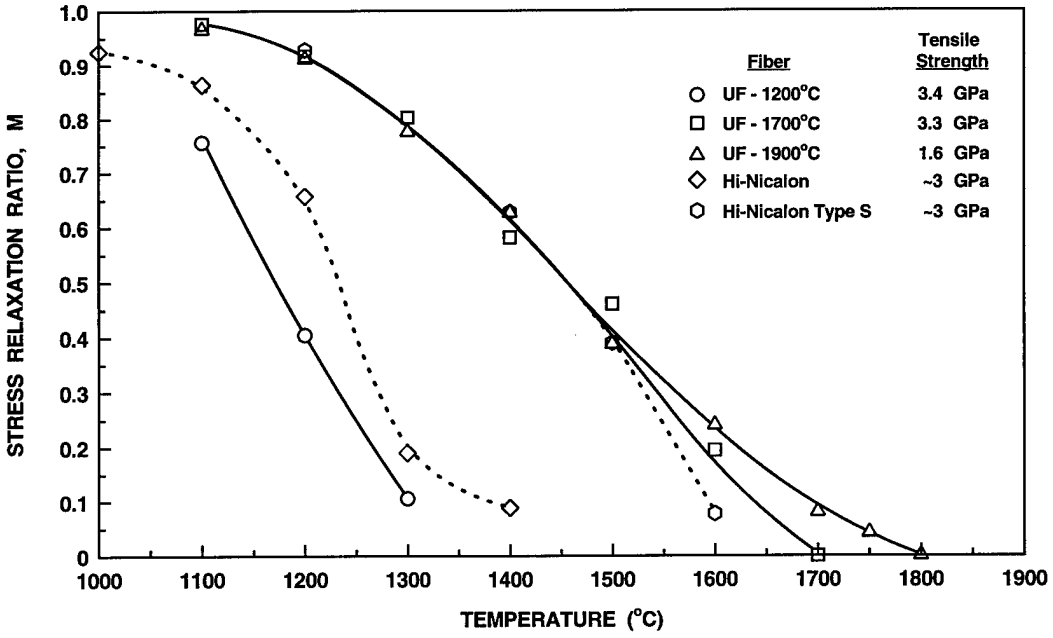

Fig. 4. Plots of stress relaxation ratio, M, vs. heat treatment temperature for as-prepared UF fibers (1200°C), heat-treated UF fibers (1700 and 1900°C), Hi-Nicalon fibers, and Hi-Nicalon Type S fibers.

oxygen are expected to begin at temperatures below 1700°C.[21-24] If these reactions caused significant flaw formation in the UF fibers, then the strength decreases would be expected to begin at lower heat treatment temperatures. Furthermore, scanning electron microscope (SEM) observations of the fibers (including the fracture surfaces) did not reveal the development of any obvious flaws which could account for the sharp decreases in strength with heat treatments above 1700°C.

A possible explanation for the more rapid decay in strength of the UF fibers with heat treatment is the presence of residual tensile stresses at the fiber surface. Such stress might arise due to the mismatch in thermal expansion coefficients between SiC and C. These stresses could become more severe as the SiC/C structure coarsens during heat treatment at higher temperatures. (In addition to growth of the β-SiC grains, the carbon regions grow into larger and more highly ordered domains when PCS-derived carbon-rich SiC fibers are heat treated at temperatures above the original fabrication temperature.[19,25] The growth of the graphitic carbon regions also has significance because graphite has a very large difference in the thermal expansion coefficients for the directions parallel and normal to the hexagonal basal planes.)

The excellent strength retention of the UF and UF-HM fibers after high temperature heat treatments (e.g., compared to fibers such as Hi-Nicalon™ and Hi-Nicalon™ Type S) offers the possibility for improved high-temperature strength retention in ceramic-matrix composites (CMC's) that are fabricated with such fibers. Furthermore, two other advantages can be realized. First, higher temperatures can be used during the processing of CMC's (e.g., to produce matrices with higher relative density) without degradation of the properties of the fibers. Second, it is possible to prepare fibers with improved creep resistance, while still retaining high tensile strength. In regard to the latter consideration, it has been shown that Hi-Nicalon™ and Hi-Nicalon™ Type S fibers become more creep-resistant after annealing heat treatments above the original processing temperature.[6,26] (This may be attributed to the increased grain sizes and/or the more highly crystallized graphitic carbon. Both microstructural changes are expected to inhibit diffusion-controlled creep processes.) The same effect (i.e., improved creep resistance in annealed fibers) was observed in the present study for the UF and UF-HM fibers. Figure 4 shows plots of the bend stress relaxation ratios, M, as a function of the heat treatment temperature for as-pyrolyzed (1200°C) UF fibers and for UF fibers which were given heat treatments for 1 h (in argon) at 1700°C and 1900°C. As expected, substantial increases in M values were obtained for the heat-treated UF fibers. The 1700°C heat-treated UF fibers not only shows greatly improved creep resistance (based on the BSR test results), but also retains high tensile strength.

Figure 4 also includes BSR data reported [6,27-29] for Hi-Nicalon™ and Hi-Nicalon™ Type S fibers. The Hi-Nicalon™ fibers have higher M values (for a given BSR test temperature) compared to the as-prepared UF fibers. This is attributed to a slightly higher initial processing temperature for the Hi-Nicalon™ fibers which, in turn, results in slightly coarser microstructures (including larger SiC crystallite sizes). The 1700°C heat-treated UF fibers have M values comparable or better (for a given BSR test temperature) than the Hi-Nicalon™ Type S fibers. This occurs despite the fact that the

grain sizes are larger for the latter fibers.[6] This observation again suggests that diffusion is inhibited in SiC-based fibers with larger amounts of excess carbon. (This manifests itself not only in the slower coarsening of SiC grains, but also in the improved creep resistance of the fibers.)

Figure 5 shows that the creep resistance (as assessed by the BSR method) for the near-stoichiometric UF-HM fibers can also be improved by annealing heat treatments. In fact, the annealed UF-HM fibers show comparable BSR behavior to that reported [27-29] for much weaker, coarse-grained Carborundum fibers. (The latter fibers were prepared by sintering of SiC powders.[30] This resulted in fibers with considerably larger grain sizes, larger diameters, and rougher surfaces compared to typical polymer-derived SiC fibers. The coarser grain sizes result in fibers with excellent creep resistance, but relatively low tensile strength.)

Takeda et al.[6] have reported that annealing heat treatments can be used to improve the creep resistance of the Hi-Nicalon™ Type S fibers (as assessed by the BSR test). However, these fibers do not retain tensile strengths as high as the UF-HM fibers after the annealing heat treatments. This is illustrated in Fig. 6 which shows plots of tensile strengths vs. M values for Hi-Nicalon™ Type S and UF-HM fibers which were subjected to various annealing heat treatments prior to BSR tests at 1400°C (for 1 h argon). It was possible to produce UF-HM fibers which had 1400°C BSR M values of ~0.9, while still retaining tensile strengths of ~3 GPa. In contrast, 1400°C BSR M values of only ~0.6 were possible in Hi-Nicalon™ Type S fibers which retained tensile strengths of ~3 GPa.

BN-Coated UF-HM fibers

UF-HM fibers with BN surface coatings were prepared by an in-situ process which is schematically illustrated in Fig. 7 (top). Boron-doped fibers were heat treated in a nitrogen-containing atmosphere. BN forms by reaction of boron at the surface with nitrogen in the atmosphere. After the initial reaction at the original SiC fiber surface, it is presumed that the increases in thickness of the coating occur by diffusion of boron from the interior of the fiber to the reaction layer, followed by chemical interdiffusion of boron and nitrogen through the growing BN layer.

Figure 7 (bottom left) shows a TEM micrograph of the BN coatings formed on the UF-HM fibers. Typical coating thicknesses were ~0.1-0.2 μm, although it may be possible to increase the thickness by using SiC fibers with higher initial boron content. Figure 7 (bottom right) shows an HRTEM micrograph of the BN layer. Electron diffraction analysis and lattice spacing measurements showed that the coating layer is hexagonal BN. The HRTEM micrograph also shows that the coating grows such that the hexagonal BN basal planes are oriented mostly perpendicular to the long axis of the UF-HM fibers.

UF-HM fibers prepared with the BN coatings retained high strength (~3 GPa) and excellent creep resistance. The effectiveness of the BN coatings for developing weak fiber/matrix interfaces in CMC's has not yet been evaluated.

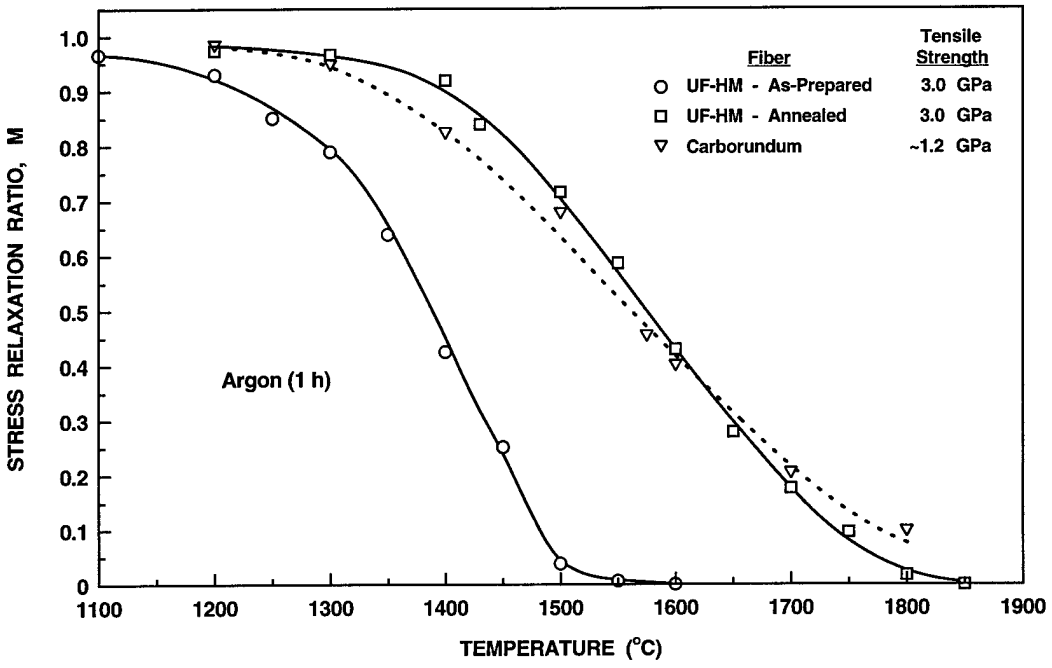

Fig. 5. Plots of stress relaxation ratio, M, vs. heat treatment temperature for as-prepared UF-HM fibers, heat-treated UF-HM fibers, and Carborundum fibers.

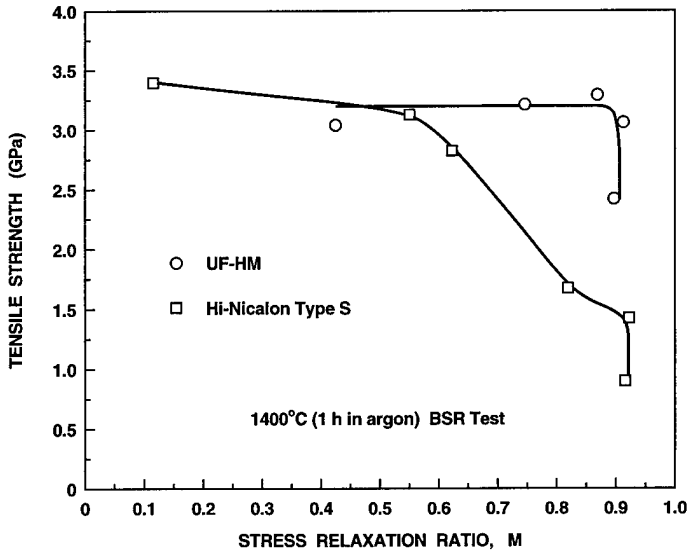

Fig. 6. Plots of tensile strength vs. stress relaxation ratio, M, for UF-HM fibers and Hi-Nicalon Type S fibers which were given varying annealing treatments in order to alter the M values. The BSR test temperature was 1400°C.

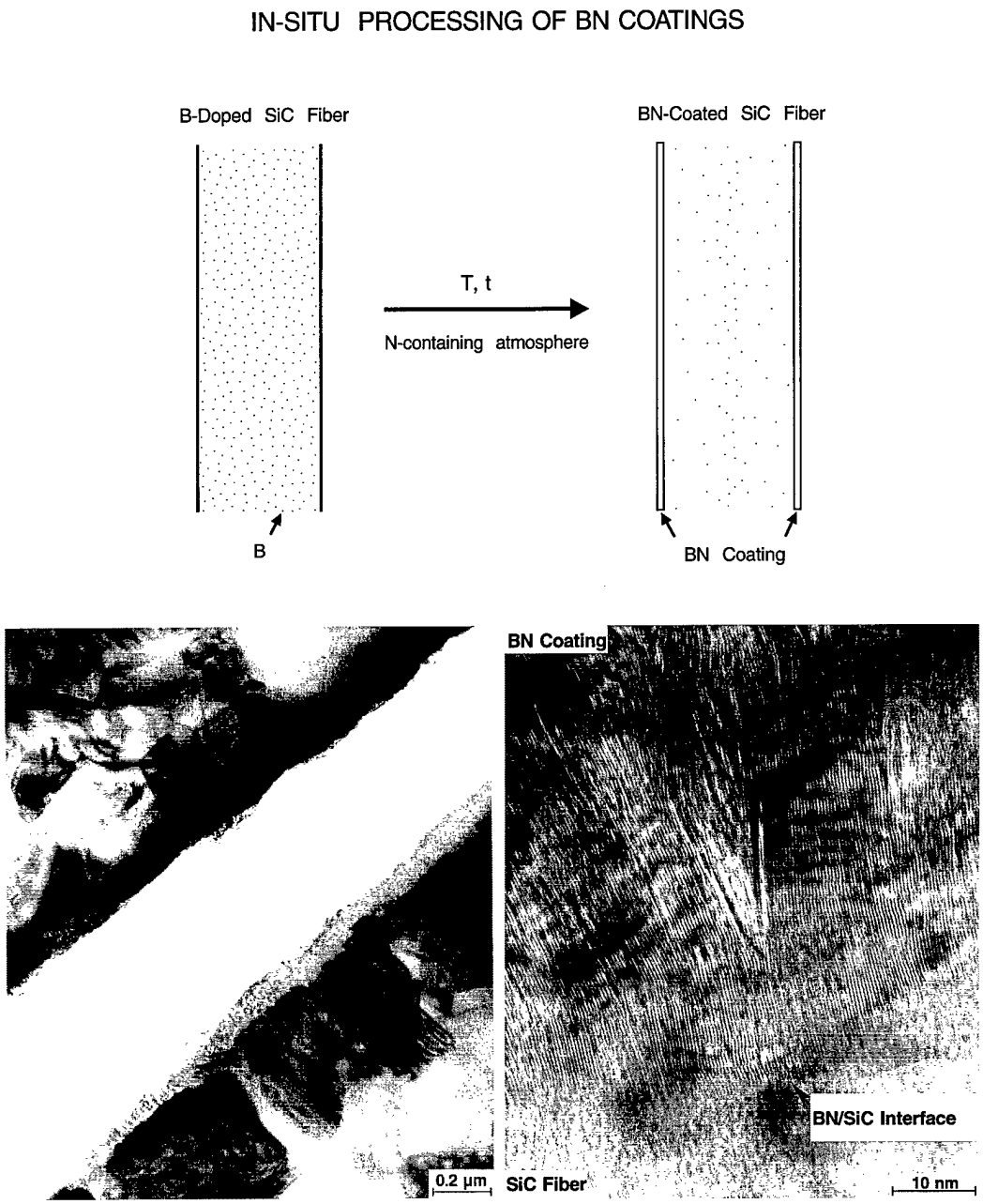

Fig. 7. Top: Schematic illustration of the formation of a BN coating on a SiC fiber by in-situ processing. Bottom left: TEM micrograph showing BN coatings and SiC fiber grains. Bottom right: HRTEM micrograph showing the BN coating/SiC fiber interface and the lattice planes of the BN coating. The BN basal planes grow with an orientation that is mostly perpendicular to the long axis of the SiC fiber.

ACKNOWLEDGEMENTS

The authors thank J.A. DiCarlo and G.N. Morscher of the NASA Lewis Research Center for assistance with the BSR measurements and helpful discussions; G.A. Staab, M. Saleem, G. Brubaker, T.J. Williams, and A.A. Morrone of the University of Florida for experimental contributions; and D. Kutikkad of the University of Missouri for the boron analysis by NAA. Support for this work by the Advanced Research Projects Agency and the Office of Naval Research (N00014-91-J-4075, N00014-93-1-0853), Air Force Office of Scientific Research, (F49620-94-1-0429, F49620-97-1-0095), and the IHPTET Fiber Development Consortium (IHP-UFLA-93A374-005, IHP-MMM-96A374-011) is gratefully acknowledged.

REFERENCES

1. M. Takeda, Y. Imai, H. Ichikawa, and T. Ishikawa, "Properties of the Low Oxygen Content SiC Fiber on High Temperature Heat Treatment", Ceram. Eng. Sci. Proc., 12 [7-8] 1007-1018 (1991).
2. M. Takeda, Y. Imai, H. Ichikawa, T. Ishikawa, N. Kasai, T. Suguchi, and K. Okamura "Thermal Stability of the Low Oxygen Content Silicon Carbide Fibers Derived from Polycarbosilane," Ceram. Eng. Sci. Proc., 13 [7-8] 209-217 (1992).
3. T. Ishikawa, "Recent Developments of the SiC Fiber Nicalon and Its Composites, Including Properties of the SiC Fiber Hi-Nicalon for Ultra-High Temperature," Composites Sci. Technol., 51 135-144 (1994).
4. M. Takeda, J. Sakamoto, Y. Imai, H. Ichikawa, and T. Ishikawa, "Properties of Stoichiometric Silicon Carbide Fiber Derived from Polycarbosilane," Ceram. Eng. Sci. Proc., 15 [4] 133-141 1994.
5. M. Takeda, J. Sakamoto, A. Saeki, Y. Imai, and H. Ichikawa, Ceram. Eng. Sci. Proc., "High Performance Silicon Carbide Fiber Hi-Nicalon for Ceramic Matrix Composites," 16 [4] 37-44 1995.
6. M. Takeda, J. Sakamoto, A. Saeki, and H. Ichikawa, Ceram. Eng. Sci. Proc., "Mechanical and Structural Analysis of Silicon Carbide Fiber Hi-Nicalon Type S," 17 [4] 35-43 1996.
7. J. Lipowitz, J.A. Rabe, and G.A. Zank, "Polycrystalline SiC Fibers from Organosilicon Polymers," Ceram. Eng. Sci. Proc., 12 [9-10] 1819-1831 (1991).
8. Y. Xu, A. Zangvil, J. Lipowitz, J.A. Rabe, and G.A. Zank, "Microstructure and Microchemistry of Polymer-Derived Crystalline SiC Fibers," J. Am. Ceram. Soc., 76 [12] 3034-3040 (1993).
9. J. Lipowitz, T. Barnard, D. Bujalski, J.A. Rabe, G.A. Zank, Y. Xu, and A. Zangvil, "Fine-Diameter Polycrystalline SiC Fibers," Composites Sci. Technol., 51 167-171 (1994).
10. J. Lipowitz, J.A. Rabe, G.A. Zank, A. Zangvil and Y. Xu, "Structure and Properties of Sylramic™ Silicon Carbide Fiber -- a Polycrystalline, Stoichiometric β-SiC Composition," Ceram. Eng. Sci. Proc., 18 [3] 147-157 (1997).
11. Wm. Toreki, G.J. Choi, C.D. Batich, M.D. Sacks, and M. Saleem, "Polymer-Derived Silicon Carbide Fibers with Low Oxygen Content," Ceram. Eng. Sci. Proc., 13 [7-8] 198-208 (1992).
12. Wm. Toreki, C.D. Batich, M.D. Sacks, M. Saleem, G.J. Choi, and A.A. Morrone, "Polymer-Derived Silicon Carbide Fibers with Low Oxygen Content and Improved Thermomechanical Stability," Composites Sci. Technol., 51 145-159 (1994).
13. M.D. Sacks, A.A. Morrone, G.W. Scheiffele, and M. Saleem, "Characterization of

Polymer-Derived Silicon Carbide Fibers with Low Oxygen Content, Near-Stoichiometric Composition, and Improved Thermomechanical Stability," Ceram. Eng. Sci. Proc., 16 [4] 25-35 (1995).

14. M.D. Sacks, G.W. Scheiffele, M. Saleem, G. Staab, T.J. Williams, and A.A. Morrone, "Polymer-Derived Silicon Carbide Fibers with Near-Stoichiometric Composition and Low Oxygen Content," pp. 3-10 in *Ceramic Matrix Composites - Advanced High Temperature Structural Materials*, Mat. Res. Soc. Symp. Proc., Vol. 365. Edited by R.A. Lowden, M.K. Ferber, J.R. Hellmann, S.G. DiPietro, and K.K. Chawla. Materials Research Society, Pittsburgh, PA, 1995.
15. G.N. Morscher and J.A. DiCarlo, "A Simple Test for Thermomechanical Evaluation of Ceramic Fibers," J. Am. Ceram. Soc., 75 [1] 136-140 (1992).
16. ASTM Test Method D3379-75, "Standard Test Method for Tensile Strength and Young's Modulus for High-Modulus Single-Filament Materials," pp. 131-134, Section 15, Vol. 15.03 in 1993 Annual Book of ASTM Standards, Section 15, Vol. 15.03, American Society for Testing and Materials, Philadelphia, PA, 1993.
17. ASTM Test Method D3800-79, Procedure B, "Standard Test Method for Density of High-Modulus Fibers," pp. 172-176, Section 15, Vol. 15.03 in 1988 Annual Book of ASTM Standards, American Society for Testing and Materials, Philadelphia, PA, 1988.
18. E. Serrano and M.D. Sacks, unpublished work.
19. G. Chollon, R. Pailler, R. Naslain, and P. Olry, "Structure, Composition, and Mechanical Behavior at High Temperature of the Oxygen-Free Hi-Nicalon Fiber," pp. 299-302 in *High-Temperature Ceramic-Matrix Composites II: Manufacturing and Materials Development*, Ceram. Trans., Vol. 59. Edited by A.G. Evans and R. Naslain. American Ceramic Society, Westerville, OH, 1995.
20. G.A. Staab and M.D. Sacks, unpublished work
21. T. Mah, N.L. Hecht, D.E. McCullum, J.R. Hoenigman, H.M. Kim, A.P. Katz, H. Lipsitt, "Thermal Stability of SiC Fibres (Nicalon)," J. Mater. Sci., 19 [4] 1191-1201 (1984).
22. G. Simon and A.R. Bunsell, "Mechanical and Structural Characterization of the Nicalon Silicon Carbide Fibre," J. Mater. Sci., 19 [11] 3649-3657 (1984).
23. T.J. Clark, R.M. Arons, J.B. Stamatoff, and J. Rabe, "Thermal Degradation of Nicalon SiC Fiber," Ceram. Eng. Sci. Proc., 6 [7-8] 576-578 (1985).
24. M.H. Jaskowiak and J.A. DiCarlo, "Pressure Effects on the Thermal Stability of Silicon Carbide Fibers," J. Am. Ceram. Soc., 72 [2] 192-197 (1989).
25. R. Bodet, X. Bourrat, J. Lamon, and R. Naslain, "Tensile Creep Behavior of Silicon Carbide-Based Fibre with a Low Oxygen Content," J. Mater. Sci., 30 661-677 (1995).
26. H.M. Yun, J.C. Goldsby, and J.A. DiCarlo, "Environmental Effects on Creep and Stress-Rupture Properties of Advanced SiC Fibers," pp. 331-336 in *High-Temperature Ceramic-Matrix Composites II: Manufacturing and Materials Development*, Ceram. Trans., Vol. 59. Edited by A.G. Evans and R. Naslain. American Ceramic Society, Westerville, OH, 1995.
27. J.A. DiCarlo, Composites Sci. Technol., "Creep Limitations of Current Polycrystalline Ceramic Fibers," 51 213-222 (1994).
28. G.N. Morscher and J.A. Dicarlo, "Creep Resistance of Advanced SiC Fibers," Proceedings of the NASA 6th Annual HITEMP Review, Cleveland, OH, 1993.
29. G.N. Morscher, unpublished results.
30. F. Frechette, B. Dover, V. Venkateswaran, and J. Kim, "High Temperature Continuous Sintered SiC Fiber for Composite Applications," Ceram. Eng. Sci. Proc., 12 [7-8] 992-1006 (1991).